Available online at www.sciencedirect.com
SCIENCE DIRECT®
PERGAMON
Progress in Aerospace Sciences 39 (2003) 467–510
PROGRESS IN AEROSPACE SCIENCES
www.elsevier.com/locate/paerosci

Wind turbine wake aerodynamics

L.J. Vermeer[a,*], J.N. Sørensen[b], A. Crespo[c]

[a] *Section Wind Energy, Faculty of Civil Engineering and Geosciences, Delft University of Technology, Stevinweg 1, 2628 CN Delft, The Netherlands*

[b] *Fluid Mechanics Section, Department of Mechanical Engineering, Technical University of Denmark, DK-2800 Kgs. Lyngby, Denmark*

[c] *Departamento de Ingeniería Energética y Fluidomecánica, ETS de Ingenieros Industriales, Universidad Politécnica de Madrid, José Gutiérrez Abascal 2, E-28006 Madrid, Spain*

Abstract

The aerodynamics of horizontal axis wind turbine wakes is studied. The contents is directed towards the physics of power extraction by wind turbines and reviews both the near and the far wake region. For the near wake, the survey is restricted to uniform, steady and parallel flow conditions, thereby excluding wind shear, wind speed and rotor setting changes and yawed conditions. The emphasis is put on measurements in controlled conditions. For the far wake, the survey focusses on both single turbines and wind farm effects, and the experimental and numerical work are reviewed; the main interest is to study how the far wake decays downstream, in order to estimate the effect produced in downstream turbines. The article is further restricted to horizontal axis wind turbines and excludes all other types of turbines.

Contents

*Corresponding author. Tel.: +31-15-2785166; fax: +31-15-2785347.

E-mail addresses: n.vermeer@citg.tudelft.nl (L.J. Vermeer), jns@mek.dtu.dk (J.N. Sørensen), crespo@enerflu.etsii.upm.es (A. Crespo).

0376-0421/$ - see front matter © 2003 Elsevier Ltd. All rights reserved.
doi:10.1016/S0376-0421(03)00078-2

1. Introduction

The conversion of wind energy to useful energy involves two processes: the primary process of extracting kinetic energy from wind and conversion to mechanical energy at the rotor axis, and the secondary process of the conversion into useful energy (mostly electrical, but also mechanical for water pumps or chemical for water desalination or hydrolyses). This paper concerns the primary process: the extraction of kinetic energy from the wind. The major field of science involved in this process is aerodynamics, but it needs meteorology (wind description) as input, and system dynamics for the interaction with the structure. The latter is important since all movement of the rotor blades, including bending of the blades out of their plane of rotation, induces apparent velocities that can influence or even destabilize the energy conversion process. Aerodynamics is the oldest science in wind energy: in 1915, Lanchester [1] was the first to predict the maximum power output of an ideal wind turbine. A major break-through was achieved by Glauert [2], by formulating the blade element momentum (BEM) method. This method, extended with many 'engineering rules' is still the basis for all rotor design codes. Recently, first results of complete Navier–Stokes calculations for the most simple wind turbine operational mode have been reported. Progress is significant in the 30-year history of modern wind energy. To name one example: a better understanding of the aerodynamics improved the efficiency of the primary process from 0.4 to 0.5 (out of a maximum of 0.592). Nevertheless, many phenomena are still not fully understood or quantified. This is due to several aspects that are unique for wind turbine aerodynamics:

- Although at present wind turbines are the biggest rotating machines on earth (up to 110 m diameter so each blade has approximately the size of the span of a Boeing 777) they operate in the lowest part of the earth boundary layer. Most aircraft try to fly high enough to avoid turbulence and extreme wind events, but for wind turbines steady wind is an off-design condition. All aerodynamic phenomena

are essentially unsteady, which, however, is still beyond the scope of current design knowledge.

- The very successful 'Danish concept' for wind turbines relies on stall for aerodynamic power limitation in high wind speeds: the increase in drag due to stall limits the torque produced at the rotor axis. All other aerodynamic objects (except military aircraft) avoid stall as much as possible because of the associated high loads and the possible loss of aerodynamic damping. Since many wind turbines rely on stall, a thorough understanding of unsteady (deep) stall is necessary.
- The flow in the blade tip- and root region is three-dimensional: for example, due to centrifugal and coriolis forces the flow in the boundary layer at the root is in spanwise direction, while the flow just outside the layer is chordwise. This effect delays stall, by which much higher lift is achieved compared to two-dimensional data. The relevance of two-dimensional data for wind turbine performance prediction is very limited.

The aerodynamic research for wind turbines has contributed significantly to the success of modern wind energy. For most unsolved problems, engineering rules have been developed and verified. All of these rules have a limited applicability, and the need to replace these rules by physical understanding and modelling is increasing. This is one of the reasons that the worldwide aerodynamic research on wind energy shows a shift towards a more fundamental approach. 'Back to basics', based on experiments in controlled conditions, is governing most research programs. This paper contributes to this by surveying all previous experiments and analyses on the flow through the rotor. For an overview on the technology development of wind turbines, see [3]. For a survey of the future R&D needs for wind energy, see [4].

2. Overview

Wind turbine wakes have been a topic of research from the early start of the renewed interest in wind energy utilisation in the late 1970s. From an outsider's point of view, aerodynamics of wind turbines may seem quite simple. However, the description is complicated, by the fact that the inflow always is subject to stochastic wind fields and that, for machines that are not pitch-regulated, stall is an intrinsic part of the operational envelope. Indeed, in spite of the wind turbine being one of the oldest devices for exploiting the energy of the wind (after the sailing boat), some of the most basic aerodynamic mechanisms governing the power output are not yet fully understood.

When regarding wakes, a distinct division can be made into the near and far wake region. The near wake is taken as the area just behind the rotor, where the properties of the rotor can be discriminated, so approximately up to one rotor diameter downstream. Here, the presence of the rotor is apparent by the number of blades, blade aerodynamics, including stalled flow, 3-D effects and the tip vortices. The far wake is the region beyond the near wake, where the focus is put on the influence of wind turbines in farm situations, so modelling the actual rotor is less important. Here, the main attention is put on wake models, wake interference, turbulence models, and topographical effects. The near wake research is focussed on performance and the physical process of power extraction, while the far wake research is more focussed on the mutual influence when wind turbines are placed in clusters, like wind farms. Then, the incident flow over the affected turbines has a lower velocity and a higher turbulence intensity, that make the power production decrease and increase the unsteady loads. In the far wake the two main mechanisms determining flow conditions are convection and turbulent diffusion and in many situations a parabolic approximation is appropriate to treat this region. It is expected that sufficiently far downstream, the deleterious effects of momentum deficit and increased level of turbulence will vanish because of turbulent diffusion of the wake.

For the near wake, the survey is restricted to the uniform, steady and parallel flow conditions. Topics which will not be addressed, but which contribute to the complexity of the general subject, are: wind shear, rotor–tower interaction, yawed conditions, dynamic inflow, dynamic stall and aeroelastics, but these are not taken along in this article. Furthermore, the emphasis is put on measurements in controlled conditions. This is guided by the realisation that, although there have been attempts to tackle dynamic inflow and yawed related topics, the basics of wind turbine aerodynamics is not fully understood. For an overview of wind turbine rotor aerodynamics in general, see [5] and for an overview of unsteady wind turbine aerodynamic modelling, see [6].

Some field experiments are directed towards wake measurements, but changes in wind force and wind direction often obscure the effects of investigation. Most recent field measurement campaigns are related to the pressure distribution over the blade. These measurements are done as an international cooperation project as IEA Annex XVIII: "Enhanced Field Rotor Aerodynamic Database" see [7]. Because this topic is outside the scope of this article, the mention will be restricted to this and the focus will be on experiments under controlled conditions (i.e. in the wind tunnel).

For the far wake, the survey focusses on both single turbines and wind farm effects, which are modelled often in a different way. Both analytical and experimental

work is analysed. In the research work of the far wake frequent reference is made to the near wake behaviour, and consequently both are difficult to separate in a review paper; the main reason is that the near wake characteristics of the flow are initial conditions for the far wake. In the study of the far wake the effect of wind shear has to be retained, as it is an important mechanism to explain some phenomena of interest. The article is further restricted to horizontal axis wind turbines and excludes all other types of turbines. Nevertheless, sufficiently far downstream, the results for the far wake, could be extended to other turbines if the overall drag of the wind turbine that originates the wake is estimated correctly.

3. Near wake experiments

In sharp contrast to the helicopter research (see [8]), good near wake experiments are hard to find in wind energy research. And also, unlike in helicopter industry, there are only few financial resources available for experiments, but the need for experimental data is nevertheless well recognized (see also [9]).

Since the start of the wind energy revival, effort has been put into experiments, both for single turbines and wind farms. During the literature survey for this article, a number of references to wind tunnel experiments have been gathered, which are summarized in Table 1. These experiments on the near wake will be assessed by several criteria to evaluate the significance: model to tunnel area ratio, Reynolds number, completeness of acquired data. The properties to evaluate concern the feasibility to make a comparison between the experimental data and results from computational codes, so the fluid dynamics must be representable for validation. The suitable rotor properties thus are the aerofoil, the Reynolds number and the wind tunnel environment (specifically the tunnel to model area ratio).

The main focus will be on experiments in controlled conditions, because these are capable of providing the essential data for comparison with numerical simulations. The drawback of wind tunnel experiments is the effect of scaling on the representation of ''real world'' issues. On the other hand, the full-scale experiments (which are mostly field experiments) are put at a disadvantage by wind shear, turbulence, changing oncoming wind in both strength and direction on the exposure of physical phenomena.

Most experiments have been performed at rather low Reynolds numbers (as related to blade chord and rotational speed), only three cases with Reynolds numbers exceeding 300,000 are known [10–12]. Running a test at low Reynolds numbers shouldn't be much of a problem as long as an appropriate aerofoil section is chosen, of which the characteristics are known for that particular Reynolds range. In this way, the model test does not resemble a full-scale turbine, but is still suitable for comparison and verification with numerical models. The same reasoning can be applied to the number of blades: although the current standard in wind turbine industry is to design three bladed wind turbines, experiments on two (or even one) bladed models can be very valuable.

Another aspect to consider is the model to tunnel area ratio. This is especially important for closed tunnels, but should also be taken into account for open-jet tunnels. Because of the mutual dependency of rotor inflow and wake structure, the performance of the rotor is influenced by the possibility of free expansion of the wake. As can be seen in the near wake experiments table, there are a great diversity of models and tunnels. The model to tunnel area ratio ranges from 1 to 125 (where the size of the model is apparently very small) to 1 to 1 (where it is clear that there cannot be any undisturbed expansion of the wake).

The most promising results are to be gained from wind tunnel experiments on full-scale rotors. However, these experiments tend to be very expensive, because of both investments in the model and the required tunnel size. There is only one known source: the NREL Unsteady Aerodynamic Experiment in the NASA-Ames wind tunnel (see [13,14]). In this case, the field test turbine of NREL, with a diameter of 10 m, was placed in the 24.4 m × 36.6 m (80 ft. × 120 ft.) NASA-Ames wind tunnel; the model to tunnel area ratio is 1 to 10.8 and the Reynolds number was 1,000,000. Although there was a considerable time to spend in the tunnel, most emphasis was put on pressure distributions over the blade and hardly any wake measurements were performed. Nevertheless, a considerable amount of data has been collected. This data will be the starting point for an international cooperation project as IEA Annex XX: ''HAWT Aerodynamics and Models from Wind Tunnel Measurements'' to analyse the NREL data to understand flow physics and to enhance aerodynamics subcomponent models.

Within the European Union, a similar project to the NREL experiment was started under the acronym ''MEXICO'' (model rotor experiments under controlled conditions). In this project, a three bladed rotor model of 4.5 m diameter will be tested in the DNW (Deutsch-Niederländische Windanlage: the German-Dutch Wind Tunnels) wind tunnel. For this experiment, the tunnel will be operated with an open test section of 9.5 m × 9.5 m; the model to tunnel area ratio is 1–3.8 and the Reynolds number will be 600,000 at 75% radius. One of the three rotor blades will be instrumented with pressure sensors at five radial locations. In the measurement campaign, also wake velocity measurements with PIV (particle image velocimetry) are planned. In this way, a correlation between the condition of the blade

Table 1

Descriptive name	TNO1	FFA	NLR	Cambridge	VTEC	MEL	TUDelft1	TUDelft2	TUDelft3	Rome
Institute or organization	TNO	FFA	NLR	University of Cambridge	Virginia Polytechnic Institute	MEL	Delft University of Technology	Delft University of Technology	Delft University of Technology	University of Rome
Country	Netherlands	Sweden	Netherlands	UK	USA	Japan	Netherlands	Netherlands	Netherlands	Italy
Leading person	P.E. Vermeulen	P.H. Alfredsson	O. de Vries	M.B. Anderson	M.A. Kotb	H. Matsumiya	L.J. Vermeer	L.J. Vermeer	L.J. Vermeer	G. Guj
Framework	National research programme	Basic research	National research programme	Ph.D.	Ph.D.	Basic research	Basic research	Basic research	Basic research	
Years	1978	1979–1981	1979	1982	~1983	1987	1985–1987	1987–1992	1983–2002	1991
Facility	Wind tunnel	Wind tunnel	Wind tunnel	Wind tunnel	Wind tunnel	Wind tunnel	Wind tunnel	Wind tunnel	Wind tunnel	Wind tunnel
Size	2.65 m by 1.2 m	2.1 m by 1.5 m octogonal	3 m by 2 m	9.2 m by 6.5 m	1.82 m by 1.82 m (6 ft by 6 ft)	1.4 m by 1.4 m	2.24 m diameter	2.24 m diameter	2.24 m diameter	0.39 m diameter
Model to tunnel area ratio	1 to 31.2	1 to 56	1 to 13.6	1 to 8.46	1 to 16.3	1 to 3.9	1 to 125	1 to 3.5	1 to 3.5	1 to 1.9
Model size	0.36 m diameter	0.25 m diameter	0.75 m diameter	3 m diameter	0.508 m diameter	0.8 m diameter	0.2 m diameter	1.2 m diameter	1.2 m diameter	0.28 m diameter
Number of blades	2	2	2	2	3	2	2	2	2	1
Reynolds number range	25,000–50,000 at 50% R	65,000 at the tip, 60,000 at 75% R	350,000 at 75% R	335,000 at 75%R	?	# N/A	18,000 at the tip, 24,000 at 75% R	240,000 at the tip, 175,000 at 75% R	240,000 at the tip, 175,000 at 75%	45,000
Airfoil(s)	Gö 804	#N/A	NACA 0012	NACA 4412	Airplane propeller (Zinger 20-6)	NACA 4415	curved plates	NACA 0012	NACA 0012	NACA 0012
Chord	Constant	Tapered	Tapered	Tapered	Tapered	Tapered	Tapered	Constant	Constant	Constant
Tip chord	0.02 m	0.025 m	0.048 m	0	#N/A	0.04 m	0.0122 m	0.08 m	0.08 m	0.03 m
Pitch	constant	Twisted	Twisted	Twisted	Twisted	Twisted	Twisted	Twisted	Twisted	Constant
Design tip-speed ratio	7.5	3.5	8	10	3	6	5	6	6	5
Solidity	0.071	0.14	0.0674	0.047	?	0.11	0.08	0.059	0.059	0.068
Measurement techniques	pitot-tube, hot wires	hot wires	pitot- and static-pressure	Hot film, LDV	3-D yawhead probe	LDV	hot wires	hot wires	hot wires	hot wires
Availability of data			on microfiche in report				Yes, on request	Yes, on request	Yes, on request	
References	[34,35]	[16,17]	[10]	[11]	[36–38]	[52]	[21–23]	[15,56,57,24]	[61–64,28,24]	[58]
Type of work	CP, CT, averaged velocity data, turbulence intensities	CP, CT, averaged velocity data, flowviz, vortex spirals	CP, CT, averaged velocities	CP, CT, averaged velocities, detailed velocities	CP, averaged velocities	Detailed velocities	CP, CT, detailed velocities, flowviz	CP, CT, detailed velocities	Tip vortex properties, flowviz	Detailed velocities

Table 1 (*continued*)

Newcastle1	Newcastle2	Edinburgh	Herriot-Watt1	Herriot-Watt2	NREL	Mie	UIUC	Mexico	Descriptive name
University of Newcastle	University of Newcastle	University of Edinburgh	Herriot-Watt University	Herriot Watt University	NREL	Mie University	University of Illinois at Urbana-Champaign	ECN	Institute or organization
Australia	Australia	UK	UK	UK	USA	Japan	USA	Netherlands	Country
P.D. Clausen	P.R. Ebert	J. Whale	I. Grant	I. Grant	M. Hand	Y. Shimizu	C.J. Fisichella	H. Snel et. al.	Leading person
National research programme	Ph.D.	Ph.D.	Project	Project			Ph.D.	Project	Framework
1985–1988	~1992–1996	~1990–1996	~1996	~1996	1999	~2000	1997–2001	2000–2005	Years
Wind tunnel	Wind tunnel	Water tank	Wind tunnel	Wind tunnel	Wind tunnel	Wind tunnel	Wind tunnel	Wind tunnel	Facility
0.26 m diameter	0.25 m diameter octagonal	400 mm by 750 mm	octagonal 1.24 m	2.13 m by 1.61 m	24.4 m by 36.6 m (80 ft × 120 ft NASA Ames)	1.8 m diameter	1.52 m by 1.52 m	9.5 m by 9.5 m (DNW)	Size
1 to 1.0	1 to 1.0	1 to 12.5		1 to 4.4	1 to 10.8	1 to 1.7	1 to 2.9	1 to 3.8	Model to tunnel area ratio
0.26 m diameter	0.25 m diameter	0.175 m diameter	0.9 m diameter	1.0 m diameter	10.08 m diameter	1.4 m diameter	1.0 m diameter	4.5 m diameter	Model size
2	2	2	2 or 3	2	2	3	1, 2 or 3	3	Number of blades
210,000 at 75%R	255,000 at 75% R	6,400–16,000	?	?	1,000,000	325,000	?	600,000 at 75% R	Reynolds number range
NACA 4418	NACA 4418	flat plate	NACA 4611 to NACA 3712	NACA 4415	NREL S809	NACA 4415	Clark-Y	DU91-W2-250, RIS∅A221, NACA 64-418	Airfoil(s)
Constant	Constant	Tapered	Tapered	# N/A	Tapered	Tapered	Constant	Tapered	Chord
0.058 m	0.06 m	0.01 m	# N/A	0.1 m	0.356 m	0.12	0.0457 m	0.085 m	Tip chord
Constant	Constant	Constant	Constant	# N/A	Twisted	Twisted	Twisted	Twisted	Pitch
4	4	6	6.7	# N/A	5	3	# N/A	6.5	Design tip-speed ratio
0.2	0.17	0.091	?	?	0.052	0.12	0.029, 0.058 or 0.087	0.085	Solidity
hot wires	hot wires	PIV	PIV	PIV, pressure taps	Pressure taps	LDV	Hot film	PIV	Measurement techniques
							As charts in thesis	After project finish	Availability of data
[53–55]	[46–50]	[40–42,44,45]	[65]	[65]	[13,14]	[12]	[51]		References
Detailed velocities	CP, detailed velocities	Detailed velocities, tip vortex properties	Tip vortex properties	Tip vortex properties	Flowviz	CP, detailed velocities, flowviz	CT, detailed velocities, tip vortex properties	CP, CT, detailed velocities, tip vortex properties	Type of work

circulation and the wake properties is expected to be achieved.

3.1. Global properties

The operational conditions of a wind turbine are described in a non-dimensional way with the C_P–λ and $C_{D_{ax}}$–λ curves. The C_P–λ curve gives the power coefficient against the tip-speed ratio, where C_P is defined as the power from the wind turbine divided by the power available from the wind through the rotor area, so $C_P = P/\frac{1}{2}\rho V_0^3 \pi R^2$ and λ is the rotor tip speed divided by the oncoming wind speed, so $\lambda = \omega R/V_0$ (similar to the reciprocal of the advance ratio in helicopter terminology). The $C_{D_{ax}}$–λ curves gives the axial force coefficient against the tip-speed ratio, where $C_{D_{ax}}$ is defined as the axial force on the total rotor divided by the reference value, so $C_{D_{ax}} = D_{ax}/\frac{1}{2}\rho V_0^2 \pi R^2$.

A lot of the references do give data for the global properties of the rotor, but only for the configuration parameters of the tests. Good practice would be to thoroughly test the rotor before trying to experiment on the wake, providing a proper documentation of the rotor for later analysis. The curves given by de Vries [10] (see Fig. 1) and Vermeer [15] (see Figs. 2 and 3) show typical examples for two different rotor models.

3.2. Flow visualisations

Flow visualisation can give information, mostly qualitative, about the flow in the vicinity of the rotor and can reveal areas of attention. It can be done either in the wake, trying to reveal rotor related flow patterns, or on the blade, trying to reveal blade related flow pattern.

One of the first flow visualisation experiments is done at FFA by Alfredsson [16,17]. Later by Anderson [11], Savino [18], Anderson [19], Eggleston [20], Vermeer [21–23] and [24], Hand [13] and Shimizu [12].

There is a distinction between two types of flow visualisation with smoke: either the smoke can be inserted into the flow from an external nozzle, so the smoke is being transported with inflow velocity and shows the cross section of the tip vortices (see Figs. 4–6), or the smoke is ejected from the model (mostly near the tip), so the smoke trails are being transported with the local velocity and show a helix trace (see Fig. 7).

The FFA experiment by Alfredsson was originally set out for wind farm effects, but was used later on for deducing parameters for a single wake. In Fig. 4, as much as six tip vortex cores can be counted, so for this two-bladed rotor this means three full revolutions. The visibility of these vortex cores is dependent on several aspects: the quality of the wind tunnel with respect to turbulence intensity, the quality of the smoke and illumination, but also on the strength of the tip vortex itself.

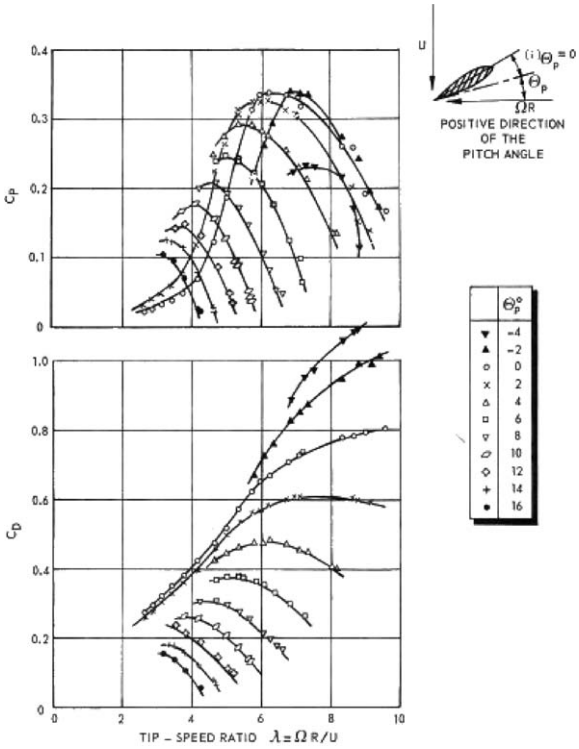

Fig. 1. Influence of pitch angle, θ_{tip}, on power coefficient (top) and rotor drag coefficient (bottom) versus tip-speed ratio λ (from [10]).

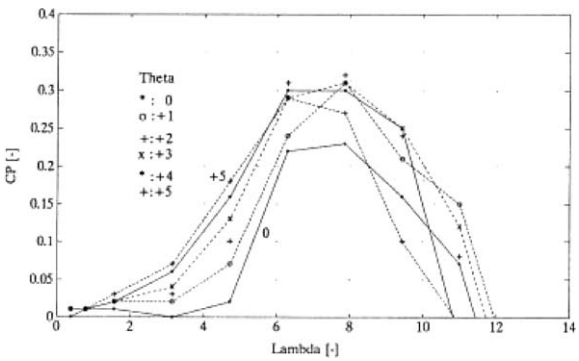

Fig. 2. Power coefficient as function of tip-speed ratio, λ, with tip pitch angle, Θ, as a parameter (from [15]).

Also at TUDelft, similar smoke pictures were taken by Vermeer [24] (see Fig. 6). Compared to the FFA pictures, these appear rather poor, which might be due to the turbulence level and the quality of the smoke nozzle. Although the rotor model is really small (0.2 m diameter), it has been used in the first phase of a long-term wake research programme. With this model, the initial measurements have been carried out and some interesting observations have been made: when setting

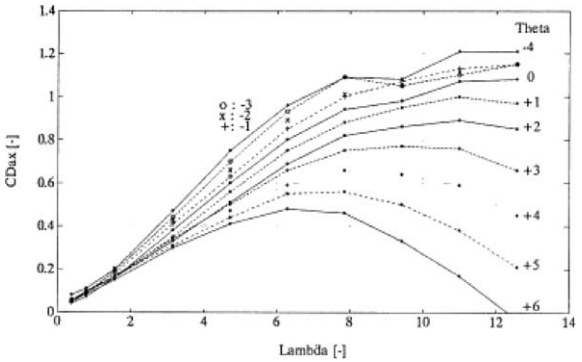

Fig. 3. Axial force coefficient as function of tip-speed ratio, λ, with tip pitch angle, Θ, as a parameter (from [15]).

Fig. 4. Flow visualisation with smoke, revealing the tip vortices (from [16]).

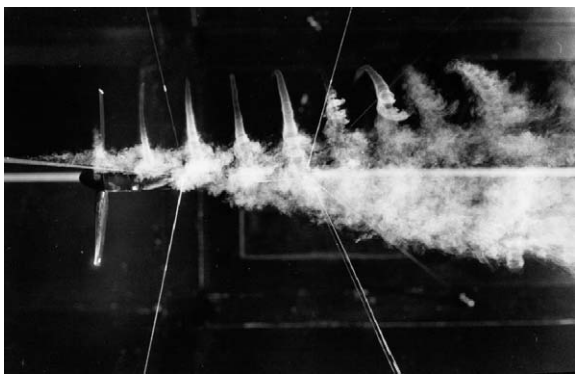

Fig. 5. Flow visualisation with smoke, revealing smoke trails being 'sucked' into the vortex spirals (from [16]).

the two blades at different pitch angles, the two tip vortex spirals appear to have each their own path and transport velocity. After a few revolutions, one tip vortex catches up with the other and the two spirals

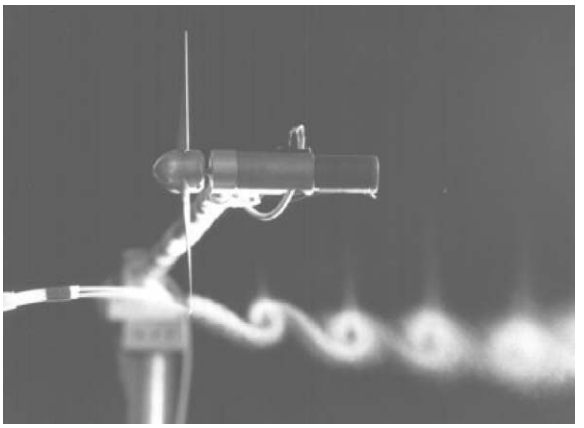

Fig. 6. Flow visualisation experiment at TUDelft, showing two revolutions of tip vortices for a two-bladed rotor (from [24]).

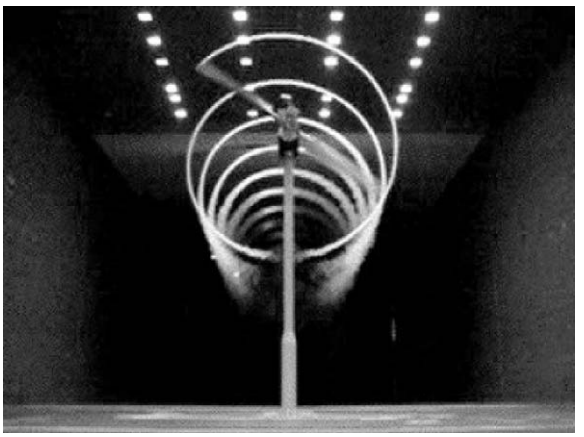

Fig. 7. Flow visualisation with smoke grenade in tip, revealing smoke trails for the NREL turbine in the NASA-Ames wind tunnel (from Hand [13]).

become entwined into one. Unluckily, there are no recordings of this phenomena.

During the full scale experiment of NREL at the NASA-Ames wind tunnel, also flow visualisation were performed with smoke emanated from the tip (see Fig. 7). With this kind of smoke trails, it is not clear whether the smoke trail reveals the path of the tip vortex or some streamline in the tip region. Also, these experiments have been performed at very low thrust values, so there is hardly any wake expansion.

A different set-up to visually reveal some properties of the wake was utilised by Shimizu [12] with a tufts screen (see Fig. 8).

Visualisation of the flow pattern over the blade is mostly done with tufts. This is a well-known technique and applied to both indoor and field experiments (see [16–20,25–27]), however since blade aerodynamics is

a related subject, but beyond the scope of this article, only one mention will be made of such an application.

Vermeer [28] has tried to correlate the flow pattern visualised by tufts on the blade with near wake velocity patterns, in order to get a better understanding of how to interpret velocity signals. Especially, the location of stall on the blade was the focus of this experiment. The hot-wire probe was located at 65% radius and recorded velocity traces over ten revolutions. There appeared to be a great difference between attached flow (Fig. 9) and stalled flow (Fig. 10). In attached flow, the velocity changes associated with the blade passages (at 90° and 270° azimuth angle) are steady and the regions associated with the remains of the boundary layer (just after 0° and 180° azimuth angle) are relatively small, in contrast to stalled flow, where the blade passages cause changing magnitude (because of fluctuating circulation) and the remains of the boundary layer is wide and dominated by erratic fluctuations.

A novel technique of blade flow visualisation has been devised by Corten [29–32] in the form of what he has entitled stall-flags. The operational principle of the stall-flags is shown in Figs. 11 and 12. The stall-flag basically consists of a hinged flap and a retroreflector, fitted on a sticker. These stickers have such a size that a few hundred can be positioned on a full-scale rotor blade. When the flow over the rotor blade is non-stalled, the flap covers the reflector, where-as in stalled conditions, the reflector will be uncovered.

Stall flags are suitable of surveying the stall behaviour of full scale wind turbines on location. By installing a powerful lightsource in the field (up to 500 m downstream of the turbine), the whole rotor area can be illuminated, revealing all visible reflectors (see Fig. 13). The stalling behaviour is recorded by a digital video camera. Subsequently, the video frames are fed into the computer, which can analyse automatically thousands of frames, thanks to the binary character of the stall flag

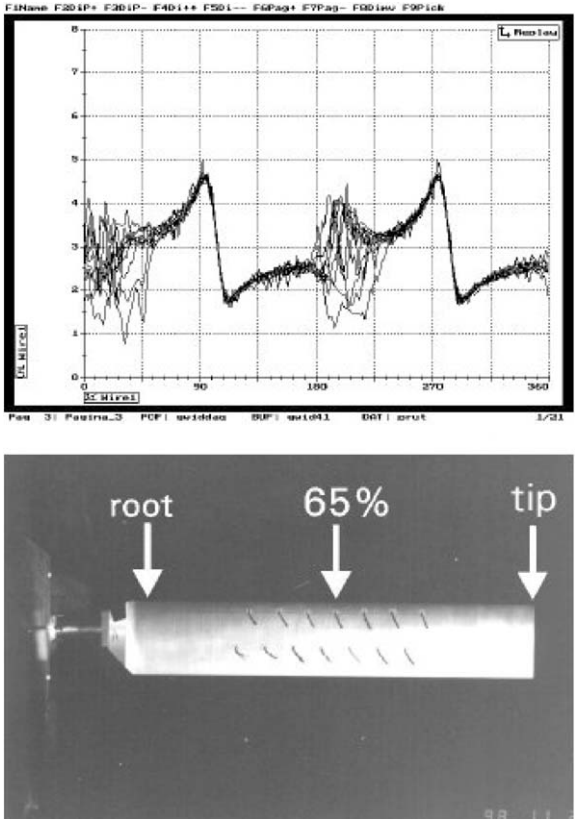

Fig. 9. Correlation between flow condition on the blade on observed velocity pattern in the near wake for non-stalled conditions (from [28]). The blade passages, recorded at 90° and 270° rotor azimuth angle, are steady.

signal. Statistical properties of the very dynamic process of stalling can be derived, so that one can determine whether the behaviour meets the design. If deviations are notified, it can be derived from the data which precise adaptations have to be made. The adaptations are made by applying vortex generators or stall strips or by pitching the blades slightly. Therefore the stall flag technique can be seen as a diagnostic tool, which also can prescribe the cure. An example of such diagnostics was the analysis of the double stall problem, see [32].

As easy as it is to visualise the tip vortex, so hard it is to do the same for the root vortex. Vermeer has tried to visualise the root vortex of the TUDelft rotor model (see [33]). In a total length of half an hour video material (at 25 frames/s), it is possible to locate a few frames on which a clear root vortex is visible. This has several causes: the root vortex is weaker than the tip vortex, the attachment of the root of the blade to the hub and the hub itself prevents a distinct vortex to be formed. As it is hard to visualise the root vortex, getting experimental data will be extremely difficult. This is regrettable,

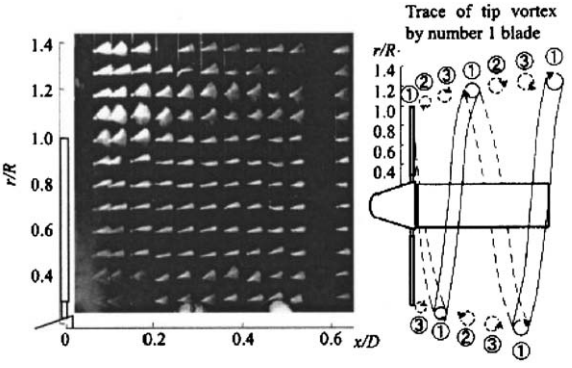

Fig. 8. Flow visualisation by tufted grid method (from Shimizu [12]).

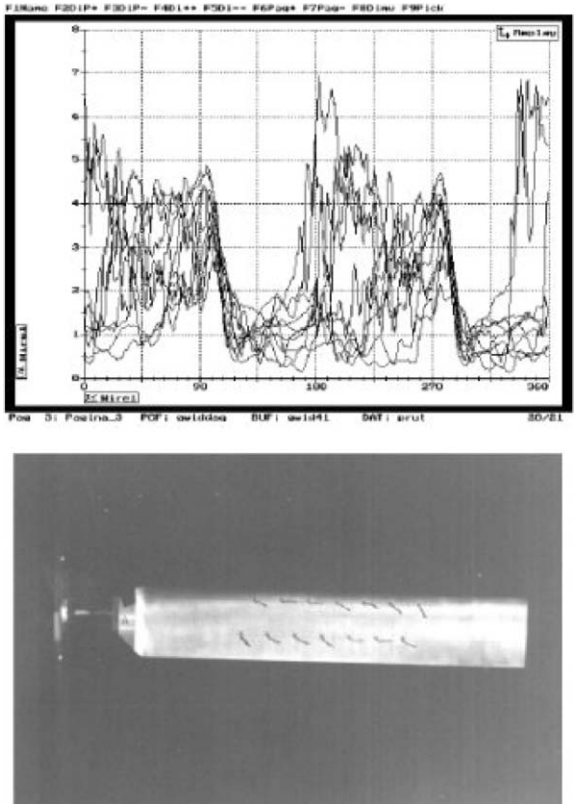

Fig. 10. Correlation between flow condition on the blade on observed velocity pattern in the near wake for stalled conditions (from [28]). The blade passages, recorded at 90° and 270° rotor azimuth angle, show changing magnitude.

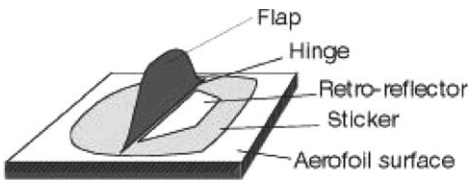

Fig. 11. The stall flag, consisting of a hinged flap and a reflector (from [32], © Nature, with permission).

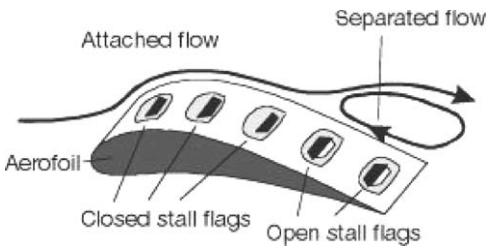

Fig. 12. Stall flags, showing the separated-flow area on an aerofoil (from [32], © Nature, with permission).

Fig. 13. Recording of stall-flag signals from the NEG Micon turbine in California (from [32], © Nature, with permission).

because calculations have shown that including or excluding the root vortex does make a lot of difference, especially under yawed conditions.

3.3. Averaged data

Averaged data dealing with velocity distribution in the wake is mostly used for attempts to analyse power and thrust, which are the global properties of a wind turbine, and do not reveal much about the physical process of power extraction. The experiments have mostly been carried out in the early years of wind turbine research (up until 1983), with modest equipment (Pitot tubes and pressure sensors), see [10,16,17,34–38]. Most data are shown at radius scale, including the rotor model axis area, e.g. see Fig. 14. This is rather directed towards wind farm research, but clearly shows the path towards near wake research in which detailed data is related to its spanwise location.

Wind profiles are also measured in non-uniform flowfields (see [36] and Fig. 15) and even in atmospheric boundary layers (see [39]).

3.4. Detailed data

Detailed wake data is acquired to provide a better understanding of the underlying physics of wind turbine aerodynamics. The experiments with detailed data are done after 1982, when more sophisticated equipment was employed. This section will be divided into two parts, one concerning velocity measurements and one concerning tip vortex properties. The experimental equipment has changed to fast response pressure sensors, hot wires (HW), laser doppler (LDV) and as a latest promising development particle image velocimetry

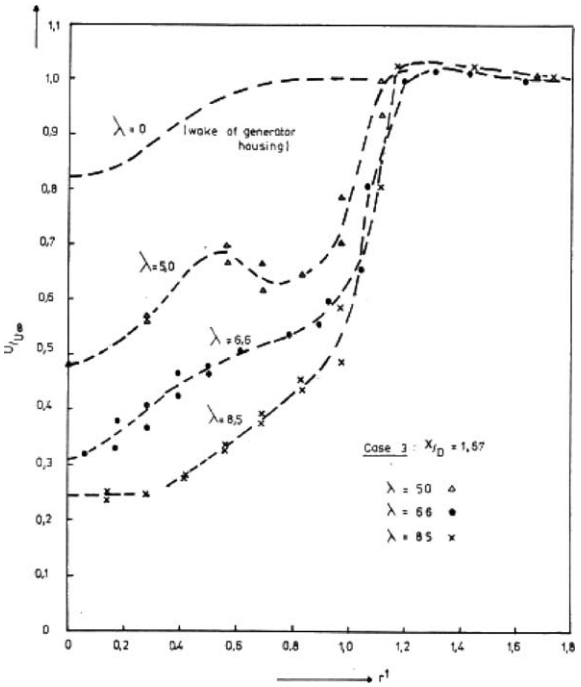

Fig. 14. Cross wind profiles, showing the velocity deficit, as a function of radial distance, with the tip-speed ratio as a parameter, for axial distance $x/D = 1.67$ (from [34]).

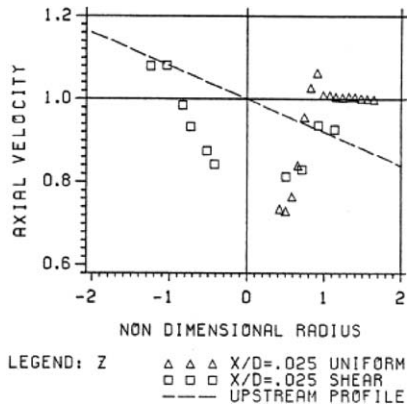

Fig. 15. Axial velocity profiles, showing the velocity deficit, at axial distance $X/D = 0.025$, for both uniform and shear flowcases together with the upstream shear profile (from [36]).

(PIV). Only a few elaborate studies are known [24,40–51]. The rest seems incidental experiments.

The study from Whale was one of the first to apply PIV to wind turbine wakes. In his case, this was done in a water tank. The major drawback here was the Reynolds number, which was very low (from 6400 to 16,000). Despite of this disadvantage, this study comprises both experiments and analysis by an advanced vortex lattice method.

The study from Ebert is very elaborate and has put a strong accent on the repeatability of the data (many runs were re-done when strict criteria on e.g. wind tunnel velocity steadiness over a run were not met), but suffers from a major drawback: the diameter of the rotor model is the same as the "diameter" of the octagonal tunnel.

In Fisichella's case, a lot of experimental data is acquired (and reported) for a rotor operated in 1, 2 or 3 bladed mode. Also, flow visualisation was done, but mostly at off-design conditions (low and high tip-speed ratios). Although the thesis of Fisichella gives a thorough overview of the research area, the analysis part is a little underexposed in his thesis.

The most comprehensive study has been carried out by Vermeer (for an overview, see [24]). The study started with measuring the global parameters of the rotor model and then advanced to cover many topics related to the near wake: detailed wake velocities, wake expansion, tip vortex strength and tip vortex propagation speed. Although the measurement sessions date from the early 1990s, there is still a lot of data-mining to be done (see next section).

3.4.1. Velocities

Detailed velocity measurements have been performed at numerous places with numerous different models in the same number of different tunnels [11,15,40–58]. Most important finding in the detailed velocity measurements in the near wake is the revelation of the passage of the rotor blades. This is shown by Tsutsui [52] with LDV (even in the rotor plane) (see Fig. 16), by Guj [58] upwind of a single blade turbine (see Fig. 17), by Ebert [48] (see Fig. 18), Fisichella [51] and by Vermeer [57,24] (see Fig. 19).

Especially at TUDelft, a lot of work has been done on trying to calculate the local bound vorticity on the blade from this very distinct velocity pattern (see [57]), but also in some other references, a comparison is made between experimental data and various calculational methods. In all comparison, attempts are made to find the match between the fluctuation related to the blade passage with the circulation as close as possible. But a recent study has shown that this approach does not give a good estimation for the bound circulation (see [59]). During this study, an analysis model, as opposed to a prediction model, was developed. This model is based upon the vortex line method (and Biot–Savart's law) and 'fed' with as many experimental data as present. The vortex distribution over the blade in radial direction is represented by a set of orthogonal functions. By using the wake geometry, as deduced from the measurements, a set of equations can be build to express the wake velocities. Because the wake velocities are measured at several axial and radial positions and sampled at 0.5°

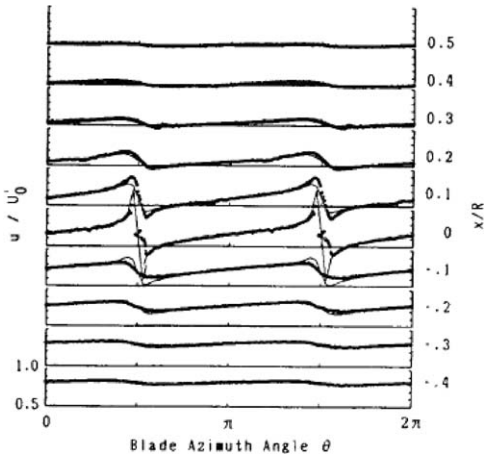

Fig. 16. Axial velocity component (at $r/R = 0.7$) as a function of rotor azimuth angle for several axial distances, both upstream and downstream of the rotor (from [52]). Blade passages are shown at $\frac{1}{2}\pi$ and $\frac{3}{2}\pi$ blade azimuth angle.

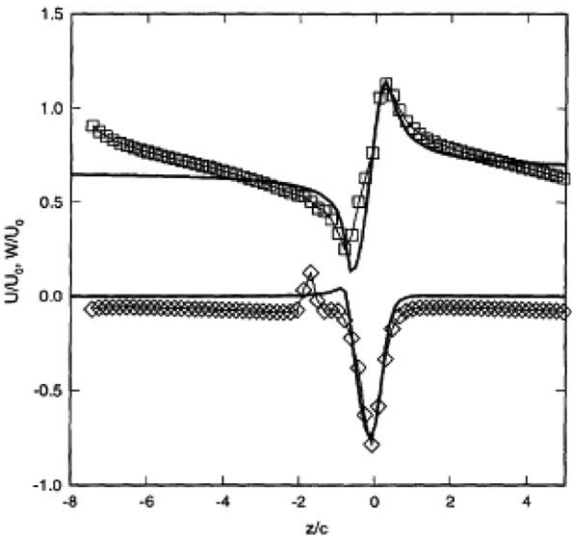

Fig. 18. Comparison of axial (top) and tangential (bottom) velocity patterns occurring at a blade passage (from [48]).

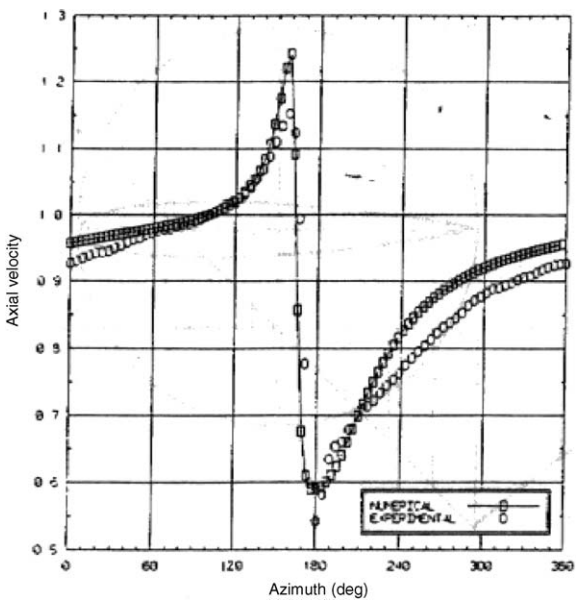

Fig. 17. Axial velocity in near wake, showing blade passage at 180°, as a function of rotor azimuth angle, for a single bladed rotor model (from [58]).

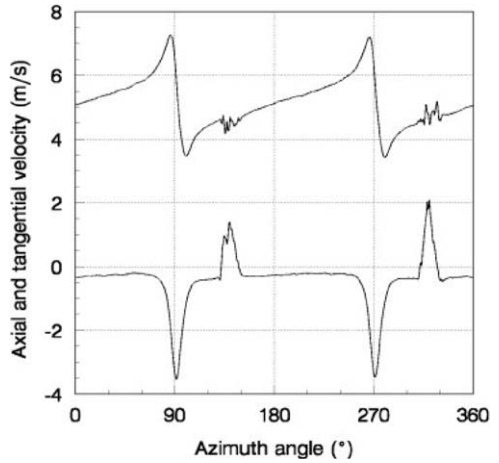

Fig. 19. Measured axial (top) and tangential (bottom) velocity components as a function of rotor azimuth angle (from [24]). The blades pass at 90° and 270° azimuth angle.

azimuth angle, a highly overdetermined set of equations is derived. By solving these equations with a least squares method, the bound circulation can be calculated, and from this distribution the wake velocities can be compared with the measured ones (see Fig. 20).

One of the major findings was that the velocity fluctuation caused by the blade passages can only partially be attributed to the bound vorticity on the blade, but when the measurement position is close to the rotor blade, also the vorticity distribution over the thickness of the blade has to be accounted for. A simulation was done to compare a single line vortex (as used in the study), with a vortex panel method (XFOIL, see [60]) with a distribution of vortices over the contour of the aerofoil, see Fig. 21. The vorticity distribution results in a different velocity fluctuation and the difference resembles the one from the analysis model, see Figs. 22 and 20.

3.4.2. Tip vortex properties

Besides wake velocities, also the properties of the tip vortices are worthwhile to investigate, because they

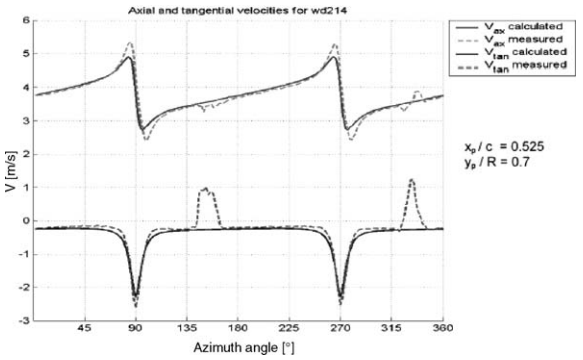

Fig. 20. Measured axial (top) and tangential (bottom) velocities as a function of rotor azimuth angle, compared to calculated velocities (from [59]).

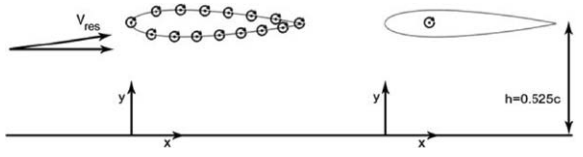

Fig. 21. Modelling of an aerofoil using a vortex distribution over its profile and a single vortex at its quarter chord point (from [59]).

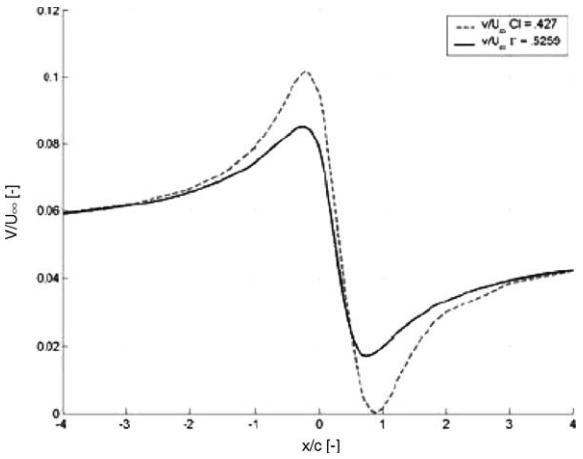

Fig. 22. Induced velocity in the near wake by a model with vortex distribution over its profile, compared to a single vortex model, see Fig. 21 (from [59]).

likewise determine the physical behaviour of the wind turbine rotor as a whole. In this respect, the interesting properties are: wake expansion (as defined by the tip vortex path), vortex spiral twist angle and also the strength of the tip vortex spiral itself. Experiments focussed on this particular area have been carried out by Vermeer [61–64], Whale et al. [45], Grant [65] and Fisichella [51].

In a series of short experiments, the above mentioned properties have been investigated by Vermeer. At first, the wake expansion was measured by locating the path of the tip vortex. This appeared to be relatively easy, because the passage of the tip vortex core along the hot-wire gives a very distinct signal, see Fig. 23.

Next a similar approach from reducing the bound vorticity has been applied to the free tip vortex in order to determine its strength: when traversing from the passage of the tip vortex further outward in radial direction, the influence of the tip vortex diminishes, see Fig. 24. From this decrease, the strength of the tip vortex can be estimated, see Fig. 25.

Vermeer [63] also did experiments on the transport velocity of the tip vortex. In a very basic way, this transport velocity was measured by taking the time the tip vortex needs to travel a certain distance, by making axial traverses with a hot-wire. Because of the use of these hot-wires, also the local flow velocity was recorded. It appeared that the propagation speed of the tip vortex spiral was lower than the local flow velocity. This can be understood by thinking of the self-induced propagation speed of a vortex ring in still air.

Whale has studied the tip vortex using PIV in a watertank and has made comparison with a vortex lattice method, see Fig. 26. Qualitative agreement is shown for the shape of the wake boundary, including downstream wake contraction, and even at the low Reynolds numbers (6400 to 16,000), quantitative agreement is shown for the tip vortex pitch.

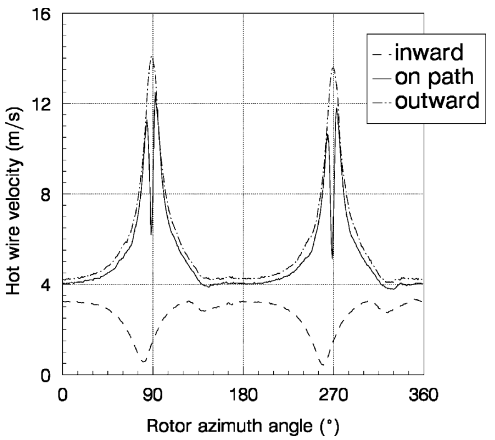

Fig. 23. Typical velocity signal when traversing over the wake boundary to detect vortex path (from [61]). The axial velocity is shown as function of rotor azimuth angle, with the tip vortex occurrences at 90° and 270°. Three radial positions are given: inside and outside of the vortex path and exactly on the vortex path, with the dip in velocity indicating the passage of the vortex core.

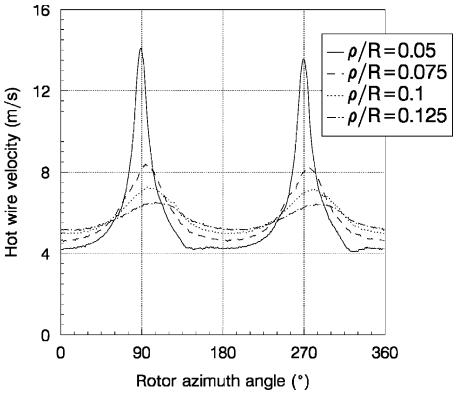

Fig. 24. Azimuthal velocity plot outside the wake boundary, showing the passage of the tip vortices at 90° and 270° azimuth angle (from [62]). The parameter ρ is the radial coordinate measured from the tip radius. The velocity peak associated with the passage of the tip vortex decreases with increasing radial distance.

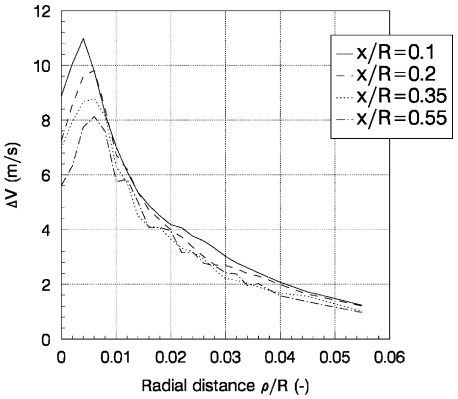

Fig. 25. The value of the peak velocity associated with the passage of the tip vortex (see Fig. 24), as a function of the radial distance from the rotor tip, for several axial distances (from [62]).

Grant [65] has used Laser sheet visualisation to measure the behaviour of the vorticity trailing from the turbine blade tips and the effect of wall interference on wake development, for various conditions of turbine yaw. Results were compared with a prescribed wake model, see Fig. 27.

4. Near wake computations

Although there exists a large variety of methods for predicting performance and loadings of wind turbines, the only approach used today by wind turbine manufacturers is based on the blade element/momentum

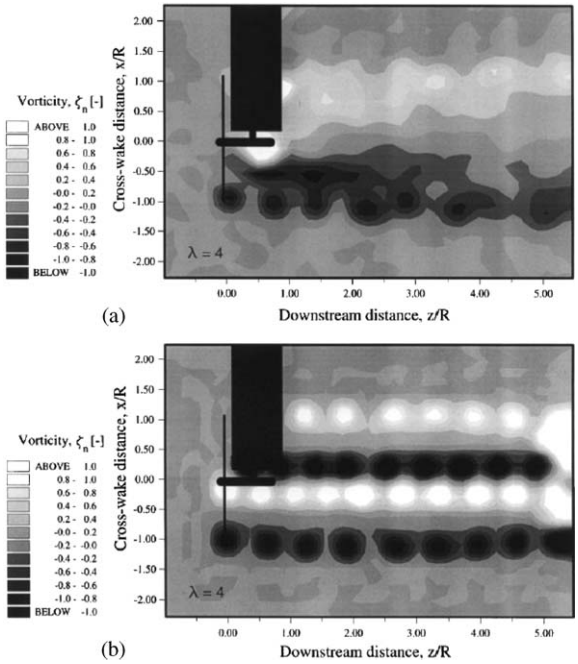

Fig. 26. Comparison of PIV measurements and ROVLM computations of vorticity contour plots of the full wake of a two-bladed flat-plate rotor (from [45]).

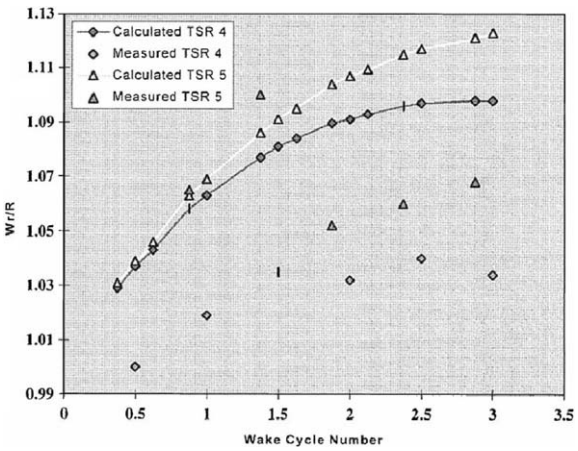

Fig. 27. Predicted and measured wake expansion for tip-speed ratios 4 and 5 in head-on flow (from [65]).

(BEM) theory. A basic assumption in the BEM theory is that the flow takes place in independent stream tubes and that the loading is determined from two-dimensional sectional aerofoil characteristics. The advantage of the model is that it is easy to implement and use on a computer, it contains most of the physics representing rotary aerodynamics, and it has proven to be accurate for the most common flow conditions and rotor

configurations. A drawback of the model is that it, to a large extent, relies on empirical input which is not always available. Even in the simple case of a rotor subject to steady axial inflow, aerofoil characteristics have to be implemented from wind tunnel measurements. The description is further complicated if we look at more realistic operating situations. Wind turbines are subject to atmospheric turbulence, wind shear from the ground effect, wind directions that change both in time and in space, and effects from the wake of neighbouring wind turbines. These effects together form the ordinary operating conditions experienced by the blades. As a consequence, the forces vary in time and space and a dynamical description is an intrinsic part of the aerodynamic analysis.

At high wind velocities, where a large part of the blade operates in deep stall, the power output is extremely difficult to determine within an acceptable accuracy. The most likely explanation for this is that the flow is not adequately modelled by static, two-dimensional aerofoil data. When separation occurs in the boundary layer, outward spanwise flow generated by centrifugal and coriolis pumping tends to decrease the boundary layer thickness, resulting in the lift coefficient being higher than what would be obtained from wind tunnel measurements on a non-rotating blade. Employing a viscous-inviscid interaction technique it has been shown by Sørensen [66] that the maximum lift may increase by more than 30% due to the inclusion of rotational effects. Later experiments of e.g. Butterfield [67], Ronsten [68], and Madsen and Rasmussen [69] have confirmed this result. To take into account the rotational effects, it is common to derive synthesized three-dimensional aerofoil data (see e.g. [70] or Chaviaropoulos and Hansen [71]). If it turns out, however, that stall on a rotating blade inherently is a three-dimensional process, it is doubtful if general values for modifying two-dimensional aerofoil characteristics can be used at high winds. In all cases there is a need to develop three-dimensional models from which parametrical studies can be performed.

When the wind changes direction, misalignment with the rotational axis occurs, resulting in yaw error. This causes periodic variations in the angle of attack and invalidates the assumption of axisymmetric inflow conditions. Furthermore, it gives rise to radial flow components in the boundary layer. Thus, both the aerofoil characteristics and the wake are subject to complicated three-dimensional and unsteady flow behaviour, which only in an approximate way can be implemented in the standard BEM method. To take into account yaw misalignment, modifications to the BEM model have been proposed by e.g. Goankar and Peters [72], Hansen [73], van Bussel [74] and Hasegawa et al. [75]. But, again, a better understanding demands the use of more representative models.

A full description of the global flow field around a wind turbine is in principle possible by solving the Navier–Stokes equations subject to unsteady inflow and rotational effects. In practice, however, the capability of present computer technology limits the number of mesh points to a maximum of about 10 millions, which is not always sufficient for a global description that includes the boundary layer on the rotor as well as and the shed vortices in the wake. As a consequence, various models have been proposed, ranging from models based on potential flow and vortex theory to CFD models based on solving the Reynolds-averaged Navier–Stokes equations.

In the following an overview of computational methods for use in wind turbine aerodynamics will be presented. The intention is not to give here an exhaustive description of numerical techniques. Rather the presentation will concentrate on describing basic features of models pertinent to the aerodynamics of horizontal-axis wind turbines.

4.1. The Navier–Stokes equations

As basic mathematical model we consider the Reynolds-averaged, incompressible Navier–Stokes equations which, with $\vec{V}$ denoting the Reynolds-averaged velocity and P the pressure, in conservative form are written as

$$\frac{\partial \vec{V}}{\partial t} + \nabla \cdot (\vec{V} \otimes \vec{V}) = -\frac{1}{\rho}\nabla P + \nu \nabla \cdot \left[\left(1 + \frac{\nu_t}{\nu}\right)\nabla \vec{V}\right] + \vec{f}, \tag{1}$$

$$\nabla \cdot \vec{V} = 0, \tag{2}$$

where t denotes time, ρ is the density of the fluid and ν is the kinematic viscosity. The Reynolds stresses are modelled by the eddy-viscosity, ν_t, and a body force, $\vec{f}$, is introduced in order to model external force fields, as done in the generalized actuator disc model. These equations constitute three transport equations, which are parabolic in time and elliptic in space, and an equation of continuity stating that the velocity is solenoidal. The main difficulty of this formulation is that the pressure does not appear explicitly in the equation of continuity. The role of the pressure, however, is to ensure the continuity equation be satisfied at every time instant. A way to circumvent this problem is to relate the pressure to the continuity equation by introducing an artificial compressibility term into this (see e.g. [76]). Thus, an artificial transport equation for the pressure is solved along with the three momentum equations, ensuring a solenoidal velocity field when a steady state is achieved. The drawback of this method is that only time-independent problems can be considered. Another approach, the pressure correction method, is to

relate the velocity and pressure fields through the solution of a Poisson equation for the pressure. This is obtained by taking the divergence of the momentum equations, resulting in the following relation:

$$\nabla^2 P = -\rho \nabla \cdot [\nabla \cdot (\vec{V} \otimes \vec{V}) - \nu_t \nabla \vec{V}], \tag{3}$$

which is solved iteratively along with the momentum equations.

As an alternative to the $\vec{V} - P$ formulation of the Navier–Stokes equations, vorticity based models may be employed, see [77,78]. The vorticity, defined as the curl of the time-averaged velocity

$$\vec{\omega} = \nabla \times \vec{V}, \tag{4}$$

may be introduced as primary variable by taking the curl of Eq. (1). This results in the following set of equations:

$$\frac{\partial \vec{\omega}}{\partial t} + \nabla \times (\vec{\omega} \times \vec{V}) = -\nu \nabla^2 \left[\left(1 + \frac{\nu_t}{\nu} \right) \vec{\omega} \right] + \nabla \times \vec{f} + Q_\omega, \tag{5}$$

$$\nabla \times \vec{V} = \vec{\omega}, \quad \nabla \cdot \vec{V} = 0, \tag{6}$$

where Q_ω contains some additional second order terms from the curl operation. The equations can be formulated in various ways. The Cauchy–Riemann part of the equations, Eq. (6), may e.g. be replaced by a set of Poisson equations

$$\nabla^2 \vec{V} = -\nabla \times \vec{\omega}. \tag{7}$$

If we consider Eq. (5) in an arbitrarily moving frame of reference we get

$$\frac{\partial \vec{\omega}^*}{\partial t} + \nabla \times (\vec{\omega}^* \times \vec{V}) = -\nu \nabla^2 \left[\left(1 + \frac{\nu_t}{\nu} \right) \vec{\omega}^* \right] + \nabla \times \vec{f} + Q_\omega, \tag{8}$$

where the vorticity vector $\vec{\omega}^*$ refers to the inertial system, i.e. $\vec{\omega}^* = \vec{\omega} + 2\vec{\Omega}$, with $\vec{\Omega} = (\Omega_x, \Omega_y, \Omega_z)$ denoting the angular velocity of the coordinate system.

The advantage of the vorticity–velocity formulation over that of the primitive variables were discussed by Speziale [79]. To summarize, these are: (1) Non-inertial effects arising from a rotation or translation of the frame of reference to an inertial frame enter the problem only through the initial and boundary conditions, as demonstrated in Eq. (8); (2) A solenoidal velocity field is automatically ensured when solving Eq. (6), thus no pressure–velocity coupling is needed; (3) The relation between velocity and vorticity is linear. The disadvantages, on the other hand, are that the Cauchy–Riemann part of the equations are overdetermined, i.e. contains more equations than unknowns, and when replacing this by Eq. (7), three Poisson equations have to be solved instead of the one for the pressure in the primitive variables formulation. Another drawback of the model is that the vorticity field must satisfy the solenoidal constraint, $\nabla \cdot \vec{\omega} = 0$, which follows directly from Eq. (4). Finally, it should be mentioned that when the formulation is employed to solve flow problems in multiple-connected domains, for each hole in the domain, the equations are subject to the following integral constraint (see e.g. [80])

$$\frac{1}{\rho} \oint_l \nabla P \, \mathrm{d}l = -\oint_l \left[\frac{\partial \vec{V}}{\partial t} + \nabla \cdot (\vec{V} \otimes \vec{V}) \right] \mathrm{d}l + \nu \oint_l \nabla \cdot \left[\left(1 + \frac{\nu_t}{\nu} \right) \nabla \vec{V} \right] \mathrm{d}l, \tag{9}$$

where l is an arbitrary circuit looping the inner body.

In a study by Hansen [81] it was concluded that the vorticity–velocity formulation is not well suited to handle high Reynolds number problems in complicated domains, but is a valuable tool for simulations of basic flow problems in Cartesian or cylindrical coordinates.

4.2. Vortex wake modelling

Vortex wake models denote a class of methods in which the rotor blades and the trailing and shed vortices in the wake are represented by lifting lines or surfaces. At the blades the vortex strength is determined from the bound circulation which is related to the local inflow field. The global flow field is determined from the induction law of Biot–Savart, where the vortex filaments in the wake are convected by superposition of the undisturbed flow and the induced velocity field. The trailing wake is generated by spanwise variations of the bound vorticity along the blade. The shed wake is generated by the temporal variations as the blade rotate. Assuming that the flow in the region outside the trailing and shed vortices is curl-free, the overall flow field can be represented by the Biot–Savart law. This is most easily shown by decomposing the velocity in a solenoidal part and a rotational part, using Helmholtz decomposition:

$$\vec{V} = \nabla \times \vec{A} + \nabla \Phi, \tag{10}$$

where $(\vec{A})$ is a vector potential and Φ a scalar potential.

The vector potential automatically satisfies the continuity equation, Eq. (2), and from the definition of vorticity, Eq. (4), we get

$$\nabla^2 \vec{A} = -\vec{\omega}. \tag{11}$$

In the absence of boundaries, this can be expressed as an integral relation,

$$\vec{A}(\vec{X}) = \frac{1}{4\pi} \int \frac{\vec{\omega}'}{|\vec{X} - \vec{X}'|} \mathrm{d}V_{\mathrm{ol}}, \tag{12}$$

where $\vec{X}$ denotes the point where the potential is computed and the integration is taken over the region where the vorticity is non-zero, designated by V_{ol}. From the definition, Eq. (10), the resulting velocity field is

obtained by

$$\vec{V}(\vec{X}) = -\frac{1}{4\pi}\int \frac{(\vec{X}-\vec{X}')\times\vec{\omega}'}{|\vec{X}-\vec{X}'|^3}\,\mathrm{d}V_{\mathrm{ol}}, \tag{13}$$

which is the most usual form of the Biot–Savart law.

In its simplest form the wake is prescribed as a hub vortex plus a spiralling tip vortex or as a series of ring vortices. In this case the vortex system is assumed to consists of a number of line vortices with vorticity distribution

$$\omega(\vec{X}) = \Gamma\delta(\vec{X}-\vec{X}'), \tag{14}$$

where Γ is the circulation, δ is the Dirac delta function and $\vec{X}'$ is the curve defining the location of the vortex lines. Combining this with Eq. (13) results in

$$\vec{V}(\vec{X}) = -\frac{1}{4\pi}\int_S \Gamma\frac{(\vec{X}-\vec{X}')}{|\vec{X}-\vec{X}'|^3}\times\frac{\partial\vec{X}'}{\partial s'}\,\mathrm{d}s', \tag{15}$$

where S is the curve defining the vortex line and s' is the parametric variable along the curve. Utilizing Eq. (15), simple vortex models can be derived to compute quite general flow fields about wind turbine rotors. In a study of Miller [82], a system of vortex rings was used to compute the flow past a heavily loaded wind turbine. It is remarkable that in spite of the simplicity of the model, it was possible to simulate the vortex ring/turbulent wake state with good accuracy, as compared to the empirical correction suggested by Glauert [2]. As a further example, a similar simple vortex model developed by Øye [83] was used to calculate the relation between thrust and induced velocity at the rotor disc of a wind turbine, in order to validate basic features of the streamtube-momentum theory. The model includes effects of wake expansion, and, as in the model of Miller, it simulates a rotor with an infinite number of blades, with the wake being described by vortex rings. From the model it was found that the axial induced velocities at the rotor disc are smaller than those determined from the ordinary streamtube–momentum theory. Based on the results a correction to the momentum method was suggested. Although the correction is small, an important conclusion was that the apparent underestimation of the power coefficient by the momentum method is not primarily caused by its lack of detail regarding the near wake, but is more likely caused by the decay of the far wake. A similar approach has been utilised by Wood and co-workers [84,85].

To compute flows about actual wind turbines it becomes necessary to combine the vortex line model with tabulated two-dimensional aerofoil data. This can be accomplished by representing the spanwise loading on each blade by a series of straight vortex elements located along the quarter chord line. The strength of the vortex elements are determined by employing the Kutta–Joukowsky theorem on the basis of the local aerofoil characteristics. As the loading varies along the span of each blade the value of the bound circulation changes from one filament to next. This is compensated for by introducing trailing vortex filaments whose strengths correspond to the differences in bound circulation between adjacent blade elements. Likewise, shed vortex filaments are generated and convected into the wake whenever the loading undergoes a temporal variation. While vortex models generally provide physically realistic simulations of the wake structure, the quality of the obtained results depends crucially on the input aerofoil data. Indeed, in order to be of practical use, aerofoil data has to be modified with respect to three-dimensional effects and dynamic stall. In particular the American NREL experiment in the wind tunnel at NASA-Ames has demonstrated that, even though two-dimensional aerofoil data exist, input aerofoil data are the main source of uncertainty and errors in load predictions, see [14].

In vortex models, the wake structure can either be prescribed or computed as a part of the overall solution procedure. In a prescribed vortex technique, the position of the vortical elements is specified from measurements or semi-empirical rules. This makes the technique fast to use on a computer, but limits its range of application to more or less well-known steady flow situations. For unsteady flow situations and complicated wake structures free wake analysis becomes necessary. A free wake method is more straightforward to understand and use, as the vortex elements are allowed to convect and deform freely under the action of the velocity field. The advantage of the method lies in its ability to calculate general flow cases, such as yawed wake structures and dynamic inflow. The disadvantage, on the other hand, is that the method is far more computing expensive than the prescribed wake method, since the Biot–Savart law has to be evaluated for each time step taken. Furthermore, free wake vortex methods tend to suffer from stability problems owing to the intrinsic singularity in induced velocities that appears when vortex elements are approaching each other. This can to a certain extent be remedied by introducing a vortex core model in which a cut-off parameter models the inner viscous part of the vortex filament. In recent years much effort in the development of models for helicopter rotor flowfields have been directed towards free-wake modelling using advanced pseudo-implicit relaxation schemes, in order to improve numerical efficiency and accuracy (e.g. [86,87]).

To analyse wakes of horizontal axis wind turbines, prescribed wake models have been employed by e.g. Gould and Fiddes [88], Robison et al. [89], and Coton and Wang [90], and free vortex modelling techniques have been utilised by e.g. Afjeh and Keith [91] and Simoes and Graham [92]. A special version of the free vortex wake methods is the method by Voutsinas [93] in which the wake modelling is taken care of by vortex

particles or vortex blobs. Recently, the model of Coton and co-workers [94] was employed in the NREL blind comparison exercise [14], and the main conclusion from this was that the quality of the input blade sectional aerodynamic data still represent the most central issue to obtaining high-quality predictions.

A generalisation of the vortex method is the so-called *boundary integral equation method* (BIEM), where the rotor blade in a simple vortex method is represented by straight vortex filaments, the BIEM takes into account the actual finite-thickness geometry of the blade. The theoretical background for BIEMs is potential theory where the flow, except at solid surfaces and wakes, is assumed to be irrotational. In such a case the velocity field can be represented by a scalar potential,

$$\vec{V} = \nabla \Phi, \tag{16}$$

where the velocity potential

$$\Phi = \phi_\infty + \phi, \tag{17}$$

is decomposed into a potential ϕ_∞ representing the free stream velocity, and a perturbation potential ϕ that through the continuity equation, Eq. (2), can be expressed as

$$\nabla^2 \phi = \frac{\partial^2 \phi}{\partial x^2} + \frac{\partial^2 \phi}{\partial y^2} + \frac{\partial^2 \phi}{\partial z^2} = 0. \tag{18}$$

Integrating this equation over discontinuity surfaces, here denoted S, Green's theorem yields

$$\phi = -\frac{1}{4\pi}\int_S \sigma \frac{1}{|\vec{X} - \vec{X}'|}\mathrm{d}S - \frac{1}{4\pi}\int_S \mu \frac{\partial}{\partial n}\frac{1}{|\vec{X} - \vec{X}'|}\mathrm{d}S, \tag{19}$$

where n is the coordinate normal to the wall, σ is the source distribution and μ is the doublet distribution. These represent the singularities at the border of the flow domain, i.e. at solid surfaces and wakes. In a rotor computation the blade surface is covered with both sources and doublets while the wake only is represented by doublets (see e.g. [95] or [96]). The circulation of the rotor is obtained as an intrinsic part of the solution by applying the Kutta condition on the trailing edge of the blade. The main advantage of the BIEM is that complex geometries can be treated without any modification of the model. Thus, both the hub and the tower can be modelled as a part of the solution. Furthermore, the method does not depend on aerofoil data and viscous effects can, at least in principle, be included by coupling the method to a viscous solver. Within the field of wind turbine aerodynamics, BIEMs has been applied by e.g. Preuss et al. [97], Arsuffi [98] and Bareiss and Wagner [99]. Up to now, however, only simple flow cases have been considered.

A method in line with the BIEM is the asymptotic acceleration potential method, developed originally for helicopter aerodynamics by van Holten [100] and later developed further to cope with wind turbines by van Bussel [101]. The method is based on solving a Poisson equation for the pressure, assuming small perturbations of the mean flow. The model has been largely used by van Bussel [101] to analyse various phenomena within wind turbine aerodynamics. Computational efficiency and range of application of the method corresponds to what is obtained by prescribed vortex wake models.

4.3. Generalized actuator disc models

In fluid mechanics the actuator disc is defined as a discontinuous surface or line on which surface forces act upon the surrounding flow. In rotary aerodynamics the concept of the actuator disc is not new. Indeed, the actuator disc constitutes the main ingredient in the one-dimensional momentum theory, as formulated by Froude [102], and in the 'classical' BEM method by Glauert [2]. Usually, the actuator disc is employed in combination with a simplified set of equations and its range of applicability is often confused with the particular set of equations considered. In the case of a horizontal axis wind turbine the actuator disc is given as a permeable surface normal to the freestream direction on which an evenly distribution of blade forces acts upon the flow. In its general form the flow field is governed by the unsteady, axisymmetric Euler or Navier–Stokes equations, which means that no physical restrictions need to be imposed on the kinematics of the flow.

The first non-linear actuator disc model for heavily loaded propellers was formulated by Wu [103]. Although no actual calculations were carried out, this work demonstrated the opportunities for employing the actuator disc on complicated configurations as e.g. ducted propellers and propellers with finite hubs. Later improvements, especially on the numerical treatment of the equations, are due to e.g. [104,105], and recently Conway [106,107] has developed further the analytical treatment of the method. In the application of the actuator disc concept for wind turbine aerodynamics, the first non-linear model was suggested by Madsen [108], who developed an actuator cylinder model to describe the flow field about a vertical-axis wind turbine, the Voight–Schneider or Gyro mill. This model has later been adapted to treat horizontal axis wind turbines. A thorough review of 'classical' actuator disc models for rotors in general and wind turbines in particular can be found in the dissertation by van Kuik [109]. Recent developments of the method has mainly been directed towards the use of Navier–Stokes equations.

In helicopter aerodynamics combined Navier–Stokes/actuator disc models have been applied by e.g. Fejtek and Roberts [110] who solved the flow about a helicopter employing a chimera grid technique in

which the rotor was modelled as an actuator disk, and Rajagopalan and Mathur [111] who modelled a helicopter rotor using time-averaged momentum source terms in the momentum equations.

In a numerical actuator disc model, the Navier–Stokes (or Euler) equations, Eqs. (1)–(3) or Eqs. (5)–(7), are typically solved by a second order accurate finite difference/volume scheme, as in a usual CFD computation. However, the geometry of the blades and the viscous flow around the blades are not resolved. Instead the swept surface of the blades is replaced by surface forces that act upon the incoming flow at a rate corresponding to the period-averaged mechanical work that the rotor extracts from the flow.

In the simple case of an actuator disc with constant prescribed loading, various fundamental studies can easily be carried out. Comparisons with experiments have demonstrated that the method works well for axisymmetric flow conditions and can provide useful information regarding basic assumptions underlying the momentum approach [112–115], turbulent wake states occurring for heavily loaded rotors [115,116], and rotors subject to coning [117,118].

When computing the flow past an actual wind turbine, the aerodynamic forces acting on the rotor are determined from two-dimensional aerofoil characteristics, corrected for three-dimensional effects, using a blade-element approach.

In Fig. 28, a cross-sectional element at radius r defines the aerofoil in the (θ, z) plane. Denoting the tangential and axial velocity in the inertial frame of reference as V_θ and V_z, respectively, the local velocity relative to the rotating blade is given as

$$V_{\mathrm{rel}} = (V_\theta - \Omega r, V_z). \tag{20}$$

The angle of attack is defined as

$$\alpha = \phi - \gamma, \tag{21}$$

where $\phi = \tan^{-1}(V_z/(\Omega r - V_\theta))$ is the angle between $\boldsymbol{V}_{\mathrm{rel}}$ and the rotor plane and γ is the local pitch angle. The

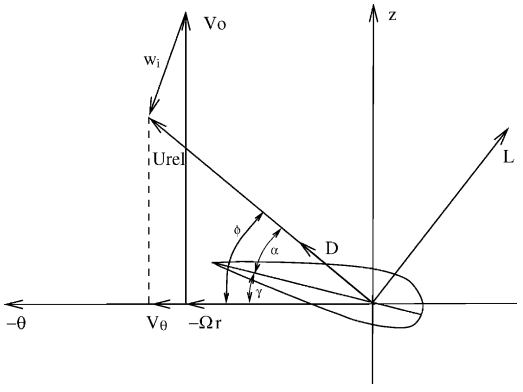

Fig. 28. Cross-sectional aerofoil element (from [119]).

distribution of surface forces, i.e. forces per unit rotor area, is given by the following expression:

$$\boldsymbol{f}_{2D} = \frac{\mathrm{d}\boldsymbol{F}}{\mathrm{d}A} = \frac{1}{2}\rho V_{\mathrm{rel}}^2 cB(C_L\boldsymbol{e}_L + C_D\boldsymbol{e}_D)/(2\pi r), \tag{22}$$

where $C_L = C_L(\alpha, Re)$ and $C_D = C_D(\alpha, Re)$ are the lift and drag coefficients, respectively, c is the chord length, B denotes the number of blades, and $\boldsymbol{e}_L$ and $\boldsymbol{e}_D$ denote the unit vectors in the directions of the lift and the drag, respectively. The lift and drag coefficients are determined from measured or computed two-dimensional aerofoil data that are corrected for three-dimensional effects. There are several reasons why it is necessary to correct the aerofoil data. First, at separation rotational effects limit the growth of the boundary layer, resulting in an increased lift as compared to two-dimensional characteristics. Various correction formulas for rotational effects have been derived using quasi three-dimensional approaches (see e.g. [120,71]). Next, the aerofoil characteristics depend on the aspect ratio of the blade. This is in particular pronounced at high incidences where the finite aspect ratio drag coefficient, C_D, is much smaller than the corresponding one for an infinite blade. As an example, for a flat plate at an incidence $\alpha = 90^\circ$ the drag coefficient $C_D = 2$ for an infinitely long plate, whereas for aspect ratios corresponding to the geometry of a wind turbine blade C_D takes values in the range $1.2 - 1.3$. In [121] it is stated that the normal force from a flat plate is approximately constant for $45^\circ < \alpha < 135^\circ$, indicating that in this range both C_L and C_D have to be reduced equally. Hansen [122] proposes to reduce C_L and C_D by an expression that takes values in range from 0.6 to 1.0, depending on the ratio between the distance to the tip and the local chord length. It should be noticed, however, that this is only a crude guideline and that most aerofoil data for wind turbine use is calibrated against actual performance and load measurements. This also explains why most manufacturers of wind turbine blades are reluctant to change well-tested aerofoil families. Yet a correction concerns unsteady phenomena related to boundary layer separation, referred to as dynamic stall. For aerofoils undergoing large temporal variations of the angle of attack, the dynamic response of the aerodynamic forces exhibits hysteresis that changes the static aerofoil data. Dynamic stall models have been developed and applied on wind turbines by e.g. Øye [123] or Leishman and Beddoes [124].

Computations of actual wind turbines employing numerical actuator disc models in combination with a blade-element approach have been carried out by e.g. Sørensen et al. [112,113] and Masson et al. [125,126] in order to study unsteady phenomena. Wakes from coned rotors have been studied by Madsen and Rasmussen [117], Masson [126], and Mikkelsen et al. [118], rotors operating in enclosures such as wind tunnels or solar

chimneys were computed by Phillips and Schaffarczyk [127], and Mikkelsen and Sørensen [128], and approximate models for yaw have been implemented by Mikkelsen and Sørensen [129] and Masson [126]. Finally, Masson and colleagues have devised techniques for employing their actuator disc model to study the wake interaction in wind farms and the influence of thermal stratification in the atmospheric boundary layer [126,130].

To demonstrate which kind of results can be achieved using an numerical axisymmetric actuator disc model, in Figs. 29 and 30 we show computed stream lines for the flow field about the Tjæreborg wind turbine at two different wind speeds. Noteworthy is the details of unsteady flow behaviour that can be obtained at small wind velocities. In fact, the streamline shown in Fig. 29 corresponds to the turbulent wake state. A main feature of the numerical actuator disc technique is the possibility of predicting transient and unsteady flow behaviour. For wind turbines unsteady effects occurs when the wind changes speed or direction, or when the rotor is subject to blade pitching actions.

This is shown in Fig. 31 where measured and computed time histories of the flapping moment of the Tjæreborg machine are compared for a case in which the pitch angle was changed in a sequence going from 0° to 2° and then back to 0°, with the value of 2° fixed in 30 s. In the calculations the pitch angle was changed instantaneously, therefore a slight difference between the two curves occurs in the initial and the final stage of the sequence. The overall behaviour of the calculations, however, is seen to be in excellent agreement with measured data.

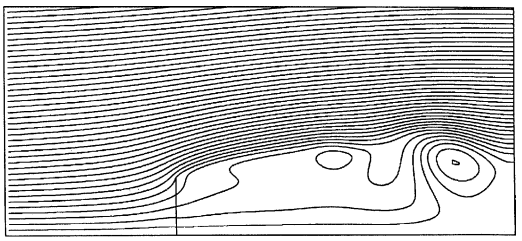

Fig. 29. Flow field about the Tjæreborg wind turbine at a wind speed of 6.5 m/s (from [113]).

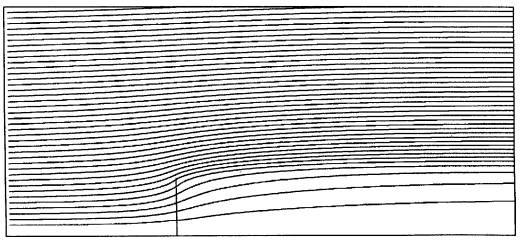

Fig. 30. Flow field about the Tjæreborg wind turbine at a wind speed of 10 m/s (from [113]).

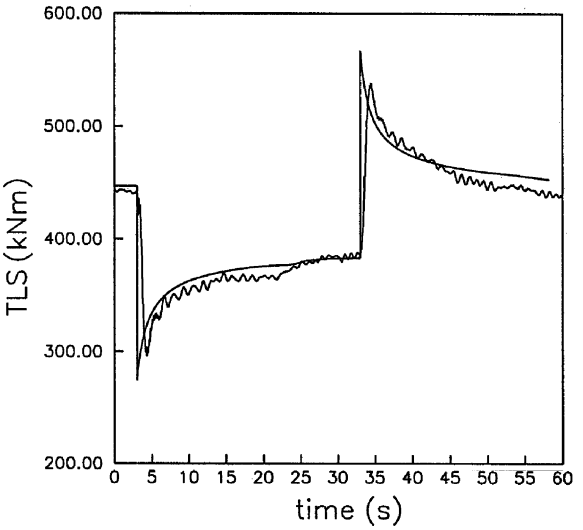

Fig. 31. Transient behaviour of the flapping moment for the Tjæreborg wind turbine subjected to instantaneous blade pitch changes (from [113]).

The main limitation of the axisymmetric assumption is that the forces are distributed evenly along the actuator disk, hence the influence of the blades is taken as an integrated quantity in the azimuthal direction. To overcome this limitation, an extended three-dimensional actuator disc model has recently been developed by Sørensen and Shen [119]. The model combines a three-dimensional Navier–Stokes solver with a technique in which body forces are distributed radially along each of the rotor blades. Thus, the kinematics of the wake is determined by a full three-dimensional Navier–Stokes simulation whereas the influence of the rotating blades on the flow field is included using tabulated aerofoil data to represent the loading on each blade. As in the axisymmetric model, aerofoil data and subsequent loading are determined iteratively by computing local angles of attack from the movement of the blades and the local flow field. The concept enables one to study in detail the dynamics of the wake and the tip vortices and their influence on the induced velocities in the rotor plane. The main motivation for developing the model is to analyse and verify the validity of the basic assumptions that are employed in the simpler more practical engineering models. In the following, we show some numerical results from computations of a 500 kW Nordtank wind turbine at a wind speed $V_0 = 10$ m/s, corresponding to a tip speed ratio of 5.8.

Fig. 32 depicts iso-vorticity contours illustrating the downstream development of the wake vortices. The bound vorticity of the blades is seen to be shed

downstream from the rotor in individual vortex tubes. These vortices persist about 2 turns after which they diffuse into a continuous vortex sheet.

Fig. 33 shows the distribution of the axial interference factor, in the rotor plane. The three blades are seen as lines with a high density of iso-lines, owing to the large changes in induced velocity that takes place across the blades. The number of iso-lines is 30 and the value between two successive lines is equidistant. The values range from -0.15 to 0.55, with peak values appearing near the mid-section of the blades (with a positive value on one side of the blade and a negative value on the other).

The development of the axial velocity distribution in the wake is depicted in Fig. 34. The velocity distributions are averaged in the azimuthal direction and plotted at axial positions $z/R = 0, 1, 2$ and 3. Outside the wake the value of the axial velocity attains the one of the undisturbed wind. A small overshoot is observed at

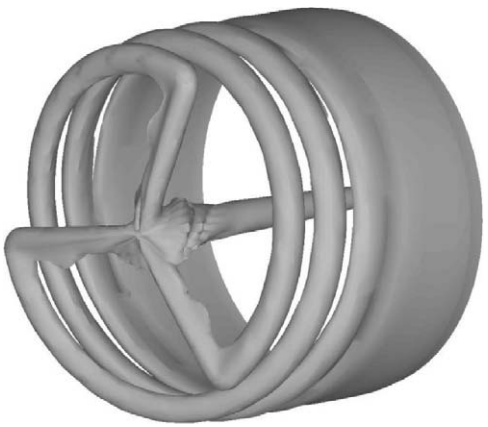

Fig. 32. Computed vorticity field showing the formation of the wake structure about the Tjæreborg wind turbine at a wind speed of 10 m/s (from [119]).

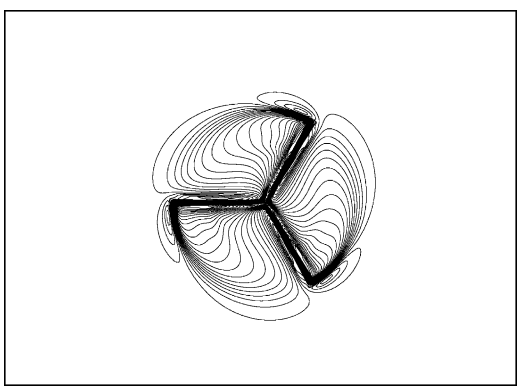

Fig. 33. Distribution of axial interference factor, $a = 1 - Vz/Vo$, in the rotor plane at a wind speed of 10 m/s (from [119]).

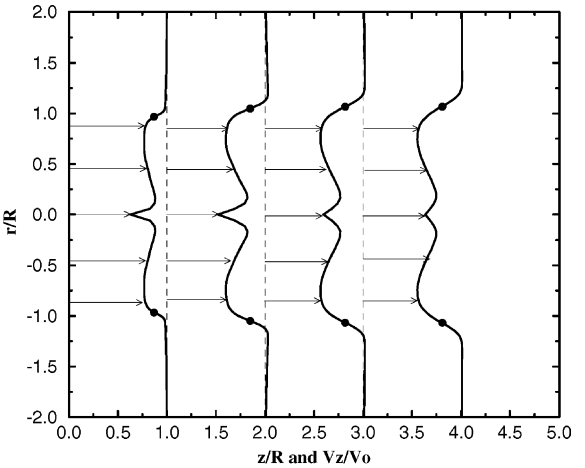

Fig. 34. Distribution of axial velocity at a wind speed of 10 m/s. The core of the tip vortices are marked by • (from [119]).

$z/R = 2$. For all velocity profiles a distinct minimum occurs at $r = 0$. This is caused by the loading on the inner part of the blade that is dominated by large drag forces. The position of the tip vortices is inferred as dots on the velocity profiles. As can be seen they are generally located midway between the wake and the external flow at the position where the gradient of the axial velocity attains its maximum value.

4.4. Navier–Stokes methods

During the past two decades a strong research activity within the aeronautical field has resulted in the development of a series of Computational Fluid Dynamics (CFD) tools based on the solution of the Reynolds-averaged Navier–Stokes (RANS) equations. This research has mostly been related to the aerodynamics of fixed-wing aircraft and helicopters. Some of the experience gained from the aeronautical research institutions has been exploited directly in the development of CFD algorithms for wind turbines. Notably is the development of basic solution algorithms and numerical schemes for solution of the flow equations, grid generation techniques and the modelling of boundary layer turbulence. These elements together form the basis of all CFD codes, of which some already exist as standard commercial software. Looking specifically on the aerodynamics of horizontal axis wind turbines, we find some striking differences as compared to usual aeronautical applications. First, as tip speeds generally never exceeds 100 m/s, the flow around wind turbines is incompressible. Next, the optimal operating condition for a wind turbine always includes stall, with the upper side of the rotor blades being dominated by large areas of flow separation. This is in contrast to the cruise

condition of an aircraft where the flow is largely attached.

The research on CFD in wind turbine aerodynamics has in Europe taken place mostly through the EU-funded collaborate projects VISCWIND [131], VISCEL [132] and the on-going project KNOW-BLADE. The participants in these projects are Risø, DTU, CRES, NTUA, VUB, FFA and DLR, who all have vast experience in developing Navier–Stokes codes. Results from the projects have been reported in e.g. [132–137]. In the US, three-dimensional computations of wind turbine rotors employing Reynolds-averaged Navier–Stokes equations have been carried out by Duque et al. [138,139] and by Xu and Sankar [140,141], who utilised a hybrid Navier–Stokes/full-potential/free wake method in order to reduce computing time.

Recently, the American NREL experiment at NASA-Ames [142] and the accompanying NREL/NWTC Aerodynamics Blind Comparison test [14] have given a lot of new insight into wind turbine aerodynamics and revealed serious shortcomings in present day wind turbine aerodynamics prediction tools. First, computations of the performance characteristics of the rotor by methods based on blade element techniques were found to be extremely sensitive to the input blade section aerodynamic data [94,143]. Indeed, predicted values of the distribution of the normal force coefficient deviated from measurements by as much as 50%. Even at low angles of attack, model predictions differed from measured data by 15–20% [14]. Next, the computations based on Navier–Stokes equations convincingly showed that CFD has matured to become a tool for predicting and understanding the flow physics of modern wind turbine rotors. The Navier–Stokes computations by Sørensen et al. [144] generally exhibited very good agreement with the measurements, except at a wind speed of 10 m/s. At this particular wind speed, onset of flow separation is taking place. Hence, it is likely that the introduction of a more physically consistent turbulence modelling and the inclusion of a laminar/turbulent transition model will improve the quality of the results. In the following we give a short description of basic elements and research areas that generally are acknowledged to be of importance for CFD solutions of wind turbine rotors.

4.4.1. Turbulence modelling

To model the Reynolds stresses various turbulence models are available, ranging from simple algebraic zero-equation models to two-equation transport models and system of transport equations for the Reynolds stresses. The turbulence modelling in itself has been an important subject for many years and the research activities within the field will probably continue for the next many years to come. Along with laminar–turbulent transition, turbulence modelling constitutes the most critical part of the flow modelling, as they do not have a universal validity, and for most practical applications, various parameters have to be calibrated to empirical data. Some of the most popular models are still the Baldwin–Lomax zero-equation model [145] and the two-equation k–ε model [146], although they exhibit problems in reproducing correctly stall characteristics of aerofoils and rotor blades (see e.g. [147,148]). In the past years refined one- and two-equation turbulence models have been developed to cope with specific flow features. In particular the k–ωSST model developed by Menter [149] has shown its capability to cope with attached and lightly separated aerofoil flows, and today this model is widely used for wind turbine computations [144]. As an alternative to the Reynolds-averaged methodology large eddy simulation (LES) techniques have been widely explored in the past years. Although LES gives a better physical representation of the eddy dynamics in separated flows, it is still limited to flow problems at moderate Reynolds numbers. As the RANS equations fail to simulate massive separation, even when simulations are performed in a time-true sense, and large eddy simulations (LES) are unaffordable, hybrid LES/RANS approaches, such as detached eddy simulation (DES), represent an attractive compromise between computing costs and accuracy. The idea behind hybrid approaches is to combine fine-tuned RANS technology in the boundary layers, and the simple power of LES in the separated regions, see [150]. In the RANS regions, the turbulence model has full control over the solution through the eddy-viscosity based closure. In the LES region, little control is left to the model, the larger eddies are resolved both in space and time, and grid refinement directly expands the range of scales in the solution. This reduces considerably the computing costs as compared to a full blown LES. The DES technique has recently been applied on the NREL Phase VI wind turbine blade under parked conditions by Johansen et al. [151].

4.4.2. Laminar–turbulent transition

Most computations of flows around rotor blades are carried out assuming that the boundary layer is fully turbulent everywhere. However, recent computational results indicate that correct treatment of flow transition is important for capturing the flow physics of aerofoils and rotor blades during stall and post-stall. There are at least two different forms of transition. If the incoming flow is largely laminar, natural transition is encountered, whereas for highly turbulent incoming flow or flow over rough surfaces, such as often found in wind engineering, the so-called *bypass* transition occurs. To predict free transition, several engineering methods based on linear stability analysis may be utilised. These range from empirical one-step methods, such as the Michel criterion [152], to methods based on solution to the Orr–Sommerfeldt equations, such as the e^n database method

of Stock and Degenhart [153]. In principle a transition prediction can take place by solving the RANS along with the Orr–Sommerfeldt equations. However, this has shown to be difficult and not very robust. Hence, most efforts have been directed towards the use of integral boundary layer methods to obtain integral boundary layer parameters, such as momentum thickness and shape parameter [137]. These are subsequently used as input to the transition model. For bypass transition, only empirical methods are presently available. Such methods rely entirely on experimental data and for bypass transition on aerodynamic configurations the body of experimental knowledge is very limited.

Within the field of wind turbine aerodynamics, transition models have for two-dimensional aerofoils been examined by Johansen and Sørensen [154], Brodeur and van Dam [155], Xu and Sankar [141], and Michelsen and Sørensen [137]. By Johansen and Sørensen [154], it was clearly demonstrated that transition prediction can be of utmost importance. For the flow past a FX 66-196 VI aerofoil, an underprediction of the lift coefficient of about 20% was obtained when assuming fully turbulent flow, whereas the use of a database method for transition prediction resulted in predictions within 1% up to stall and a small overprediction of maximum lift of about 4%.

In three dimensions transition predictions involve a number of additional complications that still remains unsolved. The determination of the stagnation point is not obvious, since it forms a line with an a priori unknown position. The boundary layer equations are more complex and involves cross-flow effects. Further, they need to be integrated along the flow on the edge of the boundary layer.

5. Far wake experiments

The far wake is the region located downstream of the near wake previously studied. As explained before, in the near wake region, immediately downstream of the rotor, vortex sheets, associated with the radial variation in circulation along the blades, are shed from their trailing edge, and roll up in a short downstream distance forming tip vortices that describe helical trajectories, as can be seen in Figs. 4–8 and 32. When the inclination angle of the helix is small enough, the layer, in which the tip vortices are located, can be interpreted as a cylindrical shear layer which separates the slow moving fluid in the wake from that on the outside. Because of turbulent diffusion, the thickness of the shear layer increases with downstream distance. Most of the turbulence that makes the wake diffuse is, at this stage, created by the shear in the wake, mainly in the shear layer. However, the shear in the external atmospheric flow also plays an important role, at least in the redistribution of the generated turbulence. At a certain distance downstream (about two to five diameters), the shear layer reaches the wake axis. This marks the end of the near wake region. After the near wake region, there is a transition region leading to the far wake region, where the wake is completely developed and, in the hypothetical absence of ambient shear flow, it may be assumed that the perturbation profiles of both velocity deficit and turbulence intensity are axisymmetric, and have self-similar distributions in the cross-sections of the wake. This property of self-similarity is the basis of the kinematic models describing wind turbine wakes. However, the presence of the ground and the shear of the ambient flow invalidate the assumption of axial symmetry and, to some extent, the hypothesis of self-similarity.

As already indicated, it is difficult to separate the research work on the near and far wakes. A typical example is shown in Fig. 35 from [156].

This figure represents the turbulent velocity profile in vertical planes at different downstream stages. It can be seen that in the annular shear layer of the near wake there is a peak in turbulence, that is largest in the upper part. Further downstream, the shear layer has diffused, and the ring-like maxima shrinks to a single maximum, that is located above the turbine axis; this upward location is clearly a reminiscent phenomenon of the near wake. The non-symmetric character of the turbulence distribution in the shear layer, is clearly associated to the non-symmetric character of the incident flow, and the maximum of turbulence in the upper part, could no be predicted with an analysis based on axial symmetry. Other aspect to be considered, when relating the far and near wakes, is that what is interpreted as turbulence in Fig. 35, is, at least partially, ordered motion associated to mean vorticity, in the previous analysis. It could be of

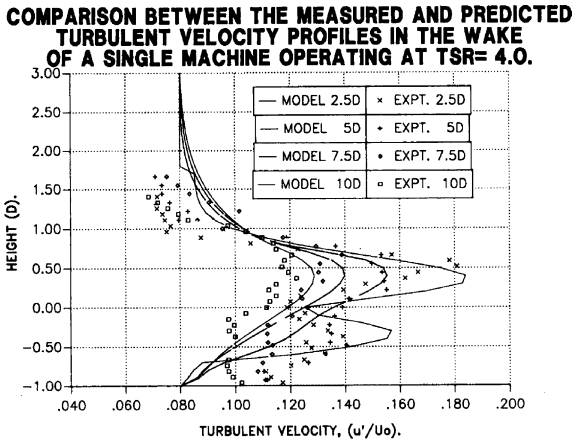

Fig. 35. Vertical turbulent velocity profile at different downstream distances. Comparison of experimental measurements in wind tunnel and model calculations (from [156]).

interest to see how the previous analysis should be modified to take into account the non-symmetric effects, and check, at least qualitatively, if this will result in larger turbulence plus vorticity production in the upper part of the shear layer. As it will be seen in the section on far wake numerics, the analysis made by Smith and Taylor [156], Fig. 35, and those of other authors [157], based on eddy-diffusivity models, and parabolic approximations, are comparatively easy, and even Crespo and Hernández [157] were able to give a theoretical estimation of the near wake peak; however, an analysis based on solving the fully elliptic equations, with complicated non-symmetric boundary conditions could be a formidable problem.

In this section, far wake measurements of both wind tunnel and field experiments will be discussed. A comparison of experimental and numerical results will be made in the following sections. In general, the conditions are better controlled in the wind tunnel experiments and consequently a better agreement with numerical results can be obtained. On the other hand, the reproduction of many aspects of the real situation of the atmospheric and environmental conditions is not easy in wind tunnel experiments, and the size of the models should be small enough to avoid blocking effects. Helmis et al. [158] argue that the length of the near wake region is overestimated in wind tunnel experiments. Högström et al. [159] indicate that wake turbulence intensity may be higher than the corresponding wind tunnel data by a factor of two, whereas velocity deficit is higher in wind tunnel data. A general review of the earlier experimental work on wind wakes prior to 1989 can be found, in [160], and regarding turbulence characteristics in [161].

5.1. Wind tunnel experiments

Most of the wind tunnel experiments were carried out before 1995. They were both for single wakes and for clusters, and were based on model rotors and static simulators. These measurements were on velocity deficits (see Figs. 36 and 37) and on turbulence characteristics (see Fig. 35 from [156]). Vermeulen and Builtjes [162] and Builtjes [163] carried out wind tunnel experiments on static simulators and investigated both velocities and turbulence structure. They found interesting results, confirmed by later research work, such as the saturation of the turbulence, that reaches an equilibrium value within the cluster, after several rows of turbines. They also found that in the wakes there is a shift in the turbulence energy spectrum towards higher frequencies; this effect is confirmed by field experiments. Similar experiments were made by Green [164]. Ross and Ainslie [39] and Ross [165] carried out experiments with rotating models in clusters, that were incorporated to the analysis of Vermeulen and Builtjes [162]; they were able to study the influence of the thrust coefficient of the turbine on the equilibrium value of the added turbulence.

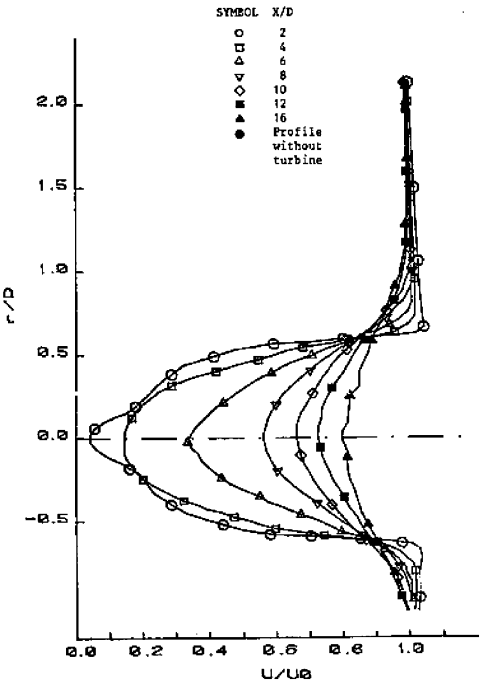

Fig. 36. Mean velocity behind turbine in freestream (from [16]).

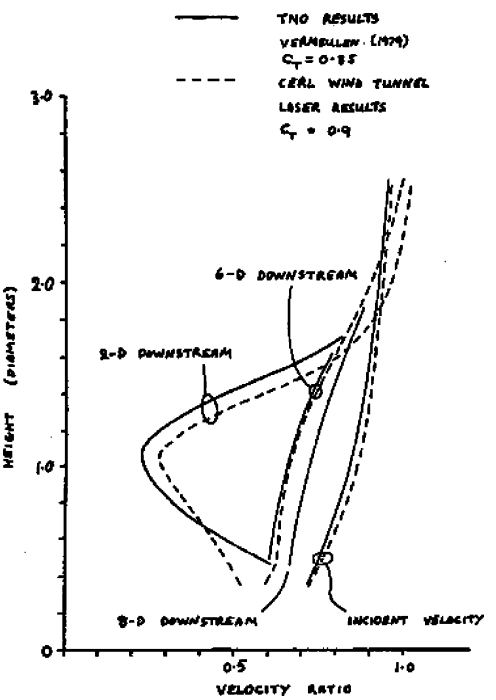

Fig. 37. Velocity deficit in boundary layer (from [39]).

Vermeulen and Builtjes [162] also measured the auto-correlation function, for several locations in the cluster, and compared it to the unperturbed upstream value. They found very similar auto-correlation functions for the perturbed flow, so that there is no difference between the turbulence structure after the first row and after multiple rows. This is probably because the typical size of the auto-correlation for all the perturbed flows is always the rotor diameter.

Several authors studied experimentally the influence of different parameters, such as downstream distance: [166,164,167,39], thrust coefficient of the wind turbine: [168,164,167], ambient turbulence: [168–170] on the added turbulence intensity. Some of these measurements have been gathered by Quarton [161] and Crespo and Hernández [157,171], that have developed analytical correlations to estimate the added turbulence intensity in the far wake, that will be presented later (Eqs. (26) and (28)). The turbulence intensity decreases with downstream distance, and increases with the thrust coefficient, but regarding the dependence with ambient turbulence, the results are not consistent, even qualitatively. In general, it is found that turbulence effects are more persistent, and that the decay of the velocity deficit is more rapid than the decay of turbulence intensity; this is also observed in large field experiments. This result is confirmed by field experiments: Højstrup [172] and Högström et al. [159] found that turbulence effects are noticeable even at 12D (diameters) and 10D downstream, respectively, whereas velocity defects are almost negligible at those distances. The correlations given later will also confirm these tendencies.

Smith [173] and Smith and Taylor [156] performed wind tunnel experiments on two rotating models of 0.27 m diameter, one located directly downstream from the other. The scale was 1/300, and they reproduced the atmospheric surface layer with an equivalent full scale roughness of 0.07 m, and a turbulence intensity of 9%. Mean and turbulent velocity and shear stress profiles were obtained at a number of locations behind the downstream machine. Their measurements were compared with the predictions of a model that is also presented in [156], and obtained a reasonable agreement. Smith and Taylor [156] observed that the maximum turbulence intensity in the far wake is located above the turbine axis, as can be seen in Fig. 35. This is probably because the turbulence in the far wake "remembers" how it was originated in the "near wake". In the near wake, turbulence production is more important in the upper part of the shear layer where the velocity gradients are more intense, and the eddy viscosity of the ambient flow is larger. As can be observed in this and other wind tunnel experiments [156,170,164,174–176] there is a well defined annular peak of turbulence intensity in this cylindrical shear layer, with its highest values in the upper part. This is also observed in field experiments and numerical models [156,177]. Crespo and Hernández [157] gave a theoretical estimation of this peak, and compared it with the previously mentioned experimental results. The added turbulent kinetic energy turned out to be $\Delta k = \Delta u^2/8$, where Δk is the turbulent kinetic energy created in the shear layer and Δu is the velocity deficit in the near wake. Within the same research program as Smith [173], Hassan et al. [176] performed similar experiments, but also included larger wind farms with different lay-outs, some of them with 15 turbines. They were the first ones to measure wind loads in wakes in a wind tunnel. They found a substantial increase in the dynamic loads when the turbines were within the array; that is to be expected because of the higher turbulence; however, they found the surprising result that the loads for some downstream rows are smaller than in upstream rows, where supposedly wake effects are more intense. Another interesting result, also confirmed by field experiments, is that highest loads do not occur when the rotor is on the wake centre, but when is only partially immersed.

A series of well planned experiments were carried out by Talmon [178,167] that used a moving model in a simulated atmospheric boundary layer; he investigated the effect of the tower, nacelle and floor of the wind tunnel on the wake. He found a downshift of the maximum velocity deficit, oppositely to what happens with the maximum turbulence intensity. These experiments have been used by Luken and Vermeulen [179] and Crespo et al. [180] to check the validity of their wake models. In the numerical calculations of Crespo et al. [180], it is shown that this downshift is mainly due to the shear of the incoming flow and the presence of the ground. Comparison of the measurements and model results is shown in Fig. 38.

The superposition of several wakes was studied by Smith and Taylor [156], who found that the wake of the downstream machine recovers more rapidly than the one upstream so that, at the same relative position, the velocity deficit is smaller in the downstream machine wake. This surprising behaviour may be explained by the enhanced momentum diffusion due to the high turbulence levels and shear stress profiles generated by the upstream machine, that leads to a faster recovery in the downstream machine. What is usually found when there is superposition of wakes is that the rate of decrease of wind velocity is smaller after crossing several rows of wind turbines, and tends to reach an equilibrium value, as can be seen in Ross and Ainslie [39], and in field experiments and numerical models that will be examined in the following sections.

The wake behaviour in complex terrain was studied by Taylor and Smith [181] in the wind tunnel. The scale was 1/1000, and the turbine was located at several positions in a flat-topped hill 0.3 m high, and 0.6 m long. A static simulator of 72 mm diameter was used for the

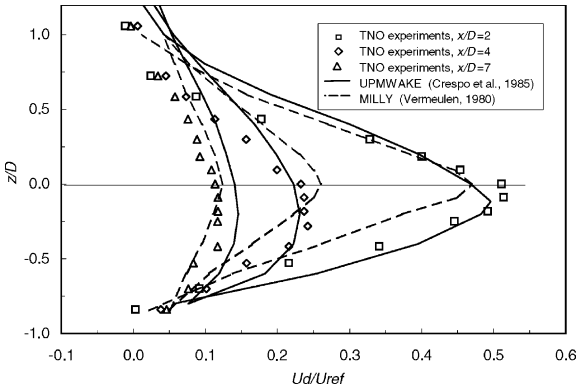

Fig. 38. Vertical distribution of maximum dimensionless velocity deficit along the wake as a function of vertical distance divided by turbine diameter for several downstream sections. Comparison of wind tunnel measurements from Vermeulen [179], and results of wake models, UPMWAKE from Crespo [180], and MILLY from Vermeulen [169].

turbine, its thrust coefficient was 0.78, including the effect of the supporting stem. The incoming flow simulates the logarithmic velocity distribution with a surface roughness of 0.2 mm and a turbulence intensity of 10.5%. Cross hot-wire anemometers were used for the wake measurements, and two mean and turbulent velocities were recorded at each point. They found that the influence of the terrain may be both significant and subtle. When the turbine is in the upstream side of the hill, there is a downwards displacement of the point of maximum velocity deficit, accompanied by a significant broadening of the lower part of the wake. As it was mentioned before this downshift also happens in flat terrain, as can be seen in [179,180], although the effect is more important in this case, probably due to the convergence of the stream lines. They also found that the wake of a turbine located upstream may also inhibit separation in the downstream side of the hill. Stefanatos et al. [182,183] and Helmis et al. [158] also studied the interaction between wake and terrain, both in wind tunnel and in large-scale tests, and from their results obtained some guidelines for the modellisation of this interaction.

Within an European project, Tindal et al. [184] have carried out wind tunnel wake studies, similar to those quoted before [156,176], that have been complemented with numerical calculations and field experiments in the Sexbierum and Nørrekaer Enge II wind farms, that will be described in the next section.

5.2. Field experiments

Relevant field experiments with a single turbine have first been made in the Näsudden turbine by Högström et al. [159], that is a 2 MW turbine of 75 m diameter. Measurements were made with a high resolution SODAR (Sonic detection and ranging) at 2D–4D downstream from the turbine, which enabled to carry out detailed studies of both mean velocity and turbulence intensity in the wake. Additional data were obtained from a tower of 145 m height, located 3D downstream, instrumented to measure velocity and temperature at six different levels, and special equipment (wind vane three axial hot film probe) to measure turbulence characteristics at three levels. These measurements, at a sampling rate of 20 Hz, could provide all turbulence moments and spectra. At a distance of 10.5 D measurements were taken with Tala Kites, that provided velocity deficit and longitudinal turbulence intensity at the centre line. A similar, although less ambitious project, was carried out in Goodnoe Hills [185] with the MOD-2 machine of 91.4 m diameter. Nevertheless, in this case the data was more difficult to interpret because of the complex orography. It was found that the wake deficit dissipated more rapidly than predicted by wind tunnel experiments, this has also been observed by Högström et al. [159], although in this case this result may be due to the orography.

Earlier work on this subject, involving several turbines, was related to the Nibe project, and measurements were made by Taylor et al. [186–188] and Højstrup [189]. The installation consisted of two machines of 40 m diameter, located 200 m apart, and four measurement towers located on the intermachine axis. One tower has five anemometers and the others seven anemometers at different heights. Average flow properties and turbulence characteristics, both turbulence spectra and turbulence intensity, were measured. A project of similar characteristics, with two turbines of 20 m diameter was that of Burglar Hill [190,191]. Højstrup [192] made also measurements of turbulence characteristics in the Tændpibe wind farm, that consists of 35 machines of 75 kW each. He used both cup and 3D sonic anemometers, the latter ones for high frequency turbulence measurements. Højstrup also performed measurements [172] in the Nørrekaer Enge II wind turbine array, that consists of 42 Nordtank turbines of 300 kW separated 6-8D. He found that the spectral distribution of increase in turbulence corresponded to a band of frequencies whose scale is of the order of the width of the wake, as in the wind tunnel experiments of Vermeulen and Builtjes [162]. For some frequencies there may be even a decrease in turbulence. This may be because the wind turbine is capable of responding to low frequency fluctuations of wind speed and extracts energy from the wind in the low frequency (large-scale) range [189]. As discussed previously, a shift of the wake spectrum towards higher frequencies has also been observed in wind tunnel experiments [162]. Nevertheless, this tendency may be reversed for wind speeds higher

than that corresponding to the maximum power coefficient, as measured by Papadopoulus et al. [193], that made measurements in the wake of a single turbine in the Samos Island wind farm. Velocity spectra were also measured in the offshore Vindeby wind farm [194], that consists of 11 machines of 450 kW which are arranged in two rows, each machine and each row separated by approximately 8D. Two instrumented masts provide measurements of ambient and wake-flow parameters. The geometry of the wind farm and the instrumentation allowed for both single and multiple-wake measurements. It was observed that there is a great variation in the length scales of turbulence in the wake region, probably because atmospheric stability, and in particular the length scale in the wake is found to be much smaller than in free flow. Tindal et al. [184] also report, from wind tunnel experiments, that in the near wake the turbulence length scale is reduced to a quarter of the free stream value. Højstrup and Courtney [195], based on data from several wind farms, indicate that the shear layers in the wake create turbulence at much smaller length scales that those seen in free turbulence. Probably what is observed is that the turbulence length scale in the wake is related to the wake width, as discussed previously in the wind tunnel experiments of Vermeulen and Builtjes [162].

Kline [196] made measurements in a Howden wind farm, in Altamont Pass in California, in a cluster of 75 turbines of 33 m diameter. Emphasis was put in estimating characteristics of gusts in wakes. Also, they report measurements of horizontal shear at 2D (diameters) and 6D downstream. Other measurements of velocities and turbulence intensities were also made in Altamont Pass in California [197,198] for clusters of smaller wind turbines.

The Zeebrugge [199,200] wind farm became operational in 1987 and has 23 turbines of 22 m diameter. Two fully equipped wind masts are installed so that unperturbed wind conditions could be measured. Recordings of 10 min data sets, including wind velocity and direction, turbulence intensity, and power output were obtained. The main purpose of the research was to investigate power production and compare the measurements with the results of different models. The effect of other obstacles, such as LNG tanks in the harbour, had to be included in the analysis.

In the Vindeby wind farm, within the ENDOW (Efficient Development of Offshore Wind Farms) project, measurements have been made using SODAR instrumentation mounted on a boat [201]. This is an interesting method to complement measurements in wakes performed with fixed meteorological masts.

5.2.1. Fatigue and loads

The most important structural effect on a wind turbine which is in the wake of a neighbouring machine is fatigue, that is due to the combined effect of increased turbulence, wind speed deficit and shear, and changes in turbulence structure that cause dynamic loading, which may excite the wind turbine structure. There is a need for revision of the standards on wind turbine design and safety, to adequately account for increased fatigue loading in wind turbine clusters; this issue has been addressed by Frandsen and Thøgersen [202]. Fatigue in wind turbine clusters has already been reviewed in [203], so that previous efforts will not be considered in much detail. Earlier work on this subject was made in the Nibe project [186,187] where special emphasis was put in measuring the wake induced loads, because of its implication in the fatigue life of the machine. Other earlier measurements of loads were made by Vølund [204] and Stiesdal [205], for machines that were 2 to 3D apart. They found increases of the standard deviation of the flapwise bending moment of the order of 100% relative to the unobstructed case. Loads were largest when the machine was exposed to half-wake conditions. Stiesdal [205] introduced the concept of equivalent load, that is the amplitude of a sinusoidal load with a fixed frequency that would generate the same fatigue damage as the actual (random) load; this concept provides a more precise fatigue measurement than the standard deviation. Measurements have been made on one wind turbine in the experimental Alsvik wind farm in Sweden [206], which has four machines sited so that the instrumented unit is exposed to 5D, 7D or 9.5D single-wake loads, depending on wind direction. The terrain is smooth and the ambient turbulence low. The wind farm layout is unique in offering many experimental possibilities. It was found that under full-wake conditions the equivalent load is increased by 10% at 9.5D and up to 45% at 5D. Their conclusion is that for low roughness and low ambient turbulence sites, as occur in offshore wind farms, the wake effects are very important for wind turbine loads and fatigue. This is probably due to the fact that under these conditions wakes are more persistent, because diffusion due to ambient turbulence is smaller in the sea. Similar results were reported by Thomsen et al. [207] in the Kappel wind farm in Denmark, that consists of 24 units of 400 kW, sited in a row on a westerly shoreline, with 3.7D separations. However, in a later paper Thomsen and Sørensen [208] observe the same relative increase in fatigue loads for an offshore wind farm and a land site wind farm. Frandsen and Christensen [209] made measurements in the large Nørrekaer Enge II wind turbine array in Denmark. Two turbines in opposite corners of the wind farm were instrumented to measure stresses in towers and blades. There was a clear increase in the standard deviation of the fluctuating load when the instrumented machine was in the direct wake of a neighbouring machine, although the integrated effect of wake and non-wake operation was significantly smaller. Frandsen and Thomsen [210]

carried out similar measurements in the Danish offshore Vindeby wind farm. Data, including equivalent loads, were recorded for two years. Despite the fairly large spacing between wind turbines, the fatigue load increase in the wake is significant, about 80%. The data obtained for several wind directions demonstrate that there is no appreciable difference between single and multiple-wake loads. Further measurements of fluctuating loads in the Vindeby wind farm were reported by Thomsen and Sørensen [208], that give measured values of the power spectrum density function of flapwise bending moment, both in free flow and in wakes, and compare them with the results of an aeroelastic code. The Sexbierum wind farm in the Netherlands consists of 18 units of 300 kW, placed in three rows, each with six machines [211]. The machines are spaced 5 or 10D apart and the rows are separated by 8D. Six meteorological towers provided information on flow characteristics. As in the Vindeby wind farm, it was found that equivalent fatigue loads under single and multiple-wake conditions were very similar.

5.2.2. Anisotropy

The anisotropy of turbulence characteristics in wakes was measured by Cleijne [212] in the Sexbierum wind farm. The six components of the symmetric turbulence stress tensor were measured. The shear stress turns out to behave similarly to the velocity shear, indicating, at least qualitatively, the validity of the eddy viscosity assumption; similar results were obtained in wind tunnel experiments by Smith [173]. In general the turbulence in the wake seems to be more isotropic than in the outside flow, although, locally, there are some peaks of turbulence intensity of the component in the wind direction, that are less intense for the turbulence intensities in the other directions. These peaks occur where the gradient of the average velocity is largest. In Figs. 39 and 40 some of these results and its comparison with the UPM-ANIWAKE model proposed by Gómez-Elvira and Crespo [213] can be observed. In Fig. 39 are given the values of the turbulence intensity in the average flow direction, $(\overline{u'^2})^{1/2}/u_0$ and vertical direction, $(\overline{w'^2})^{1/2}/u_0$. The other component of the turbulence stress tensor that is not represented, $(\overline{v'^2})^{1/2}$, has values in between them. The peaks can be clearly observed in the shear layer, and the anisotropy in these peaks is smaller than in the unperturbed flow outside the wake. The turbulence is even more isotropic in the center of the wake, where all the turbulence components, including the horizontal one not represented, have approximately the same value. The longitudinal turbulence intensity decreases below its ambient value, and the vertical one increases, so that both become equal in the center of the near wake. In Fig. 40 is presented the non-diagonal components of the turbulence stress tensor, $(\overline{u'v'})^{1/2}$, corresponding to the correlation of the fluctuations of the two horizontal components of velocity; it also has peak values in the shear layer, and is zero in the wake centre.

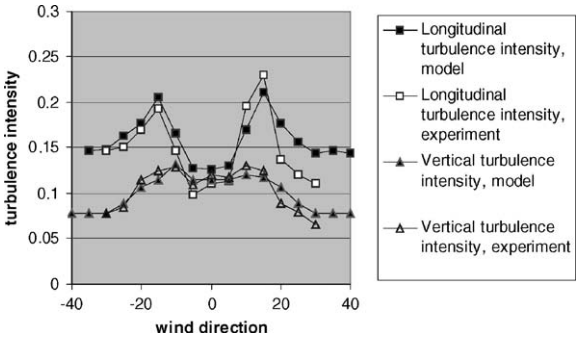

Fig. 39. Turbulence intensity in the average flow direction, $(\overline{u'^2})^{1/2}/u_0$ and vertical direction, $(\overline{w'^2})^{1/2}/u_0$, at a downstream distance of 2.5D, in a horizontal plane. Comparison of measurements in the Sexbierum wind farm from [212], and UPM-ANIWAKE model from [213].

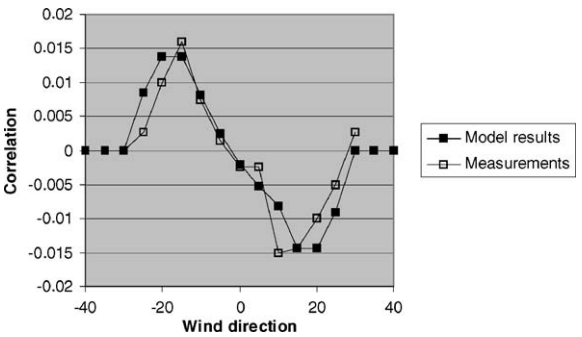

Fig. 40. Correlation of the fluctuations of the two horizontal components of velocity, $(\overline{u'w'})^{1/2}/u_0$, at a downstream distance of 2.5D, in a horizontal plane. Comparison of measurements in the Sexbierum wind farm from [212], and UPM-ANIWAKE model from [213].

5.2.3. Atmospheric stability

Another important aspect is the influence of atmospheric stability on wake behaviour. Some interesting experimental results have been presented by Magnusson [214] and Magnusson and Smedman [177]. They performed experiments in the Alsvik wind farm and measured at 4.2D, 6.1D and 9.6D downstream of a machine. They found that, for unstable stratification with Richardson number (Ri) values smaller than -0.05, the velocity deficit is independent of stability, while it increases linearly with Ri in the interval $-0.05 < Ri < 0.05$; this is due to the fact that in a stable atmosphere there is less diffusion of the velocity deficit. More recently they found [215] that for $0.25 < Ri$ there is

a tendency for the deficit to decrease, which would indicate more effective mixing.

5.2.4. Coherence

Coherence is another magnitude of interest, and is defined as the absolute value of the normalized two-point spectrum. It represents the degree to which two wind speeds at points separated in space are alike in their time histories. It could be useful to estimate the duration of a gust whose size should be large enough to engulf a rotor, and also to translate the spectra from an Eulerian frame to a rotating frame as seen by the turbine blades. Højstrup [172] has made measurements in the Nørrekaer Enge II wind farm, of the spectral coherence, both vertical and lateral, in wakes of wind turbines. He found that there is a small influence of the wake on vertical coherence, and that the lateral coherence was only modified in the near wake. Nevertheless, this result may be influenced by the fact that in these experiments the distances between the two points were small compared to the size of the wake.

6. Far wake modelling

In this section the numerical research on the far wake will be presented. Much of it has already been reviewed by Crespo et al. [203], so that previous contributions in this field will not be examined in much detail. The first subsection will be dedicated to individual wakes in flat terrain, that are easy to characterize with few parameters, and provide information of basic interest that can be easily arranged. However, the usual situation of practical interest, that will be discussed next, is that many wind turbines are located in a wind farm with irregular terrain, where the different wakes interact.

6.1. Individual wakes

6.1.1. Kinematic models

The first approach to study wind–turbine wakes was introduced in a seminal paper by Lissaman [216] with a so-called kinematic model. Kinematic models are based on self-similar velocity deficit profiles obtained from experimental and theoretical work on co-flowing jets. The wake description starts after the wake has expanded; and are assigned different types of transverse velocity profiles for the near, transition and far wake regions. Lissaman [216] and Voutsinas et al. [217] used velocity profiles obtained from models on co-flowing jets by Abramovich [218]. Vermeulen [169] used a Gaussian type of profile quite similar to that of Abramovich [218], and Katic et al. [219] simplified the problem further and assumed a top-hat profile everywhere. The reference value of the velocity deficit is usually obtained from global momentum conservation, using as input the thrust coefficient of the machine. The wake growth is due to the added effects of the ambient turbulence and the turbulence created by the shear in the wake. Vermeulen [169] added another term: the turbulence created by the turbine itself. Katic et al. [219] simply assumed that the wake radius increases linearly with downstream distance; the proportionality constant must be adjusted by comparison with experiments. The ground effect is simulated by imaging techniques. Lissaman [216] included a symmetrical turbine and added the velocity deficits of both the real and image turbine, so that drag conservation is satisfied. Crespo et al. [220] use an antisymmetric wake so that velocity deficits are subtracted and give zero perturbation at the ground. The differences in the results are not important, and it is not clear which procedure is more appropriate.

6.1.2. Field models

The field models follow a different approach and calculate the flow magnitudes at every point of the flow field. The earlier models assumed axial symmetry, such as the simple model proposed by Sforza et al. [221], that used the linearized momentum equation in the main flow direction, with constant advective velocity and a constant eddy diffusivity. They made small-scale experiments, and the agreement was reasonable, considering the simplicity of the model. A more complete parabolic model, EVMOD, was developed by Ainslie [222,223] assuming an eddy viscosity method for turbulence closure. The eddy viscosity is represented by a simple analytical form based on Prandtl's free shear layer model, but which also includes a contribution from ambient turbulence. This eddy viscosity is an average value over a cross-section. At small downstream distances, the eddy viscosity is modified by an empirical filter function to account for the lack of equilibrium between the mean velocity field and the developing turbulence field. Several constants appear in the problem, that are adjusted by comparison with particular experiments. The model is fairly simple and gives reasonable results when compared with wind tunnel experiments [179,224]. For large-scale experiments, the results are corrected by taking into account meandering effects. Nevertheless, some aspects such as the downshift of the wake centreline, or the upward displacement of the maximum turbulence intensity, can never be well predicted by models with axial symmetry. To reproduce such effects, models which retain three-dimensional effects are needed.

6.1.3. Boundary layer wake models

Crespo et al. [220,225] developed the UPMWAKE model in which the wind turbine is supposed to be immersed in a nonuniform basic flow corresponding to the surface layer of the atmospheric boundary layer. The properties of the nonuniform incident flow over the

wind turbine are modelled by taking into account atmospheric stability, given by the Monin–Obukhov length, and the surface roughness. The modelling of the turbulent transport terms is based on the k–ε method for the closure of the turbulent flow equations, previously presented. Finite-difference methods were used in the discretization of the equations. A parabolic approximation was made and the equations were solved numerically by using an alternate-direction implicit (ADI) method. The developed wake model is three-dimensional and pressure variations in the cross-section have to be retained in order to calculate transverse velocities. Crespo and Hernández [226,225] and Crespo et al. [180,227] compared UPMWAKE results with the results of wind-tunnel experiments obtained by Luken et al. [224] and those of field experiments using full-scale machines [186]. The code can predict effects such as the downward tilt of the wake centreline, as shown in Fig. 38, the upward displacement of the point of maximum added turbulence kinetic energy, as shown in Fig. 35, or the different vertical and horizontal growths of the wake width.

Another approach was followed by Taylor [228] and Liu et al. [229], that retained Coriolis forces and assumed that the pressure gradients were given by the geostrophic wind. However, this assumption cannot be justified because the length scale of the wake is not sufficiently large for the Coriolis forces to play a dominant role; indeed, they can be neglected, and the pressure field will be that resulting from the momentum conservation in the wake. If a parabolic approximation is made, pressure variations across the wake can be neglected in the momentum equation for the main flow direction, but not for the momentum components in the transverse direction, particularly when there is neither axial nor two-dimensional symmetry. Taylor's model [228] was two-dimensional, and the equations were linearized around a basic flow. Liu et al.'s model [229] was three-dimensional, and included atmospheric stability effects.

Smith and Taylor [156] and, in more detail, Taylor [230] presented a non-symmetric two-equation model that is in many ways similar to the three-equation model of Crespo et al. [220]. They neglected transverse velocities and just solve the momentum equation in the axial direction. To model the turbulent viscosity they use a k–L method, where the turbulent length scale, L, is related to the width of the wake. The comparison with their wind-tunnel experimental results is very good, as can be seen in Fig. 35, although a comparison with full-scale Nibe measurements showed that the model overestimates the values of the velocity deficit. They attributed this discrepancy to meandering and obtained better agreement when they corrected for this effect using the method proposed by Ainslie [223].

Based on the model developed by Ainslie [223], the company Garrad and Hassan has developed the code EVFARM, described by Adams and Quarton [231]. The code incorporates two alternative semi-empirical models to calculate wake turbulence. Adams and Quarton [231] use both EVFARM and UPMWAKE codes in combination with machine load predictive tools to provide a method for fatigue load prediction. As part of this study, a comprehensive validation of both codes is made using the wind tunnel measurements of Hassan [232]. A better agreement with experiments is found if a downstream displacement of the origin is considered. In the initial region of the wake some important discrepancies were also observed between the results of UPMWAKE and the Nibe measurements published by Taylor et al. [186]. On the other hand, by eliminating the boundary layer approximation used in UPMWAKE, Crespo et al. [227] proposed an elliptic model to deal simultaneously with the axial pressure gradients and diffusion effects by retaining both the axial and transverse diffusion terms. Their model therefore describes both the evolution of the expansion region and the diffusion processes in the near wake. No fundamental differences between the results of the elliptic and parabolic models were found, and displacement of the origin was apparently not necessary. Another reason for the discrepancies observed between models and experiments in the near wake may be the uncertainty involved in the radial distribution of the initial velocity deficit, that has been studied by several authors, [230,233–235] and is discussed in more detail in the first part of this review. Schepers [236] found that, by using a Gaussian profile for the initial velocity deficit, a significative improvement of the agreement with experimental results is obtained.

6.1.4. Hybrid models

An alternative approach that requires less computing capacity is the multi-parametric wake model of Voutsinas et al. [237,238], which was further developed by Cleijne et al. [235]. This model divides the wake into the rotor region, the near wake region and the far wake region, and applies a vortex particle method in the rotor region, a field model in the near wake region, and, in the far wake region, explicit self-similar expressions similar to those used in the kinematic models. Different assumptions are made to match the different regions. The method was partially successful in simulating the experimental results of the Nibe turbines given in Taylor [188]. Later, Magnusson et al. [239] applied the model to reproduce the experimental results of the Alsvik wind farm. Explicit expressions for wake characteristics obtained from this work were later applied to study the noise emissions from wind farms [240].

All these models use a closure scheme, based on zero, one or two equation models, to calculate the turbulence transport terms, and assume an isotropic turbulence

field. Transport equations for the Reynolds stresses have only been used occasionally. Ansorge et al. [241] used a Reynolds-stress turbulence model based on the commercial code PHOENICS and obtained reasonable results. More recently Gómez-Elvira and Crespo [213] have extended UPMWAKE by using an explicit falgebraic model for the components of the turbulent stress tensor. The constants of the new model, UPMANIWAKE, have been adjusted, so that it will reproduce the logarithmic layer of the basic flow and the corresponding stress tensor. The new model has a low computational cost, and its results are compared to experimental data from the Sexbierum wind farm [212], as can be seen in Figs. 39 and 40, previously commented, and a reasonable agreement is obtained.

6.2. Wind farm wake models

6.2.1. Single wake superposition

A wind farm consists of many wind turbines whose wakes can interact, and whose turbines may be affected by the wakes of several machines located upstream. Wind farm codes usually rely on the results of single wake calculations, and make superposition assumptions to take into account the combined effect of different wakes. The linear superposition of the perturbations created by wakes of different machines in a wind farm model was first used by Lissaman [216] in a classical paper, although this assumption fails for large perturbations as it overestimates velocity deficits and could lead to the absurd result of negative velocities when many wakes superimpose. Instead, Katic et al. [219] assumed linear superposition of the squares of the velocity deficits. In this case, the cumulative effect, when there are many wakes, will be smaller than that calculated for linear superposition, and, in general, this assumption provides better agreement with experimental results than the linear superposition, although, apparently, there is no physical reason for it. The corresponding code, named PARK, was applied by Beyer et al. [242] for the optimization of wind farm configurations using genetic algorithms. As already mentioned, Smith and Taylor [156] found, for a particular experimental configuration of two machines in a row, that the wake velocity of the downstream machine recovers more rapidly than the one upstream. By making a number of crude assumptions concerning the momentum transfer within the downstream wake that is imbedded in the upstream wake, Smith and Taylor [156] were able to formulate a semi-empirical superposition law that works quite well. However, it is cumbersome and can only be applied for the interaction of the wakes of two turbines in a row. When there are many turbines in a line it has been observed experimentally [200] that while the first turbine produces full power, there is a significant decrease of power in the second turbine, with practically no further loss in successive machines. Based on these observations, and on the results of the calculations of Crespo et al. [227], Van Leuven [200] assumed in his farm model (WINDPARK) that a given turbine is only affected by the wake of the closest upstream turbine, obtaining good agreement in comparison with measurements made at the Zeebrugge wind farm.

6.2.2. Elliptic wake models

Crespo et al. [227] applied an elliptic model for studying the interaction of the wakes from two turbines in two configurations: abreast and in a line. There was good agreement with experimental results, and, when other superposition assumptions were compared, it was found that the linear superposition worked well for the two machines abreast, in which velocity deficits in the interference region are small. However, for the two turbines placed in a row the linear superposition overestimated the velocity deficit, as was to be expected. Recently, this model has been improved by Sotiropoulos et al. [243] by a more detailed analysis of the rotor and inclusion of terrain effects; the results are in fair agreement with measurements in the Alsvik wind farm [239] and in wind tunnel. When the results of the elliptic model [227] are considered, it can be observed that the truly elliptic effects, such as axial pressure variations, only occur very close to the turbine, so that the parabolic approximation may be a suitable approach for studying wake interactions over most of the region where this interaction occurs. Moreover, to extend the fully elliptic code to a wind farm consisting of many machines, besides consuming a lot of calculation time, would require very powerful computers and would therefore be of little practical interest for modelling wind farms.

6.2.3. Parabolic wake models

Because of the above, Crespo et al. [244] have developed a code, UPMPARK, extending the parabolic UPMWAKE code for a single wake to the case of a park with many machines. No assumptions are required regarding the type of superposition or the type of wake to be used, as all the wakes and their interactions are effectively calculated by the code. In UPMPARK, the conservation equations solved are the same as those for the single wake code, UPMWAKE, as specified in Crespo and Hernández [225], and turbulence is closed using a k–ε model. Adams and Quarton [231] extended the UPMWAKE model to wind farms using a procedure quite similar to that of UPMPARK; this extended code has been incorporated in a wind farm design support tool, named FYNDFARM (Fatigue Yield Noise Design Farm) [245].

Usually wind farm models make the assumption that the terrain is flat and that the unperturbed wind velocity is uniform, an assumption which is not reasonable in

many cases of interest since, as is well known, terrain irregularities can be used to enhance or concentrate wind power. For terrains that are moderately complex, the simple procedure of adding the velocity perturbations of the wake and terrain should give an approximate flow field; this or equivalent procedures were applied in [226,231,200]. In the Monteahumada wind farm the velocity irregularities of the terrain and the velocity deficit created by a single wake are both of a similar order of magnitude; from its analysis it is shown, [246], that, for a moderately irregular terrain, the linear superposition of wake and terrain effects gives reasonable results. More elaborated models to take into account terrain effect on wakes are proposed by Voutsinas et al. [247], Stefanatos et al. [182], Hemon et al. [248], and Migoya et al. [249].

6.2.4. CFD code calculations

Numerical calculations using commercial CFD codes were made by several authors, [241,250] to study wake and terrain interaction for simple configurations, but their extension to wind farms of typical size will be computationally expensive. More recently, Chaviaropoulos and Douvikas, [251], and Ivanova and Nadyozhina, [252], have developed their own in-house CFD methods that deal simultaneously with terrain and wake effects. In [252] the turbines are considered as distributed roughness elements; this approach will be discussed later. In [251] a k–ω model for closure was used, the numerical results were compared with experimental measurements, and the accuracy of the simulation is fair. The method was applied to sets of one and two turbines and also seems to be computationally expensive for conventional wind farms.

As mentioned previously Taylor and Smith [181], Stefanatos et al. [182,183], and Helmis et al. [158] gave some guidelines for the modellisation of the terrain–wake interaction.

6.2.5. Offshore wind farm wakes

A related problem arises in offshore wind farms where, when the wind blows from land to sea, there is an internal boundary layer, whose development is superposed on that of the wakes, as mentioned by Crespo and Gómez [253]. As the surface roughness of the sea is usually much smaller than the corresponding roughness on land, it is to be expected that wind velocity will be greater and turbulence intensities lower than for equivalent inland stations. Consequently, turbulent diffusion of the wake will also be lower and wake effects will probably be more persistent downstream. Wake effects in offshore wind farms obtained from both experiments and numerical models are reported by Frandsen et al. [194], Crespo et al. [254,243] and their effect on fatigue loading by Frandsen [255]. Recently, within the ENDOW project, the performance of several wake models in offshore wind farms has been evaluated [256]. A total of seven models have been proposed within the ENDOW project: an axisymmetric semi-analytical engineering model (Risø), an advanced code based on computational fluid dynamics, that is coupled to an aeroelastic model (Risø), an analytical model based on Taylor's hypothesis for closure (Upsala University), two axisymmetric models based on eddy-viscosity assumption for turbulence closure (Garrad Hassan, and Oldenburg University), a fully elliptic 3D turbulent Navier–Stokes model with k–ε assumption for closure (Robert Gordon University, RGU), and a modification of UPMWAKE made by ECN (Netherlands Energy Research Foundation) [236]. Comparisons were made of the results of the different models and with experimental results in Vindeby and Bockstigen wind farms. In all cases large discrepancies appear in the near wake region, see Figs. 41 and 42.

Compared to the Vindeby experimental results, all the models overestimate the wake effects in the case of low ambient turbulence (6%), and give acceptable results in the case of higher ambient turbulence (8%). The 3D models, ECN and RGU, predict downward shift of the maximum velocity deficit, that is also confirmed by experimental results, as previously mentioned, see Fig. 38. The superposition of several wakes in double and quintuple wake cases is being also examined within the ENDOW project [257], and preliminary results point out the importance of including correct values of the ambient turbulence intensity. Another issue addressed by ENDOW, is how to link wake models with atmospheric boundary layer models; this is also in its

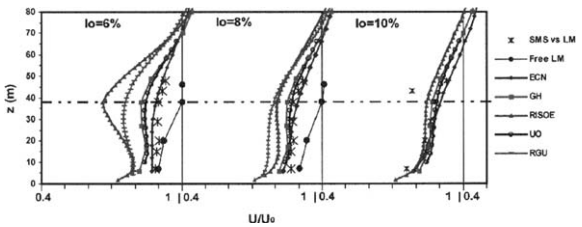

Fig. 41. Example results from the ENDOW project: cross wind profiles in vertical direction (from [256]).

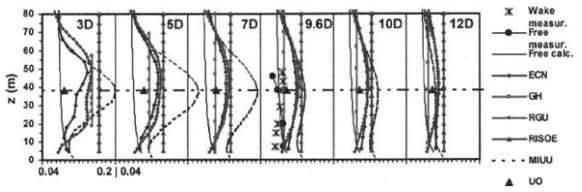

Fig. 42. Example results form the ENDOW project: turbulence in the wake (from [256]).

preliminary stages, and it does not seem to contemplate the superposition of wake and local terrain effects yet [258]. This linking provides the input needed for the wake models, assuming that the calculated atmospheric conditions are uniform along the wind farm.

6.2.6. Generic wind farm wake models

Another approach to model wind farms is to consider that the turbines behave as distributed roughness elements. Several models were proposed by Newman [259] and Bossanyi [260]. They assumed a logarithmic wind profile for the unperturbed wind, which includes ground roughness as a parameter. The presence of the turbines increases the value of the roughness. Frandsen [261] gave an explicit expression relating the artificial surface roughness to the wind turbine characteristics and its spacing within the wind farm.

Recently, the distributed roughness model has been used by Crespo el al. [262] to estimate how the large offshore wind farms may change the local wind climate, and how in turn this change of the climate will affect the local behaviour of the wind farm. In a first approach, the large wind farm is simulated by an artificial roughness as proposed in [261]. An internal boundary layer is considered that starts developing at the leading edge of the farm until it reaches, sufficiently far downstream (if the wind farm is large enough), the top of the planetary boundary layer, after that a new equilibrium region is reached. This will occur in a large distance, so that presumably, most of the wind farm will be immersed in the developing internal boundary layer. From the calculation of the internal boundary layer, the flow conditions are obtained at a certain reference height, these are then used as boundary conditions for UPMPARK. In [262] a large wind farm has been considered, that has 384 turbines of 1.5 MW rated power each; the evolution of the local turbulence intensity at hub height, as the distance from the leading edge increases, is calculated, and is presented in Fig. 43. A comparison is made with an equilibrium value predicted by Frandsen and Thogersen [202], that will be presented later in Eq. (30).

A different approach was used by Hegberg [263] that analysed the equilibrium region by establishing a global balance of Coriolis, pressure and drag forces.

Recent work on local wind climate, within and downwind of large offshore wind turbine clusters, was presented in a meeting for experts at the Risø Laboratory, that is reviewed by Frandsen and Barthelmie [264]. In this meeting, it was pointed out that the new understanding of resistive flows can be obtained from other areas of fluid dynamics, such as flow behind buildings and in forest canopies [265].

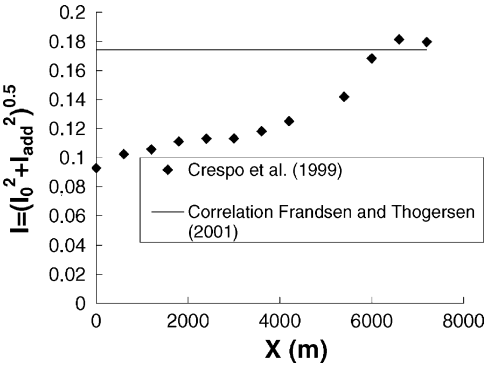

Fig. 43. Local turbulence intensity at hub height, as function of the distance from the leading edge of the wind farm, from [262]. Comparison with an analytical prediction for equilibrium conditions in an infinitely large wind farm, from [202], see Eq. (30).

7. Far wake: engineering expressions

7.1. Velocity deficit

In many cases it is of interest for the designer to have, as an alternative to numerical models, analytical expressions which can estimate the order of magnitude and the tendencies of the most important parameters characterising wake evolution. Regressions or correlations of this type were obtained by different authors to describe single wake behaviour, [226,224,159,266,215], for the velocity deficit and the width of the wake. For the velocity deficit in the far wake, these correlations are usually of the type:

$$\frac{\Delta V}{V_{\text{hub}}} = A\left(\frac{D}{x}\right)^n, \tag{23}$$

where V_{hub} is the incident wind velocity at hub height, x is the downstream distance, D the wind–turbine radius, and A and n are constants. In some cases, to extend the range of validity of this equation to smaller values of x, its origin is displaced. The constant A will depend on turbine characteristics, fundamentally on the thrust coefficient, C_{T} or the induced velocity factor, a, and will increase with either of them. These constants are in the range $1<A<3$, and $0.75<n<1.25$, respectively. If we consider an axisymmetric wake we can apply classical results, see for example the book of Schlichting [267]. For the case of a turbulent wake that is diffusing with zero ambient turbulence, $n=2/3$, [268], and for a laminar wake, or equivalently when diffusion is controlled by a constant ambient turbulent diffusivity, $n=1$.

Instead of using the non-dimensional distance, x/D, Magnusson and Smedman, [266,215], expressed wake diffusion as a function of the transport time $t=x/V_{\text{hub}}$

made dimensionless with t_0, the transport time where the near wake ends. Their correlation takes the form

$$\frac{\Delta V}{V_{\text{hub}}} = C_2 \ln\left(\frac{t_0}{t}\right) + C_{\text{T}}, \tag{24}$$

valid for $t > t_0$, and for t_0 in neutral atmosphere they give

$$t_0 = C_1 \frac{1}{f} \ln\left(\frac{H}{z_0}\right) \frac{D}{2H}, \tag{25}$$

where H is the turbine height, z_0 is the surface roughness of the ground, f is the rotational frequency of the turbine, and C_1 and C_2 are constants, taken respectively equal to 1 and 0,4, in [215].

7.2. Turbulence intensity

Correlations for turbulence intensity in the far wake have been given in [224,162,159,161,171,157,266,268]. Crespo and Hernández [157,171], give the following expression for the added turbulence intensity, created by the turbine:

$$\Delta I = 0.73 a^{0.83} I_{\infty}^{-0.0325} \left(\frac{D}{x}\right)^{0.32}. \tag{26}$$

The turbulence intensity, I, is defined as the ratio of the standard deviation of the wind velocity in the average wind direction, divided by the average wind velocity. It is assumed that the wind turbine creates an additional turbulent kinetic energy that should be added to the ambient one, consequently, ΔI will be,

$$\Delta I = \sqrt{I^2 - I_{\infty}^2}, \tag{27}$$

where I_{∞}, is the ambient turbulence intensity. This expression was obtained by fitting with the numerical results of UPMWAKE, and was validated by comparison with experimental results, both of wind tunnel and field experiments (many of them compiled by Quarton [161]). A similar expression was proposed in [161], obtained by fitting with experimental results:

$$\Delta I = 4.8 C_{\text{T}}^{0.7} I_{\infty}^{0.68} \left(\frac{x_N}{x}\right)^{0.57} \tag{28}$$

where the drag coefficient, C_{T}, has been used instead of the induced velocity factor a, and the diameter has been substituted by the near wake length, x_N, that is of the order of 1D–3D. Frandsen and Thogersen [202] proposed the following correlation based on measurements:

$$\Delta I = \frac{1}{1.5 + 0.3(x/D)\sqrt{V_{\text{hub}}}}, \tag{29}$$

where V_{hub} is related to C_{T}. The decay with downstream distance is smaller in Eq. (26), $x^{-0.32}$, than in Eq. (28), $x^{-0.57}$ and in Eq. (29), that for large values of x, will be like x^{-1}. In [159] a decay like $x^{-0.5}$ is obtained. In [268] it is observed that the behaviour should be like $x^{-1/3}$; this corresponds to the classical situation of a wake developing in an ambient with no turbulence [267]. If only field experiments are used, in Eq. (28) the exponent will be 0.37, whereas, from wind tunnel experiments made at TNO [160], the behaviour is estimated to be like $x^{-0.7}$. In any case it should be noticed that the decay of turbulence intensity, ΔI, is slower than the decay of the velocity deficit, ΔV. Frandsen [269] has plotted the three correlations: (26), (28), and (29), with different coefficients, in order to fit to some experimental results. These are shown in Fig. 44. It can be seen that the agreement of the correlation of Crespo and Hernández [157], Eq. (26), is appropriate for large distances, whereas that of Quarton [161]), Eq. (28), gives a better fitting for smaller distances.

7.3. Wind farm wake expressions

For wind turbine clusters Luken [160] proposed a correlation for the equilibrium value of the turbulence intensity reached in a row of turbines, using the experimental results of Builtjes and Vermeulen [162], in which the turbulence decayed like $x^{-1.64}$, x being the distance between machines. Frandsen et al. [194] presented correlations giving values of the average velocity, turbulence intensity, turbulence scale and width of the wake at different positions of each machine in a row as functions of their operating characteristics. These correlations are obtained by making the best fit with numerical results from UPMPARK, and are validated by comparison with measurements made in Vindeby wind farm. Frandsen and Thogersen [202], based on the distributed roughness model of Frandsen [261], considered the case of an infinitely large wind farm that perturbs the whole boundary layer, and estimated the value of the added turbulence intensity deep inside the

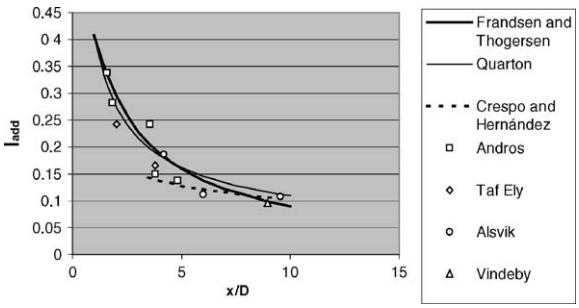

Fig. 44. Maximum, added hub height wake turbulence measured in four different cases, compared with the three correlations: (26), (28), and (29), with adjusted coefficients. Wind velocities in the range 9 m/s$< U <$11 m/s. The experimental data were compiled by Ghaie (Personal communication to Frandsen, 1997). Figure taken from [269].

farm to be

$$\Delta I = \frac{0,36}{1 + 0.2\sqrt{x_r x_f}/D/\sqrt{C_T}} \quad (30)$$

where x_r is the separation of rows, and x_f the separation of files. This equation gives a maximum value of $\Delta I = 0.36$ that is equal to the one obtained by Crespo and Hernández [157], for the annular peak of turbulence intensity in the cylindrical shear layer formed in the near wake. This correlation agrees well with the predictions made in [262], as can be seen in Fig. 43.

The effect of atmospheric stability (expressed in terms of the Richardson number) on velocity deficit decay was taken into account in the correlation given by Magnusson and Smedman [177].

All these correlations have been compared with some experimental results and show at least an acceptable degree of agreement, although more work is needed to carry out a full comparison both among these correlations and with experimental results.

8. Concluding remarks

At a time when it is realised that the matter of interest is really complicated, it is worthwhile to review the work that has been done. Hopefully, this overview will provide a point of departure for 'plunging' into the subject.

8.1. Near wake

With regards to the near wake experiments, it can be concluded that the wealth of experimental data for helicopters is regrettably not present for wind turbines. In this respect, it is not the quantity that matters, because even when restricting to the uniform, static, non-yawed case, there is a lot of experimental work done on wind turbine near wakes. However, most of these experiments tend to be fragmentarily carried out, meaning they deal only with a limited set of rotor properties. The experiments themselves certainly achieve their own described goal. But most of them seem to be individual and limited efforts. In a larger perspective, by the great diversity in rotor models and wind tunnels, it is extremely difficult to make a comparison between the different experiments and trying to combine them to gain an added value appears to be unfeasible.

The lack of an extensive data set with such basic aerodynamic rotor properties is often felt as a large deficiency, in both the scientific and the engineering environment, for comparison with calculational codes. So, initiatives like the measurement campaign by NREL in the NASA-Ames wind tunnel and the EU-funded "MEXICO" project (with forthcoming measurements in the DNW wind tunnel) are highly appreciated, but definitely need to have a continuous follow-up.

Near wake computations can be carried out by various numerical techniques, ranging from inviscid lifting line/surface methods to viscous Navier–Stokes based methodologies. Each method has its own advantages and limitations. While e.g. prescribed vortex wake methods are fast to run on a computer but leaves much of the physics to a priori given assumptions, Navier–Stokes based methods offer very detailed insight in the flow behaviour but are very computing costly. There is no doubt, however, that full-blown Navier–Stokes simulations now are reaching a level where they convincingly have matured to become the most important predictive tool for predicting and understanding aerodynamics of modern wind turbines.

8.2. Far wake

With regards to far wake analysis, wind turbine wakes have been extensively studied both experimentally and analytically. Nevertheless, their knowledge is far from being satisfactory. Many of the numerical models proposed show an acceptable degree of agreement with the experiments with which they are compared. However, the assumptions and coefficients that are chosen are such that the agreement with some particular experiments may be good, although the overall validity has not been checked in more general situations. There is a clear need for serious and conscious checks against independent data, as it is made in the project ENDOW, [256,257]. The models which depend on the least simplifying assumptions are better suited in dealing with different configurations and in reproducing wake development in more detail. Some aspects of individual wake modelling, such as near wake representation, influence of atmospheric stability, appropriate turbulence modelling, or convergence problems, are still issues of active research. Some of these aspects are more relevant to the offshore wind farms, many of which are expected to be installed in future. While greater emphasis used to be directed to the estimation of velocity deficits and farm efficiency in terms of energy production, research is nowadays more oriented to other issues, such as estimating magnitudes related to the structural and fatigue behaviour, or fluctuations in the electrical energy produced by machines affected by upstream wakes. For this, it is necessary to know the turbulence characteristics of the flow (turbulence intensity, correlations and spectrum), and wind shear data. An issue of some importance, and in which some progress has been made, is the non-isotropic nature of the turbulence of ambient atmospheric flow, in contrast to the more isotropic turbulence in the wakes. One of the most important difficulties that has not been treated satisfactorily is the choice of appropriate input parameters to define

ambient unperturbed flow, particularly in complicated terrains. Usually, a comparison with wind tunnel experiments is reasonably straightforward, but when field experiments are used for comparison there are many difficulties and effects like meandering, that have not yet been satisfactorily modelled. The results obtained from experimental and modelling studies for terrains of varying roughness and the appearance of internal boundary layers, such as those observed in large wind farms located near the coast or offshore, should be incorporated into the description of ambient flow. The problem is that it is difficult to envisage general solutions, and we will always be solving particular problems that, at most, could only point to general tendencies.

Acknowledgements

Thanks to everyone who has contributed to this article: Gijs van Kuik for writing the introduction on wind energy and proof-reading, Gerard van Bussel for proof-reading and "restructuring advice", and Gustave Corten for his help with the stall-flag pictures.

References

[1] Lanchester FW. A contribution to the theory of propulsion and the screw propeller. Trans Inst Naval Archi. 1915;57:98.
[2] Glauert H. Aerodynamic theory, vol. 4. Berlin, Germany: Julius Springer: 1935. p. 169–360 (Chapter Division L).
[3] van Kuik G. 25 years of wind turbine technology development. In: Watson R, editor. European Wind Energy Conference 1997, IWEA, Slane, Ireland, 1997. p. 21–4.
[4] Thor S-E, Weis-Taylor P. Long-term research and development needs for wind energy for the time frame 2000–2020. Wind Energy 2002;5(1):73–5.
[5] Snel H. Review of the present status of rotor aerodynamics. Wind Energy 1998;1(S1):46–69.
[6] Leishman JG. Challenges in modelling the unsteady aerodynamics of wind turbines. Wind Energy 2002;5 (2–3):85–132.
[7] Schepers JG, et al., Final report of IEA Annex XVIII: enhanced field rotor aerodynamic database. Technical report ECN-C–02-016, ECN, Petten, The Netherlands, February 2002.
[8] Conlisk AT. Modern helicopter rotor aerodynamics. Progr Aerospace Sci 2001;37(5):419–76.
[9] Landgrebe AJ, Cheney MC. Rotor wakes—key to performance. In: Aerodynamics of Rotary Wings, AGARD, Marseilles, France, 1972. p. 1/1–1/19.
[10] de Vries O. Wind-tunnel tests on a model of a two-bladed horizontal axis wind turbine and evaluation of an aerodynamic performance calculation method. Technical report NLR TR 79071 L, NLR, Amsterdam, The Netherlands, June 1979.
[11] Anderson MB, Milborrow DJ, Ross NJ. Performance and wake measurements on a 3 m diameter horizontal axis wind turbine. Comparison of theory, wind tunnel and field test data. Technical report, University of Cambridge, Department of Physics, Cavendish Lab., Cambridge, U.K., April 1982.
[12] Shimizu Y, Kamada Y. Studies on a horizontal axis wind turbine with passive pitch-flap mechanism (performance and flow analysis around wind turbine). J Fluids Eng 2001;123:516–22.
[13] Hand M, Simms D, Fingersh L, Jager D, Cotrell J, Schreck S, Larwood S. Unsteady aerodynamics experiment phase vi: Wind tunnel test configurations and available data campaigns. Technical report NREL/TP-500-29955, NREL, December 2001.
[14] Schreck S. The NREL full-scale wind tunnel experiment introduction to the special issue. Wind Energy 2002;5 (2–3):77–84.
[15] Vermeer N. A new rotor model for aerodynamic measurements in the improved open jet wind tunnel (in dutch). In: National Wind Energy Conference 1990, Lunteren, The Netherlands, 1990. p. 441–5.
[16] Alfredsson P-H, Dahlberg J-Å. A preliminary wind tunnel study of windmill wake dispersion in various flow conditions. Technical Note AU-1499, Part 7, FFA, Stockholm, Sweden, September 1979.
[17] Alfredsson P-H, Dahlberg J-Å. Measurements of wake interaction effects on power output from small wind turbine models. Technical Note HU-2189, Part 5, FFA, Stockholm, Sweden, June 1981.
[18] Savino JM, Nyland TW. Wind turbine flow visualization studies. In: Proceedings of the Windpower '85 Conference, Washington, DC: American Wind Energy Association, 1985. p. 559–64.
[19] Anderson CG, Niven AJ, Jamieson P, Knight RR, Milborrow DJ. Flow visualization on rotating blades. In: 9th British Wind Energy Association Conference, 1987. p. 169–76.
[20] Eggleston DM, Starcher K. Comparative studies of the aerodynamics of several wind turbines using flow visualization. J Solar Energy Eng 1990;112:301–9.
[21] Vermeer NJ. Velocity measurements in the near wake of a model rotor (in dutch). In: Fourth Dutch National Wind Energy Conference, Noordwijkerhout, The Netherlands, 1988. p. 209–12.
[22] Vermeer NJ. Velocity measurements in the near wake of a model rotor. In: European Wind Energy Conference 1989, Glasgow, UK, 1989. p. 532–5.
[23] Vermeer NJ, van Bussel GJW. Velocity measurements in the near wake of a model rotor and comparison with theoretical results. In: Fifteenth European Rotorcraft Forum, Amsterdam, The Netherlands, 1989. p. 20/1–20/14.
[24] Vermeer LJ. A review of wind turbine wake research at TUDelft. In: A Collection of the 2001 ASME Wind Energy Symposium Technical Papers. New York: ASME, 2001. p. 103–13.
[25] Wentz W, Ostawari C, Manor D, Snyder M. Horizontal axis wind turbine wake and blade flow studies from model

tests. In: Fourth ASME Wind Energy Symposium. Dallas, TX, 1985. p. 235–44.
[26] Butterfield CP. Aerodynamic pressure and flow-visualization measurement from a rotating wind turbine blade. In: Eighth ASME Wind Energy Symposium, ASME, Houston, TX, 1989. p. 245–56.
[27] Dexin H, Ming C, Dahlberg J, Ronsten G. Flow visualization on a rotating wind turbine blade. Technical report FFA-TN 1993-28, FFA, Bromma, Sweden, June 1993.
[28] Vermeer LJ, Timmer WA. Identification of operational aerofoil state by means of velocity measurements. In: European Wind Energy Conference 1999, Nice, France, 1999. p. 168–71.
[29] Corten GP. Visualization of the stalled area on large wind turbine blades. In: Zervos A. editor. 1996 European Union Wind Energy Conference. Göteborg, Sweden: H.S. Stephens & Associates; 1996. p. 1055–8.
[30] Corten GP. The stall flag method: proof of concept. In: Proceedings of the 17th ASME Wind Energy Symposium held in conjunction with the 36th AIAA Aerospace Meeting and Exhibit. New York: ASME, 1998. p. 31–43.
[31] Corten GP. Flow separation on wind turbine blades. PhD thesis, Utrecht University, The Netherlands, January 2001.
[32] Corten GP, Veldkamp HF. Insects can halve wind-turbine power. Nature 2001;412(6842):41–2.
[33] Vermeer LJ. Video recordings of root vortex flow visualisation, unpublished video material, January 2002.
[34] Vermeulen P. A wind tunnel study of the wake of a horizontal axis wind turbine. Technical report 78-09674, TNO,'s Gravenhage, The Netherlands, September 1978.
[35] Vermeulen P. Studies of the wake structure of model wind turbine generators. Technical report 79-012904, TNO,'s Gravenhage, The Netherlands, November 1979.
[36] Kotb MA, Schetz JA. Windmill flowfield with non-uniform approach flow. In: European Wind Energy Conference, 1984. p. 500–5.
[37] Kotb MA, Schetz JA. Wind turbine blade mean and turbulent flowfield measurements. In: European Wind Energy Association Conference, 1986. p. 387–90.
[38] Kotb MA, Abdel Haq MM. A rigid wake model for a horizontal axis wind turbine. Wind Eng 1992;16(2): 95–108.
[39] Ross JN, Ainslie JF. Wake measurements in clusters of model wind turbines using laser doppler anemometry. In: Proceedings of the Third BWEA Wind Energy Conference, Cranfield, 1981. p. 172–84.
[40] Whale J, Anderson CG. An experimental investigation of wind turbine wakes using particle image velocimetry. In: 1993 European Community Wind Energy Conference and Exhibition, Lübeck-Travemünde, Germany, 1993. p. 457–60.
[41] Helmis CG, Whale J, Papadopoulos KH, Anderson CG, Asimakopoulos DN, Skyner DJ. A comparative laboratory and full-scale study of the near wake structure of a wind turbine. In: Tsipouridis JL, editor. European Wind Energy Conference 1994, Thessaloniki, Greece, 1994. p. 465–71.
[42] Whale J, Papadopoulos KH, Anderson CG, Helmis CG, Skyner DJ. A study of the near wake structure of a wind turbine comparing measurements from laboratory and full-scale experiments. Solar Energy 1996;56(6):621–33.
[43] Whale J, Bareiss R, Wagner S, Anderson CG. The wake structure of a wind turbine rotor—comparison between PIV measurements and free-wake calculations. In: Zervos A. editor. Proceedings of the 1996 European Wind Energy Conference. Göteborg, Sweden: H.S. Stephens & Associates; 1996. p. 695–8.
[44] Whale J. Investigating fundamental properties of wind turbine wake structure using particle image velocimetry. In: 10th IEA Symposium on Wind Turbine Aerodynamics. Vienna: IEA, 1996.
[45] Whale J, Anderson CG, Bareiss R, Wagner S. An experimental and numerical study of the vortex structure in the wake of a wind turbine. J Wind Eng Ind Aerodyn 2000;84:1–21.
[46] Ebert PR, Wood DH. Three dimensional measurements in the wake of a horizontal axis wind turbine. In: Tsipouridis JL, editor. European Wind Energy Conference 1994, Thessaloniki, Greece, 1994. p. 460–4.
[47] Ebert PR. Aspects of the aerodynamics of horizontal axis wind turbines, PhD thesis, Department of Mechanical Engineering, University of Newcastle (N.S.W.), 1996.
[48] Ebert PR, Wood DH. The near wake of a model horizontal-axis wind turbine: Part 1: experimental arrangements and initial results. Renewable Energy 1997;12:225–43.
[49] Ebert PR, Wood DH. The near wake of a model horizontal-axis wind turbine: Part 2: general features of the three-dimensional flowfield. Renewable Energy 1999;18:513–34.
[50] Ebert PR, Wood DH. The near wake of a model horizontal-axis wind turbine: Part 3: properties of the tip and hub vortices. Renewable Energy 2001;22:461–72.
[51] Fisichella CJ. An improved prescribed wake analysis for wind turbine rotors. PhD thesis, University of Illinois, Urbana, Illinois, USA, April 2001.
[52] Tsustui Y, Matsumya H. Ldv measurements of flow field around a wind turbine. In: Windpower 1987, 1987. p. 381–6.
[53] Clausen PD, Wood DH. The phase and time dependence of the wake of a wind turbine. In: 9th Australasian Fluid Mechanics Conference, Auckland, New Zealand, 1986. p. 416–9.
[54] Clausen PD, Piddington DM, Wood DH. An experimental investigation of blade element theory for wind turbines. Part 1. mean flow results. J Wind Eng Ind Aerodyn 1987;25:189–206.
[55] Clausen PD, Wood DH. An experimental investigation of blade element theory for wind turbines. Part 2. Phase-locked averaged results. J Wind Eng Ind Aerodyn 1988;31:305–22.
[56] Vermeer N, van Bussel GJW. Velocity measurements in the near wake of a model rotor and comparison with theoretical results. In: European Community Wind Energy Conference 1990, Madrid, Spain, 1990. p. 218–22.
[57] Vermeer LJ. Local circulation on rotating wind turbine blades from velocity measurements in the wake of a model rotor. In: British Wind Energy Association Annual Wind Energy Conference 1992, Nottingham, UK, 1992. p. 117–21.

[58] Guj G, Terzitta M, Arsuffi G. Velocity measurements upstream of a windmill rotor model. Wind Eng 1991;15(5):248–60.
[59] Mast EHM. Estimating the circulation distribution using near wake velocity measurements, Master thesis WE-03190, Section Wind Energy, Delft University of Technology, Delft, The Netherlands, March 2003.
[60] Drela M. XFOIL: an analysis and design system for low Reynolds number airfoils. In: Conference on Low Reynolds Number Airfoil Aerodynamics, University of Notre Dame, 1989.
[61] Vermeer LJ. Measurements on the properties of the tip vortex of a rotor model. In: Tsipouridis JL, editor. European Wind Energy Conference 1994, Thessaloniki, Greece, 1994. p. 805–8.
[62] Vermeer LJ, Briaire JJ, van Doorne C. How strong is a tip vortex? In: British Wind Energy Association Annual Wind Energy Conference 1995, Warwick, UK, 1995. p. 59–64.
[63] Vermeer N. How fast is a tip vortex? In: Nineth IEA Symposium on the Aerodynamics of Wind Turbines, Stockholm, Sweden, 1995. p. 15–20.
[64] Vermeer N, van Bemmelen J, Over E. How big is a tip vortex? In: Tenth IEA Symposium on the Aerodynamics of Wind Turbines, Edinburgh, UK, 1996. p. 77–82.
[65] Grant I, et al. An experimental and numerical study of the vortex laments in the wake of an operational, horizontal-axis, wind turbine. J Wind Eng Ind Aerodyn 2000;85:177–89.
[66] Sørensen JN. Three-level, viscous-inviscid interaction technique for the prediction of separated flow past rotating wings. AFM report 86-07, Department of Fluid Mechanics, The Technical University of Denmark, 1986.
[67] Butterfield CP. Three-dimensional airfoil performance measurements on a rotating wing. In: EWEC'89 European Wind Energy Conference and Exhibition, Peter Peregrinus Ltd, 1989. p. 90–4.
[68] Ronsten G. Static pressure measurements on a rotating and a non-rotating 2.375 m wind turbine blade—comparison with 2d calculations. In: Hulle FV, Smulders P, Dragt J, editors. Wind Energy: Technology and Implementation, Amsterdam EWEC '91: Elsevier Science Publishers, 1991. p. 214–20.
[69] Madsen HA, Rasmussen F. Measured airfoil characteristics of three blade segments on a 19 m hawt rotor. In: McAnulty K, editor. Proceedings of the Third IEA Symposium on the Aerodynamics of Wind Turbines, ETSU, Harwell, 1990. p. 7.1–7.13.
[70] Snel H. Scaling laws for the boundary layer flow on rotating windturbine blades. In: McAnulty K, editor. Proceedings of the Fourth IEA Symposium on the Aerodynamics of Wind Turbines, ETSU, Harwell, 1991. p. 5.1–5.20.
[71] Chaviaropoulos PK, Hansen MOL. Investigating three-dimensional and rotational effects on wind turbine blades by means of a quasi-3D Navier–Stokes solver. J Fluids Eng 2000;197:330–6.
[72] Gaonkar GH, Peters DA. Effectiveness of current dynamic-inflow models in hover and forward flight. J Amer Helicopter Soc 1986;31(2):47–57.
[73] Hansen AC. Yaw dynamics of horizontal axis wind turbines: final report. NREL Technical report 442-4822, Nat Renewable Energy Lab, 1992.
[74] van Bussel GJW. Induced velocity distribution and axial loads on yawed rotors. In: Tsipouridis JL, editor. European Wind Energy Conference 1994, Thessaloniki, Greece, 1994. p. 834–9.
[75] Hasegawa Y, Kkikuyama K, Tanimoto M, van Bussel GJW. Calculation of yawed inflow effects on a horizontal axis wind turbine rotor by an asymptotic acceleration potential method. In: Zervos A. editor. 1996 European Union Wind Energy Conference. G-öteborg, Sweden: H.S. Stephens & Associates; 1996. 753–6.
[76] Peyret R, Taylor TD. Computational methods for fluid flows. Berlin: Springer; 1983.
[77] Gatski TB, Grosch CE, Rose ME. The numerical solution of the Navier–Stokes equations for 3-dimensional unsteady incompressible flows by compact schemes. J Comput Phys 1989;82:298–329.
[78] Hansen MOL, Sørensen JN, Shen WZ. vorticity-velocity formulation of the 3D Navier–Stokes equations in cylindrical co-ordinates. Int J Numer Methods Fluids 2003;41:29–45.
[79] Speziale CG. On the advantages of the vorticity-velocity formulation of the equations of fluid dynamics. Report CR-178076, ICASE 86/18, NASA Langley Research Center, Hampton, 1986.
[80] Daube O, Guermond JL, Sellier A. Sur la formulation vitesse-tourbillon des équations de navier-stokes en écoulement incompressible. CR Acad Sci Paris 1991; 313(II):377–82.
[81] Hansen MOL. Vorticity-velocity formulation of the navier-stokes equations for aerodynamic flows. PhD dissertation AFM 94-07, Department of Fluid Mechanics, Technical University of Denmark, 1994.
[82] Miller RH. The aerodynamic and dynamic analysis of horizontal axis wind turbines. J Wind Eng Ind Aerodyn 1983;15:329–40.
[83] Øye S. A simple vortex model. In: McAnulty K, editor. Proceedings of the Third IEA Symposium on the Aerodynamics of Wind Turbines, ETSU, Harwell, 1990. p. 4.1–5.15.
[84] Koh SG, Wood DH. Formulation of a vortex wake model for horizontal-axis wind turbines. Wind Eng 1991;15(4):196–210.
[85] Wood DH. On wake modelling at high tip speed ratios. Wind Eng 1992;16(5):291–303.
[86] Bagai A, Leishman JG. Rotor free-wake modeling using a pseudoimplicit relaxation algorithm. J Aircraft 1995; 32(6):1276–85.
[87] Bhagwat M, Leishman JG. Accuracy of straight-line segmentation applied to curvilinear vortex filaments. J Amer Helicopter Soc 2001;46(2):166–9.
[88] Gould J, Fiddes SP. Computational methods for the performance prediction of hawts. In: Hulle FV, Smulders P, Dragt J, editors. Wind Energy: Technology and Implementation. Amsterdam EWEC '91: Elsevier Science Publishers, 1991. p. 29–33.
[89] Robison DJ, Coton FN, Galbraith RAM, Vezza M. Application of a prescribed wake aerodynamic prediction

scheme to hotizontal axis wind turbine in axial flow. Wind Eng 1995;19(1):41–51.
[90] Coton FN, Wang T. The prediction of horizontal axis wind turbine performance in yawed flow using an unsteady prescribed wake model. Proceedings of the Institution of Mechanical Engineers, Part A. J Power Energy 1999;213:33–43.
[91] Afjeh AA, Keith TG. A simplified free wake method for horizontal-axis wind turbine performance prediction. Trans ASME J Fluids Eng 1986;108:303–9.
[92] Simoes FJ, Graham JMR. Prediction of loading on a horizontal axis wind turbine using a free vortex wake model. In: Proceedings of the BWEA Conference, 1991.
[93] Voutsinas SG, Beleiss MA, Rados KG. Investigation of the yawed operation of wind turbines by means of a vortex particle method. In: AGARD Conference Proceedings, vol. 552. 1995. p. 11.1–11.
[94] Coton FN, Wang T, Galbraith RAM. An examination of key aerodynamic modelling issues raised by the NREL blind comparison. Wind Energy 2002;5:199–212.
[95] Katz J, Plotkin A. Low-speed aerodynamics: from wing theory to panel methods. New York: McGraw-Hill; 1991.
[96] Cottet GH, Koumoutsakos PD. Vortex methods: theory and practice. New York: Cambridge University Press; 2000.
[97] Preuss RD, Suciu EO, Morino L. Unsteady potential aerodynamics of rotors with applications to horizontal-axis windmills. AIAA J 1980;18(4):385–93.
[98] Arsuffi G. A general formulation for aerodynamic analysis of wind turbine. In: Proceedings of the Second IEA Symposium on the Aerodynamics of Wind Turbines, Department of Fluid Mechanics, Technical University of Denmark, 1989.
[99] Bareiss R, Wagner S. A hybrid wake model for hawt. In: McAnulty K, editor. Proceedings of the Sixth IEA Symposium on the Aerodynamics of Wind Turbines, ETSU, Harwell, 1993. p. 7.1–.10.
[100] van Holten Th. The computation of aerodynamic loads on helicopter blades in forward flight using the method of the acceleration potential. Report VTH-189, Department of Aerospace Engineering, Delft, The Netherlands, 1975.
[101] van Bussel GJW. The aerodynamics of horizontal axis wind turbine rotors explored with asymptotic expansion methods. Doctoral dissertation. Technische Universiteit Delft, The Netherlands, 1995.
[102] Froude RE. On the part played in propulsion by difference of fluid pressure. Trans Roy Inst Naval Arch 1889;30:390–405.
[103] Wu TY. Flow through a heavily loaded actuator disc. Schiffstechnik 1962;9:134–8.
[104] Greenberg MD, Powers SR. Nonlinear actuator disc theory and flow field calculations, including nonuniform loading. NASA CR 1672, NASA, 1970.
[105] Greenberg MD. Nonlinear actuator disc theory. Z Flugwissensch 1972;20(3):90–8.
[106] Conway J. Analytical solutions for the actuator disk with variable radial distribution of load. J Fluid Mech 1995;297:327–55.
[107] Conway J. Exact actuator disk solution for non-uniform heavy loading and slipstream contraction. J Fluid Mech 1998;365:235–67.
[108] Madsen HA. The actuator cylinder a flow model for vertical axis wind turbines. PhD dissertation, Aalborg University Centre, 1982.
[109] van Kuik GAM. On the limitations of froude's actuator disc concept. PhD thesis, Eindoven University of Technology, Eindhoven, Netherlands, February 1991.
[110] Fejtek I, Roberts L. Navier–Stokes computation of wing/rotor interaction for a tilt rotor in hover. AIAA J 1992;30(11):2595–603.
[111] Rajagopalan RG, Mathur SR. Three dimensional analysis of a rotor in forward flight. J Amer Helicopter Soc 38(3).
[112] Sørensen JN, Myken A. Unsteady actuator disc model for horizontal axis wind turbines. J Wind Eng Ind Aerodyn 1992;39:139–49.
[113] Sørensen JN, Kock CW. A model for unsteady rotor aerodynamics. J Wind Eng Ind Aerodyn 1995;58:259–75.
[114] Sørensen JN, Mikkelsen R. On the validity of the blade element momentum theory. In: Helm P, Zervos A, editors. Proceedings of the 2001 European Wind Energy Conference and Exhibition, WIP-Renewable Energies, Munchen, 2001. p. 362–6.
[115] Madsen HA. A CFD analysis for the actuator disc flow compared with momentum theory results. In: Pedersen B, editor. Proceedings of the 10th IEA Symposium on the Aerodynamics of Wind Turbines, Department of Fluid Mechanics, Technical University of Denmark, 1996. p. 109–24.
[116] Sørensen JN, Shen WZ, Munduate X. Analysis of wake states by a full-field actuator disc model. Wind Energy 1998;1:73–88.
[117] Madsen HA, Rasmussen F. The influence of energy conversion and induction from large blade deflections. In: Proceedings of the European Wind Energy Conference, James & James, 1999. p. 138–41.
[118] Mikkelsen R, Sørensen JN, Shen WZ. Modelling and analysis of the flow field around a coned rotor. Wind Energy 2001;4:121–35.
[119] Sørensen JN, Shen WZ. Numerical modelling of wind turbine wakes. J Fluids Eng 2002;124(2):393–9.
[120] Snel H, Houwink R, Piers WJ. Sectional prediction of 3D effects for separated flow on rotating blades. In: Proceedings of the ECWEC '93 Conference, 1993. p. 395–9.
[121] Hoerner SF. Fluid-dynamic drag. Hoerner Fluid Dynamics, Brick Town, N.J. USA, 1965.
[122] Hansen MOL. Polar for NACA 63-415 airfoil. Report ET-AFM-9902, Technical University of Denmark, Department of Energy Engineering, Lyngby, Denmark, 1999.
[123] Øye S. Dynamic stall simulated as time lag of separation, In: McAnulty K, editor. Proceedings of the Fourth IEA Symposium on the Aerodynamics of Wind Turbines, ETSU, Harwell, 1991. p. 6.1–.7.
[124] Leishman JG, Beddoes TS. A semi-empirical model for dynamic stall. J Amer Helicopter Soc 1989;34(3):3–17.
[125] Masson C, Ammara I, Paraschivoiu I. An aerodynamic method for the analysis of isolated horizontal-axis wind turbines. Int J Rotating Mach 1997;3:21–32.
[126] Masson C. Viscous differential/actuator disk method and its applications. In: Thor S-E, editor. Proceedings of the

15th IEA Symposium on the Aerodynamics of Wind Turbines, FOI, Swedish Defence Research Agency, 2002. p. 65–80.
[127] Phillips D, Schaffarczyk AP. Blade-element and actuator-disk models for a shrouded wind-turbine. In: Thor S-E, editor. Proceedings of the 15th IEA Symposium on the Aerodynamics of Wind Turbines, FOI, Swedish Defence Research Agency, 2002. p. 95–105.
[128] Mikkelsen R, Sørensen JN. Modelling of wind tunnel blockage. In: Thor S-E, editor. Proceedings of the 15th IEA Symposium on the Aerodynamics of Wind Turbines, FOI, Swedish Defence Research Agency, 2001. p. 41–51.
[129] Mikkelsen R, Sørensen JN. Yaw analysis using a numerical actuator disc model. In: Pedersen B, editor. Proceedings of the 14th IEA Symposium on the Aerodynamics of Wind Turbines, Department of Fluid Mechanics, Technical University of Denmark, 2000. p. 53–9.
[130] Ammara I, Leclerc C, Masson C. A viscous three-dimensional differential/actuator-disk method for aerodynamic analysis of wind farms. J Solar Energy—T ASME 2002;124(4):345–56.
[131] Sørensen JN. VISCWIND viscous effects on wind turbine blades. ET-AFM 9902, Department of Fluid Mechanics, The Technical University of Denmark, 1999.
[132] Chaviaropoulos PK, Nikolaou IG, Aggelis K, Sørensen NN, Montgomerie B, von Geyr H, Hansen MOL, Kang S, Voutsinas S, Dyrmose SZ. Viscous and aeroelastic effects on wind turbine blades: The VISCEL project. In: Helm P, Zervos A, editors. Proceedings of the 2001 European Wind Energy Conference and Exhibition, WIP-Renewable Energies, Munchen, 2001. p. 347–50.
[133] Hansen MOL, Sørensen JN, Michelsen JA, Sørensen NN. A global Navier–Stokes rotor prediction model. In: AIAA Paper 97-0970, 1997.
[134] Sørensen NN, Hansen MOL. Rotor performance predictions using a Navier–Stokes method. In: AIAA Paper 98-0025, 1998.
[135] Sørensen NN, Michelsen JA. Aerodynamic predictions for the unsteady aerodynamics experiment phase-ii rotor at the national renewable energy laboratory. In: AIAA Paper 2000-0037, 2000.
[136] Kang S, Hirsch C. Features of the 3D viscous flow around wind turbine blades based on numerical solutions. In: Helm P, Zervos A, editors. Proceedings of the 2001 European Wind Energy Conference and Exhibition, WIP-Renewable Energies, Munchen, 2001. p. 495–8.
[137] Michelsen JA, Sørensen NN. Current developments in Navier–Stokes modelling of wind turbine rotor flow. In: Helm P, Zervos A, editors. Proceedings of the 2001 European Wind Energy Conference and Exhibition, WIP-Renewable Energies, Munchen, 2001. p. 367–72.
[138] Duque EPN, van Dam CP, Hughes S. Navier–Stokes simulations of the NREL combined experiment phase II rotor. In: AIAA Paper 99-0037, 1999.
[139] Duque EPN, Johnson W, van Dam CP, Cortes R, Yee K. Numerical predictions of wind turbine power and aerodynamic loads for the NREL phase ii combined experiment rotor. In: AIAA Paper 2000-0038, 2000.
[140] Xu G, Sankar LN. Computational study of horizontal axis wind turbines. In: AIAA Paper 99-0042, 1999.
[141] Xu G, Sankar LN. Effects of transition, turbulence and yaw on the performance of horizontal axis wind turbines. In: AIAA Paper 2000-0048, 2000.
[142] Fingersh L, Simms D, Hand M, Jager D, Cortrell J, Robinson M, Schreck S, Larwood S. Wind tunnel testing of NREL's unsteady aerodynamics experiment. In: AIAA Paper 2001-0035, 2001.
[143] Tangler JL. The nebulous art of using wind tunnel aerofoil data for predicting rotor performance. Wind Energy 2002;5:245–57.
[144] Sørensen NN, Michelsen JA, Schreck S. Navier–Stokes predictions of the NREL phase vi rotor in the nasa ames 80 ft × 120 ft wind tunnel. Wind Energy 2002;5:151–69.
[145] Baldwin BS, Lomax H. Thin layer approximation and algebraic model for separated turbulent flows. AIAA Paper 78-257.
[146] Launder BE, Spalding DB. The numerical computation of turbulent flows. Comput Meth Appl Mech Eng 1974;3:269–89.
[147] Haase W, Brandsma F, Elsholz E, Lechziner M, Schwamborn D. Euroval—an european initiative in validation of cfd codes, Notes on numerical fluid mechanics, vol. 42. Braunschweig: Vieweg; 1993.
[148] Haase W, Chaput E, Elsholz E, Lechziner M, Muller UR. ECARP—european computational aerodynamic research project: validation of cfd codes and assessment of turbulence models, Notes on numerical fluid mechanics, vol. 58. Braunschweig: Vieweg; 1997.
[149] Menter FR. Zonal two-equation model k–ω models for aerodynamic flows. In: AIAA Paper 93-2906, 1993.
[150] Spalart PR. Strategies for turbulence modelling and simulations. Int J Heat Fluid Flow 2000;21:252–63.
[151] Johansen J, Sørensen NN, Michelsen JA, Schreck S. Detached-eddy simulation of flow around the NREL phase vi blade. Wind Energy 2002;5:185–97.
[152] Michel R. Etude de la transition sur les profiles d'aile: Etablissement d'un critere de determination de point de transition et calcul de la trainee de profile incompressible. ONERA TR 1/1578A, 1951.
[153] Stock HW, Degenhart E. A simplified e^n method for transition prediction in two-dimensional, incompressible boundary layers. Zeitschrift für Flugwissenschaften 13.
[154] Johansen J, Sørensen JN. Prediction of laminar/turbulent transition in airfoil flows. J Aircraft 1999;36(4):731–4.
[155] Brodeur RR, van Dam CP. Transition prediction for a two dimensional Navier–Stokes solver applied to wind-turbine airfoils. In: AIAA Paper 2000-0047, 2000.
[156] Smith D, Taylor GJ. Further analysis of turbine wake development and interaction data. In: Q.D.C., F. V. C, editors. Proceedings of the 13th BWEA Wind Energy Conference, Swansea, UK, 1991. p. 325–31.
[157] Crespo A, Hernández J. Turbulence characteristics in wind-turbine wakes. J Wind Eng Ind Aerodyn 1996;61:71–85.
[158] Helmis CG, Papadopoulos KH, Asimakopoulos DN, Papageorgas PG, Soilemes AT. An experimental study of the near wake structure of a wind turbine operating over complex terrain. Solar Energy 1995; 54(6):413–28.
[159] Högstrom U, Asimakopoulos DN, Kambezidis H, Helmis CG, Smedman A. A field study of the wake

behind a 2 mw wind turbine. Atmos Environ 1988;22(4):803–20.
[160] Luken E. The wind loads of wind turbines in clusters—literature survey. Report 89-160, TNO Division of Technology for Society, 1989.
[161] Quarton DC. Characterization of wind turbine wake turbulence and its implications on wind farm spacing. Final Report ETSU WN 5096, Department of Energy of the UK. Garrad-Hassan Contract, 1989.
[162] Vermeulen PEJ, Builtjes PJH. Turbulence measurements in simulated wind turbine clusters. Report 82-03003, TNO Division of Technology for Society, September 1982.
[163] Builtjes PJH. The interaction of windmill wakes. In: Proceedings of the 2nd International Symposium on Wind Energy Systems, BHRA Fluid Engineering, Amsterdam, Netherlands, 1978. p. B5-49-58.
[164] Green DRR. Near wake wind tunnel studies. ETSU-WN-5040/P1 Report, Loughborough University, March 1986.
[165] Ross JN. Measurements of velocity in wind tunnel studies of windmill arrays using laser anemometry. LM/Phys./133, Central Electricity Research Laboratories, July 1979.
[166] Green DRR, Alexander AJ. Measurement of velocity and turbulence profiles in flow situations relevant to wind turbine performance. Final Report on ETSU contract E/5A/CON/5003/177/026, Loughborough University, May 1985.
[167] Talmon AM. The wake of a horizontal axis wind turbine model, measurements in uniform approach flow and in a simulated boundary layer, Report 85-01021, TNO Division of Technology for Society, August 1985.
[168] Milborrow DJ, Ross JN. The influence of turbulence and rotor thrust on wind turbine wake characteristics. Memorandum TPRD/L/AP/0098/M83, CERL, 1983.
[169] Vermeulen PEJ. An experimental analysis of wind turbine wakes. In: Proceedings of the 3rd International Symposium on Wind Energy Systems. BHRA Fluid Engineering, Lyngby, Denmark, 1980. p. 431–50.
[170] Alfredson PH, Dahlberg JÅ, Bark FH. Some properties of the wake behind horizontal axis wind turbines. In: Proceedings of the 3rd International Symposium on Wind Energy Systems, BHRA Fluid Engineering, Lyngby, Denmark, 1980. p. 469–84.
[171] Crespo A, Hernández J. Analytical correlations for turbulence characteristics in the wakes of wind turbines. In: Garrad AD, Palz W, Scheller S, editors. Proceedings of the 1993 European Community Wind Energy Conference. Germany: Travemünde; 1993. p. 436–9.
[172] Højstrup J. Spectral coherence in wind turbine wakes. J Wind Eng Ind Aerodyn 1999;80:137–46.
[173] Smith D. Multiple wake measurements and analysis. In: Davies TD, Halliday JA, Palutikov JP, editors. Proceedings of the 12th BWEA Wind Energy Conference. UK: Norwich; 1990. p. 53–6.
[174] Papaconstantinou A, Bergeles G. Hot-wire measurements of the flow field in the vicinity of a HAWG rotor. J Wind Eng Ind Aerodyn 1988;31:133–6.
[175] Ainslie JF, Hassan U, Parkinson HG, Taylor GJ. A wind tunnel investigation of the wake structure within small wind turbine farms. Wind Eng 1990;14:24–8.
[176] Hassan U, Glendinning AG, Morgan CA. A wind tunnel investigation of the wake structure and machine loads within small wind turbine farms. In: Davies TD, Halliday JA, Palutikov JP, editors. Proceedings of the 12th BWEA Wind Energy Conference. Norwich, UK 1990. p. 47–52.
[177] Magnusson M, Smedman AS. Influence of atmospheric stability on wind turbine wakes. Wind Eng 1994; 18(3):139–52.
[178] Talmon AM. A wind tunnel investigation into the effects of tower and nacelle on wind turbine wake flow. Report 84-08479, TNO Division of Technology for Society, July 1984.
[179] Luken E, Vermeulen PEJ. Development of advanced mathematical models for the calculation of wind turbine wake-interaction effects. In: Palz W, Sesto E, editors. Proceedings of EWEC'86, Rome, Italy, 1986. p. 423–7.
[180] Crespo A, Hernández J, Fraga E, Andreu C. Experimental validation of the UPM computer code to calculate wind turbine wakes and comparison with other models. J Wind Eng Ind Aerodyn 1988;27:77–88.
[181] Taylor GJ, Smith D. Wake measurements over complex terrain. In: Quarton DC, Fenton VC, editors. Proceedings of the 13th BWEA Wind Energy Conference, Swansea, UK, 1991. p. 335–42.
[182] Stefanatos NC, Voutsinas SG, Rados KG, Zervos A. A combined experimental and numerical investigation of wake effects in complex terrain. In: Tsipouridis JL, editor. Proceedings of EWEC'94, Thessaloniki, Greece, 1994. p. 484–90.
[183] Stefanatos NC, Morfiadakis EE, Glinou GL. Wake measurements in complex terrain. In: Zervos A, Ehmann H, Helm P, editors. Proceedings of the 1996 European Union Wind Energy Conference, Göteborg, Sweden, 1996. p. 773–7.
[184] Tindal AJ, Garrad AD, Schepers G, Bulder B, Hutting H, Verheij F. Dynamic loads in wind farms. In: Garrad AD, Palz W, Scheller S, editors. Proceedings of the 1993 European Community Wind Energy Conference, Travemünde, Germany, 1993. p. 477–80.
[185] Baker RW, Walker SN. Wake velocity deficit measurements at the Goodnoe Hills MOD-2 Site. Report, Report No. BPA 84-15, DOE/BP/29182-15, 1985.
[186] Taylor GJ, Milborrow DJ, McIntosh DN, Swift-Hook DT. Wake measurements on the nibe windmills. In: Garrad A, editor. Proceedings of the 7th BWEA Wind Energy Conference, Oxford, UK, 1985. p. 67–73.
[187] Taylor GJ. Fluctuating loads on a wind turbine operating in a wake. In: Galt J, editor. Proceedings of the 9th BWEA Wind Energy Conference, Edinburgh, UK, 1987. p. 55–62.
[188] Taylor GJ. Wake measurements on the nibe windturbines in Denmark. Part 2: Data collection and analysis. Final Report CEC Contract No. EN3-W.0039.UK(H1), National Power, London, 1990.
[189] Højstrup J. Wake measurements on the nibe windturbines in Denmark. Appendix 1. Nibe wake 2. Final Report CEC Contract no. EN3W.0039.UK(H1), Risø, 1990.
[190] Scott AM. Wake interaction studies on the HWP-300/22 and WEG MS-1 WTGs on Burgar Hill, Orkney. Report

on UK DOEN Contract E/5A/CON/5039/1277, James Howden and Co Ltd, 1987.
[191] Haines RS, Milborrow DJ, Page DI, Scott AD, Stevenson WG, Taylor GJ. Wake interaction studies on the HWP-300/22 and WEG MS-1 WTGs on Burgar Hill, Orkney, UK. In: Palz W, Sesto E, editors. Proceedings of EWEC'86, vol. 1, Rome, Italy, 1986. p. 453–8.
[192] Højstrup J. Turbulence measurements in a wind farm. In: Davies TD, Halliday JA, Palutikov JP, editors. Proceedings of the 12th BWEA Wind Energy Conference, Norwich, UK, 1990. p. 59–63.
[193] Papadopoulos KH, Helmis CG, Soilemes AT, Papageorgas PG, Asimakopoulos DN. Study of the turbulent characteristics of the near-wake field of a medium sized wind turbine operating in high wind conditions. Solar Energy 1999;80:121–36.
[194] Frandsen S, Chacón L, Crespo A, Enevoldsen P, Gómez-Elvira R, Hernández J, Højstrup J, Manuel F, Thomsen K, Sørensen P. Measurements on and modelling of offshore wind farms. Report Risø-R-903(EN), Risø, 1996.
[195] Højstrup J, Courtney MS. Turbulence in wind farms, In: Garrad AD, Palz W, Scheller S, editors. Proceedings of the 1993 European Community Wind Energy Conference, Travemünde, Germany, 1993. p. 383–6.
[196] Kline J. Turbulence characteristics at Howden wind park I. In: AWEA conference "windpower 88", Honolulu, Hawaii, USA, 1988.
[197] Simon RL, Matson DF, Fuchs JM. Wake effects in a Fayette 95-II5 wind turbine array, Report SERI/STR-217-3186, Fayette Manufacturing Company, September 1987.
[198] Nierenberg R. Free flow variability and wake energy deficit studies in the Altamont pass, California: results of the DOE-AEC CFT program. In: AWEA conference "windpower 88", Honolulu, Hawaii, USA, 1988.
[199] Van Leuven J, Stevens D. The wind farm of Zeebrugge: Experimental set-up. J Wind Eng Ind Aerodyn 1988; 27:139–44.
[200] Van Leuven J. The energetic effectiveness of a cluster of wind turbines. PhD thesis, Universite Catholique de Louvain, Institut des Sciences Naturelles Appliquees, 1992.
[201] Folkerts L, Barthelmie R, Sanderhof P, Ormel F, Eecen P, Stobbe O. Sodar wind velocity measurements of offshore wind turbine wakes. Wind Eng 2001;25(5): 301–6.
[202] Frandsen S, Thøgersen ML. Integrated fatigue loading for wind turbines in wind farms by combining ambient turbulence and wakes. Wind Eng 1999;23(6): 327–40.
[203] Crespo A, Hernández J, Frandsen S. A survey of modelling methods for wind-turbine wakes and wind farms. Wind Energy 1994;2:1–24.
[204] Vølund P. Loads on a horizontal axis wind turbine operating in a wake. In: Van Hulle FJL, Smulders PT, Dragt JB, editors. Proceedings of EWEC'91, Amsterdam, Netherlands, 1991. p. 605–9.
[205] Stiesdal H. Wake loads on the Bonus 450 kW II turbine. In: Clayton BR, editor. Proceedings of the 14th BWEA Wind Energy Conference, Nottingham, UK, 1992. p. 183–9.
[206] Dahlberg JÅ, Poppen M, Thor SE. Load/fatigue effects on a wind turbine generator in a wind farm. In: Van Hulle FJL, Smulders PT, Dragt JB, editors. Proceedings of EWEC'91, Amsterdam, Netherlands, 1991. p. 251–5.
[207] Thomsen K, Bindner H, Pedersen TF. Fatigue loads on a pitch regulated wind turbine operating in a coastal wind turbine array. Report Risø-R-743(EN), Risø, 1994.
[208] Thomsen K, Sørensen P. Fatigue loads for wind turbines operating in wakes. J Wind Eng Ind Aerodyn 1999;55(1):61–72.
[209] Frandsen S, Christensen CJ. Structural loads in large wind farm arrays. In: Tsipouridis JL, editor. Proceedings of EWEC'94, vol. III, Thessaloniki, Greece, 1994. p. 116–22.
[210] Frandsen S, Thomsen K. Change in fatigue and extreme loading when moving wind farms offshore. Wind Eng 1997;21(3):197–214.
[211] Adams BM, Quarton JGDC, Schepers, Bulder B, Dahlberg JÅ, Morfiadakis E. Dynamic loads in wind farms. In: Tsipouridis JL, editor. Proceedings of EWEC'94, Thessaloniki, Greece, 1994. p. 756–61.
[212] Cleijne JW. Results of Sexbierum wind farm. Report 92-388, TNO-MT, Apeldoorn, Netherlands, 1992.
[213] Gómez-Elvira R, Crespo A. An explicit algebraic turbulent model to reproduce the anisotropy of the momentum turbulent flows in a wind turbine wake. In: accepted for publication in Proceedings of EWEC'2003 Madrid, Spain, 2003.
[214] Magnusson M. Full-scale wake measurements at Alsvik wind farm, Sweden. In: Tsipouridis JL, editor. Proceedings of EWEC'94, Thessaloniki, Greece, 1994. p. 472–7.
[215] Magnusson M, Smedman AS. Air flow behind wind turbines. J Wind Eng Ind Aerodyn 1999;80:169–89.
[216] Lissaman PBS. Energy effectiveness of arbitrary arrays of wind turbines. In: AIAA Paper 79-0114, 1979. p. 1–7.
[217] Voutsinas SG, Rados KG, Zervos A. On the analysis of wake effects in wind parks. Journal of Wind Eng Ind Aerodyn 1990;14(4):204–19.
[218] Abramovich GN. The theory of turbulent jets. Cambridge, MA: MIT Press; 1963.
[219] Katic I, Højstrup J, Jensen NO. A simple model for cluster efficiency. In: Palz W, Sesto E, editor. Proceedings of EWEC'86, Rome, Italy, 1986. p. 407–10.
[220] Crespo A, Manuel F, Moreno D, Fraga E, Hernández J. Numerical analysis of wind turbine wakes. In: Bergeles G, Chadjivassiliadis J, editors. Proceedings of the Delphi Workshop on Wind Energy Applications, Delphi, Greece, 1985. p. 15–25.
[221] Sforza PM, Sheering P, Smorto M. Three-dimensional wakes of simulated wind turbines. AIAA J 1981;19(9): 1101–7.
[222] Ainslie JF. Development of an eddy viscosity model for wind turbine wakes. In: Garrad A, editor. Proceedings of the 7th BWEA Wind Energy Conference, Oxford, UK, 1985. p. 61–6.
[223] Ainslie JF. Calculating the field in the wake of wind turbines. J Wind Eng Ind Aerodyn 1988;21:213–24.
[224] Luken E, Talmon A, Vermeulen PEJ. Evaluation of two mathematical wind turbine wake models in various types of flows. Report 86-07, TNO-MT, 1986.

[225] Crespo A, Hernández J. Numerical modelling of the flow field in a wind turbine wake. In: Proceedings of the 3rd Joint ASCE/ASME Mechanics Conference, Forum on Turbulent Flows. ASME, FED-vol. 76, La Jolla, CA, USA, 1989. p. 121–7.

[226] Crespo A, Hernández J. A numerical model of wind turbine wakes and wind farms. In: Palz W, Sesto E, editors. Proceedings of EWEC'86, vol. 2, Rome, Italy, 1986. p. 111–5.

[227] Crespo A, Manuel F, Hernández J. Numerical modelling of wind turbine wakes. In: Palz W, editor. Proceedings of the 1990 European Community Wind Energy Conference, Madrid, Spain, 1990. p. 166–70.

[228] Taylor PA. On wake decay and row spacing for wecs farms. In: Proceedings of the 3rd International Symposium on Wind Energy Systems, BHRA Fluid Engineering, Lyngby, Denmark, 1980. p. 451–68.

[229] Liu M, Vocke M, Myers T. Mathematical model for the analysis of wind turbine wakes. Journal of Energy 1983;7(1):73.

[230] Taylor GJ. Development of an improved eddy viscosity model. Wake and wind farm modelling. Final Report TNO-Report 93-374, National Power, London, 1993.

[231] Adams BM, Quarton DC. Dynamic loads in wind farms. Final Report, Joule Project JOU2-CT92-0094 (Edited by Garrad Hassan, 1996).

[232] Hassan U. A wind tunnel investigation of the wake structure within small wind farms. Report. ETSU Report No. WN5113, Garrad-Hassan, 1993.

[233] Magnusson M. Near wake behaviour of wind turbines. J Wind Eng Ind Aerodyn 1999;80:147–67.

[234] Zervos A, Huberson S, Hemon A. Three-dimensional free wake calculation of wind turbine wakes. J Wind Eng Ind Aerodyn 1988;27:65–76.

[235] Cleijne JW, Crespo A, Huberson S, Taylor GJ, Voutsinas SG. Wake and wind farm modelling. Report 93-374, TNO-MT, Apeldoorn, Netherlands, 1993.

[236] Schepers JG. ENDOW: Validation and improvement of ECN's wake model. ECN-C–03-034, ECN, March 2003.

[237] Voutsinas SG, Glekas JP, Zervos A. Investigation of the effect of the initial velocity profile on the wake development of a wind turbine. J Wind Eng Ind Aerodyn 1992;39:293–301.

[238] Voutsinas SG, Rados KG, Zervos A. On the effect of the rotor geometry on the formation and the development of its wake. J Wind Eng Ind Aerodyn 1992;39:283–91.

[239] Magnusson M, Rados KG, Voutsinas SG. A study of the flow downstream of a wind turbine using measurements and simulations. Wind Eng 1996;20(6):389–403.

[240] Pothou KP, Voutsinas SG, Huberson S, Kuhlmann M, Rawlinson-Smith R. Investigation of noise emissions from wind parks and their impact to the design of parks by means of the noisepark software. In: Petersen EL, Jensen PH, Rave K, Helm P, Ehmann H, editors. Proceedings of the 1999 European Union Wind Energy Conference, Nice, France, 1999. p. 97–100.

[241] Ansorge T, Fallen M, Günther P, Ruh C, Wolfanger T. Numerical simulation of wake-effects in complex terrain and application of a Reynolds-stress turbulence model. In: Tsipouridis J, editor. Proceedings of EWEC'94, Thessaloniki, Greece, 1994. p. 448–53.

[242] Beyer HG, Rüger T, Schäfer G, Waldl HP. Optimization of wind farm configuration with variable number of turbines. In: Zervos A, Ehmann H, Helm P, editors. Proceedings of the 1996 European Union Wind Energy Conference. Göteborg, Sweden, 1996. p. 1073–6.

[243] Sotiropoulos DP, Koukas A, Stephanatos NC, Voutsinas SG. Numerical investigation of wake effects in offshore wind farms using a 3d navier-stokes solver. In: Petersen EL, Jensen PH, Rave K, Ehmann HPH, editors. Proceedings of the 1999 European Union Wind Energy Conference. Nice, France, 1999. p. 254–7.

[244] Crespo A, Chacón L, Hernández J, Manuel F, Grau JC. UPMPARK: a parabolic 3D code to model wind farms, In: Tsipouridis JL, editor. Proceedings of EWEC'94, Thessaloniki, Greece, 1994. p. 454–9.

[245] Bulder BH. Fynd farm—a wind farm design support tool. In: Proceedings of the European Wind Energy Conference, Dublin Castle, Ireland, 1997. p. 246–8.

[246] Crespo A, Manuel F, Grau JC, Hernández J. Modelization of wind farms in complex terrain. Application to the monteahumada wind farm. In: Garrad AD, Palz W, Scheller S, editors. Proceedings of the 1993 European Community Wind Energy Conference, Travemünde, Germany, 1993. p. 436–9.

[247] Voutsinas SG, Rados KG, Zervos A. The effect of the non-uniformity of the wind velocity field in the optimal design of wind parks. In: Palz W, editor. Proceedings of the 1990 European Community Wind Energy Conference, Madrid, Spain, 1990. p. 181–5.

[248] Hemon A, Huberson S, Zervos A. Numerical study of wind turbine operation in complex terrain. In: Quarton DC, Fenton VC, editors. Proceedings of the 13th BWEA Wind Energy Conference, Swansea, UK, 1991. p. 343–50.

[249] Migoya E, Crespo A, García J, Moreno F, Jiménez A. Comparative study of the behaviour of several wind-turbines in a wind farm. In: Proceedings of EWEC'2003 Madrid, Spain, 2003, Accepted for publication.

[250] Günther P, Fallen M, Wolfanger T. Numerical wake simulation of a hawt considering topography and using a mesoscale turbulence model. In: Garrad AD, Palz W, Scheller S, editors. Proceedings of the 1993 European Community Wind Energy Conference, Travemünde, Germany, 1993. p. 448–50.

[251] Chaviaropoulos PK, Douvikas DI. Mean wind field prediction over complex terrain in the presence of wind turbines. In: Petersen EL, Jensen P, Rave K, Helm P, Ehmann H, editors. Proceedings of the 1999 European Union Wind Energy Conference, Nice, France, 1999. p. 1208–11.

[252] Ivanova LA, Nadyozhina ED. Numerical simulation of wind farm influence on wind flow. Wind Eng 2000; 24(4):257–70.

[253] Crespo A, Gómez-Elvira R. Effect of the proximity of land on wind farm performance for offshore flow. In: Proceedings of the European Seminar OWEMES'97, La Magdalene, Sardinia, Italy, 1997. p. 33–41.

[254] Crespo A, Chacón L, Manuel F, Gómez-Elvira R, Hernández J. Modelization of offshore wind farms. Effect of the surface roughness of the sea. In: Zervos A, Ehmann H, Helm P (editors). Proceedings of the 1996

European Union Wind Energy Conference, Göteborg, Sweden, 1996. p. 644–7.
[255] Frandsen S. Fatigue loading on offshore wind power stations. In: Zervos H, Ehmann A, Helm P, editors. Proceedings of the 1996 European Union Wind Energy Conference, Göteborg, Sweden, 1996. p. 990–4.
[256] Rados K, Larsen G, Barthelmie R, Schlez W, Lange B, Schepers G, Hegberg T, Magnusson M. Comparison of wake models with data for offshore windfarms. Wind Eng 2001;25(5):271–80.
[257] Schlez W, Umaña A, Barthelmie R, Larsen G, Rados K, Lange B, Schepers G, Hegberg T. ENDOW: improvement of wake models within offshore wind farms. Wind Eng 2001;25(5):281–7.
[258] Schepers G, Barthelmie R, Rados K, Lange B, Schlez W. Large offshore wind farms: linking wake models with atmospheric boundary layer models. Wind Eng 2001; 25(5):307–16.
[259] Newman BG. Near wake behaviour of wind turbines. Energy Conversion 1977;16:169–71.
[260] Bossanyi EA, Maclean C, Whittle GE, Dunn PD, Lipman NH, Musgrove PJ. The efficiency of wind turbine clusters. In: Proceedings of the 3rd International Symposium on Wind Energy Systems, BHRA Fluid Engineering, Lyngby, Denmark, 1980. p. 401–16.
[261] Frandsen S. On the wind speed reduction in the center of large clusters of wind turbines. J Wind Eng Ind Aerodyn 1992;39:261–5.
[262] Crespo A, Frandsen S, Gómez-Elvira R, Larsen SE. Modelization of a large wind farm, considering the modification of the atmospheric boundary layer. In: Petersen EL, Jensen PH, Rave K, Helm P, Ehmann H (editors). Proceedings of the 1999 European Union Wind Energy Conference, Nice, France, 1999. p. 1109–13.
[263] Hegberg T. The effect of large windfarms on the atmospheric boundary layer. In: Proceedings of the Global Wind Power Conference 2002, Paris, France, 2002.
[264] Frandsen S, Barthelmie R. Local wind climate whithin and downwind of large offshore wind turbine clusters. Wind Eng 2002;26(1):51–8.
[265] Hunt J, Eames I. The disappearance of laminar and turbulent wakes in complex flows. J Fluid Mech 2002; 457:111–32.
[266] Magnusson M, Smedman AS. A practical method to estimate wind turbine wake characteristics from turbine data and routine wind measurements. Wind Eng 1996; 20(2):73–92.
[267] Schlichting H. Boundary layer theory. New York: McGraw-Hill; 1968.
[268] Larsen GC, Højstrup J, Madsen HA. Wind fields in wakes. In: Zervos A, Ehmann H, Helm P, editors. Proceedings of the 1996 European Union Wind Energy Conference, Göteborg, Sweden, 1996. p. 764–8.
[269] Frandsen S. Turbulence and turbulence-generated fatigue loading in wind turbine clusters. Report in draft form Risø-R-1188(EN), Risø, Roskilde, Denmark, 2003.